This is to certify that the
thesis entitled

ELECTROCHEMICAL IMPEDANCE SPECTROSCOPY BASED SENSORS FOR NDE OF CFRP/CONCRETE BOND IN BEAMS

presented by

Sangdo Hong

has been accepted towards fulfillment
of the requirements for the

M.S. degree in Civil Engineering

P.B. Harichandran
Major Professor's Signature

August 21, 2003
Date

ELECTROCHEMICAL IMPEDANCE SPECTROSCOPY BASED SENSORS FOR NDE OF CFRP/CONCRETE BOND IN BEAMS

By

Sangdo Hong

A THESIS

Submitted to
Michigan State University
in partial fulfillment of the requirements
for the degree of

MASTER OF SCIENCE

Department of Civil and Environmental Engineering

2003

ABSTRACT

ELECTROCHEMICAL IMPEDANCE SPECTROSCOPY BASED SENSORS FOR NDE OF CFRP/CONCRETE BOND IN BEAMS

By

Sangdo Hong

Electrochemical impedance spectroscopy (EIS) based sensor technology is used for the NDE of the bond between external CFRP reinforcement and concrete in beams. Copper tape on the surface of the CFRP sheet, stainless steel wire embedded in the concrete, and reinforcing bars were used as the sensing elements. Laboratory experiments were designed to test the capability of the sensors to detect the debonding of the CFRP from the concrete and to study the effect of short-term (humidity and temperature fluctuations and chloride content) and long-term (freeze-thaw and wet-dry exposure and rebar corrosion) environmental conditions on the measurements. The CFRP sheet was debonded from the concrete and impedance measurements were taken between various pairs of electrodes at various interfacial crack lengths. The dependence of the impedance spectra, and of the parameters obtained from equivalent circuit analysis, on the interfacial crack length was studied. Capacitance parameters in the equivalent circuit were used to assess the global state of the bond between CFRP sheets and concrete. Impedance measurements taken between embedded wire sensors were used to detect the location of debonded regions.

To my parents, wife and daughters

ACKNOWLEDGMENTS

This research was funded by Michigan State Department of Transportation. This contribution is gratefully acknowledged.

I would like to express my sincere gratitude to Dr. R. Harichandran whose supervision and guidance were heightened not only by his friendly nature, but also by his genuine concern and understanding. I also would like to thank Dr. A. Al-Ostaz and Dr. G. Davis for their collaboration and the MS guidance committee members, Dr. P. Soroushian and Dr. A. Varma for their support. I would like to express my great appreciation to Mr. S. Ravanbakhsh for his effort and help throughout this research.

TABLE OF CONTENS

LIST OF TABLES

LIST OF FIGURES

Chapter 1

Introduction

Many structures built in the past need strengthening and retrofitting to overcome deficiencies caused by increased load demands, environmental deterioration and structural aging. Thirty-five percent of all bridges in the U.S. are estimated to be structurally deficient and require repair, strengthening, widening or replacement (Karbhari 2000). To overcome structural deficiencies, composite materials such as fiber reinforced polymers (FRP) are being increasingly used for strengthening and retrofitting. Carbon-fiber reinforced polymer (CFRP) is a well-known high performance composite material used to strengthen reinforced concrete structural components.

For flexural strengthening of beams, CFRP plate or sheets are bonded to the tension face. This is a simple and convenient technique for strengthening and retrofitting structures (Rahimi et al. 2001). Unlike steel plates, FRP plates do not suffer from corrosion problems. However, the interfacial bond between FRP and concrete can deteriorate due to environmental and load-related issues leading to debonding durability and delamination.

Structural components strengthened or retrofitted with FRP behave as composite components, and their strengths are calculated by taking this into account. Interfacial bonding between the adherents plays a significant role in achieving composite behavior and increasing strength.

Concrete structures with FRP plates can exhibit a brittle failure mode if the FRP debonds from the concrete. Debonding of the plates and ripping of concrete are common

failure modes in concrete structures rehabilitated with FRP plates (Nguyen et al. 2001). The ripping of concrete and debonding of the FRP are initiated due to high localized stress concentration in the interface layer (Buyukozturk 1998).

It is therefore of interest to identify the integrity of interfacial bonding between the concrete structure and the FRP. Detection of debonding is crucial in characterizing the strength of the structural composite components, since composite action can only be achieved with a strong interfacial bond. Nondestructive evaluation (NDE) techniques can be very useful to detect the debonding between composite materials and concrete structures.

1.1 Background

Carbon-fiber-reinforced polymer (CFRP) is a common high-performance composite material used to retrofit and strengthen concrete structures by bonding the CFRP to concrete. The bond between the CFRP and concrete plays a crucial role in achieving composite action. Therefore, monitoring the integrity of the bond between two materials is important. There are several ways to detect or monitor the debonding between FRP and concrete. The tap test, the acoustic emission (AE) technique, and the ultrasonic pulse velocity (UPV) inspection method are some of the methods being promoted for this purpose.

The tap test is the simplest method that can be carried out in the field. It is conducted with a coin or a special hammer. The inspectors listen to the acoustic sounds generated by tapping and qualitatively evaluates them for detecting disbonds. The main advantage of using this technique is that the tap test does not require sophisticated or expensive equipment. The tap test works because different acoustic sounds are generated depending

on whether the FRP is bonded to the concrete or not. The major disadvantage of using this technique is that the method depends on subjective interpretation by the inspectors. Also the inspector must be able to get close to the FRP/concrete surface to conduct the test. This is often problematic for bridge beams.

Acoustic emission (AE) inspection is based on the detection of sound waves generated by the structures that are stressed (Dai et al. 1997). When concrete structures rehabilitated with FRP are subjected to stress, the concrete and FRP materials generate an AE signal. AE sources include the debonding between FRP and concrete, cracking in concrete, and plastic deformation and debonding of aggregate in concrete structures rehabilitated with FRP (Mirmiran et al. 1999). The major advantage of using the AE technique is that the integrity of structures can be monitored in real time, and the source of the AE source center can be determined as well. The main disadvantage is that the structures have to be monitored constantly. One of the main obstacles to having real time measurements is supplying power to instruments used on civil structures in remote areas. In addition to supplying the power, the AE technique suffers from the Kaiser effect. The Kaiser effect is the phenomena that an AE signal is not generated until the previous maximum load is exceeded. This Kaiser effect leads to the problem that the AE technique cannot detect pre-existing disbonds.

The ultrasonic pulse velocity (UPV) test is an NDE method similar to the AE technique. AE tests are passive tests that analyze the signal generated by concrete structures under applied loads. The UPV technique uses the characteristics of a pulse signal that travels through the structure. The variation of UPV is used to detect the cracks in the structures (Mirmiran et al. 2001). Although the UPV technique is a successful

nondestructive evaluation tool, it has one main disadvantage: the UPV measurements are not easy to interpret. UPV is a function of the stiffness and density of components, and concrete structures rehabilitated with FRP produce complicated ultrasonic signals (Olajide et al. 2000). This complication makes it difficult to isolate disbonds using the UPV test.

Electrochemical impedance spectroscopy (EIS) is a method that has been used to study moisture penetration and debonding between two bonded composites (Davis et al. 1999). This work explores the potential of EIS to detect debonding of CFRP from concrete.

1.2 Electrochemical Impedance Spectroscopy – Background

The basic concepts of electrochemical impedance spectroscopy (EIS) are reviewed in this section. The term "impedance" is a generalization of the term "resistance". Electrical resistance is the ability of a material to resist the flow of electrical current. Electrical resistance is defined in terms of the ratio between voltage (V) and current (I) by Ohm's law.

$$R = \frac{V}{I} \tag{1-1}$$

Current is a measure of the flow of electrical charge. Voltage is the change in energy that would be experienced by a charge when it travels from location A to location B.

1.2.1 Impedance

Electrochemical impedance (EI) is the resistance to current in an electrochemical cell. EI is generally obtained by measuring the current or voltage across a pair of electrodes due to an applied electrical stimulus (voltage or current). Impedance is most

commonly obtained through the amplitude and phase shift of the sinusoidal response relative to a sinusoidal input.

Electrical resistance is independent of the frequency of harmonic (sinusoidal) AC voltage. However, electrical impedance (Z) is dependent on frequency. When the excitation signal is harmonic, the response signal is also harmonic at the same frequency with an amplitude and phase angle. The impedance (Z) is a complex-valued quantity and is defined as the ratio between the excitation voltage V(t), and the response current I(t):

$$Z = \frac{V(t)}{I(t)} \tag{1-2}$$

For a harmonic AC excitation signal, V(t) may be expressed as

$$V(t) = V_o e^{j\omega t} = V_o(\cos \omega t + j \sin \omega t) \tag{1-3}$$

where ω is the circular natural frequency of the applied voltage (expressed in radian/second) and V_0 is the amplitude of the excitation signal. The harmonic current response I(t) may be expressed as

$$I(t) = I_o e^{j(\omega t - \phi)} = I_o[\cos(\omega t - \phi) + j\sin(\omega t - \phi)] \tag{1-4}$$

where I_0 is the amplitude of the harmonic current and ϕ is the phase shift. The electrical impedance in Eq. (1-2) is then

$$Z = Z_o e^{j\phi} = Z_o(\cos\phi + j\sin\phi) \tag{1-5}$$

where $Z_0 = V_0 / I_0$

Impedance, Z, is generally complex-valued. The impedance of a resistor, R, is Z_R = R and is real-valued. The impedance of a capacitor, C, is purely imaginary and is Z_C = $1/(j\omega C)$, where $j = \sqrt{-1}$ and ω is the circular natural frequency in rad/sec of the applied voltage. The constant phase element (CPE) is often used in an equivalent circuit to

represent the response of real-world electrochemical systems. Electrochemical systems sometimes do not response ideally because some properties of the electrochemical system are not homogeneous and often there are distributed elements in addition to lumped elements in the system. The impedance of the CPE is

$$Z_{CPE} = A(j\omega)^{-\alpha} \tag{1-6}$$

When $\alpha = 1$ (maximum value), the CPE is equivalent to a capacitor with A = 1/C (the inverse of the capacitance), and when $\alpha = 0$ (minimum value), the CPE is equivalent to a resistor with A = R.

For linear impedance elements in series, the equivalent impedance is

$$Z_{eq} = Z_1 + Z_2 + Z_3 \tag{1-7}$$

For linear impedance elements in parallel, the reciprocal of the impedance is

$$\frac{1}{Z_{eq}} = \frac{1}{Z_1} + \frac{1}{Z_2} + \frac{1}{Z_3} \tag{1-8}$$

1.2.2 Electrochemical impedance spectroscopy and equivalent circuit analysis

Traditionally, electrochemical impedance spectroscopy (EIS) has been used to detect coating deterioration and substrate corrosion, and the EIS technique is performed in an electrolyte with counter and reference electrodes (Scully et al. 1989). The counter electrode works as a supplier to pass sufficient current into the electrolyte. The reference electrode maintains invariant potential in an electrochemical measurement and serves as a reference point on the measurements of the working electrode. The working electrode is a transducer responding to the excitation signal. Figure 1-1 shows the typical electrochemical cell used in traditional EIS. Use of an external electrolyte is cumbersome in the field. However, it is possible to use *in-situ* electrodes to measure the impedance in

the ambient condition without submerging the electrochemical cell using a modified EIS technique (Davis et al. 2000).

Electrochemical theories have been proposed to explain the charge transfer process that occurs in electrode/electrolyte systems (Bard et al. 1980). Figure 1-2 shows the charge transfer process in the electrochemical system. When a metal electrode is immersed and activated in a solution, it will react with the solution. From this reaction, positive charges or negative charges are accumulated on the surface of the metal. An electrical double layer exists at the surface between each electrode and the electrolyte (pore fluid in the case of concrete). Ions in the electrolyte can only approach the electrode up to the outer surface of the double layer. Charge transfer between ions and the electrode involves long-range electrostatic forces, so that their interaction is essentially independent of the chemical properties of ions. Charge transfer through the electrolyte occurs by the diffusion of ions. At low excitation frequencies, the impedance to current flow is controlled by the rate of diffusion, while at high frequencies, the impedance is controlled by the kinetics of the charge transfer processes at the electrode/electrolyte interface.

In the modified EIS technique, an AC voltage is applied between the counter and the reference/working electrode. In this method the reference and working electrodes are combined into a single electrode. The complex impedance spectrum is then measured as a function of frequency. Two methods of analyzing the impedance spectra are common.

1. The first method is to simply compare the raw impedance spectra from different measurements and make inferences. The spectra can be plotted in many different ways. The conventional presentations are the Bode magnitude

plot (log impedance magnitude vs log frequency), Bode phase angle plot (phase angle vs log frequency), Nyquist plot (imaginary part of impedance vs real part of impedance), real impedance plot (real parts of impedance vs log frequency or log real parts of impedance vs log frequency), and imaginary impedance plot (imaginary parts of impedance vs log frequency). The magnitudes of impedance, phase angles, real impedances or imaginary impedances are compared over the entire frequency range or over specific frequency ranges.

2. The second method is to analyze the impedance spectra by using an equivalent circuit model. In this method, the parameters of an electrical circuit which has a theoretical impedance similar to the measured impedance are estimated, and spectra are compared based on the differences in the estimated parameters. Typical equivalent circuits are shown in Figure 1-3. Figure 1-3 (a) shows a circuit used for corrosion studies (Macdonald 1987) and Figure 1-3 (b) shows the circuit used to study an adhesive bond (Davis et al. 1999). Different equivalent circuits can be used to approximate a measured impedance spectrum, and some experience is required to select an appropriate circuit.

1.3 Use of EIS for Detection of Interfacial Degradation—A Literature Review

In-situ sensors have been adapted to detect moisture ingress and coating deterioration. Davis et al. (1999) found a strong correlation between low frequency impedance measurements and moisture ingress into coatings. They found that the initial

coating resistance was very high, but as the coating degrades due to moisture ingress, the coating resistance decreases in the low frequency region.

An *in-situ* corrosion sensor previously used in monitoring coating degradation and substrate corrosion of metals has been used to detect moisture ingress and crack propagation in structural adhesive bonds. This sensor technology has also been used to inspect the integrity of composite/composite bonds. Davis et al. (1999) conducted wedge tests on bonded glass-reinforced and graphite-reinforced composites to assess the integrity of the bond using EIS sensor technology. The wedge was driven into the specimen until the two adherents separated and impedance measurements were taken. The impedance typically increased in magnitude in the high-frequency region as the crack propagated. Figure 1-4 shows the results of the wedge test.

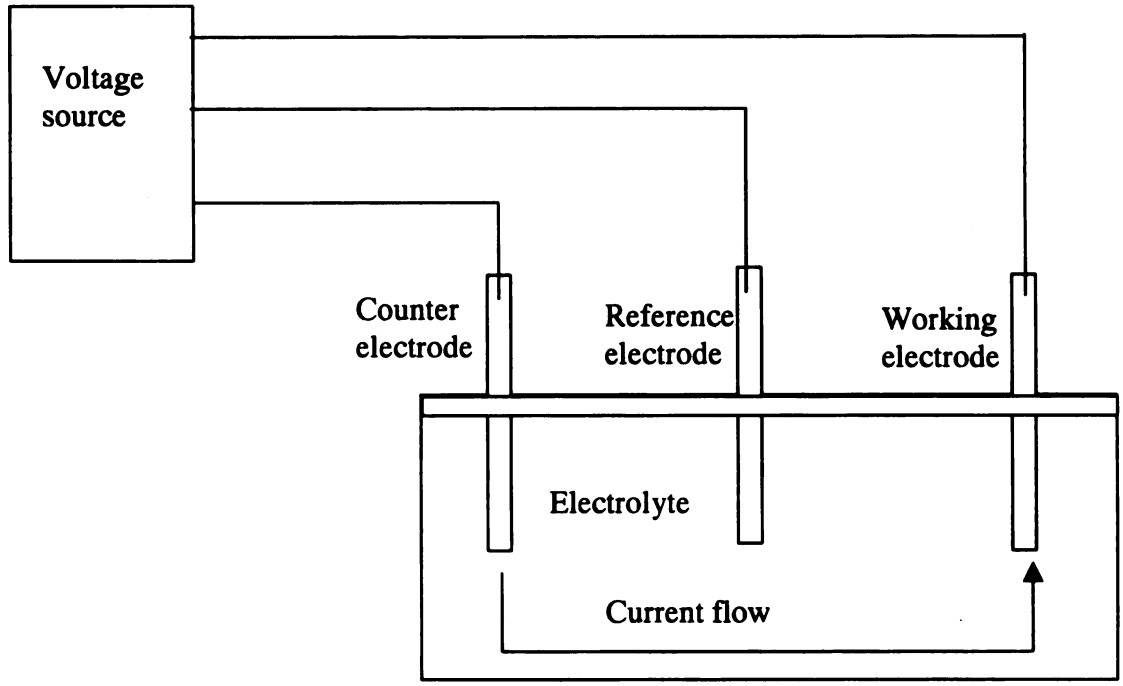

Figure 1-1 Typical electrochemical cell

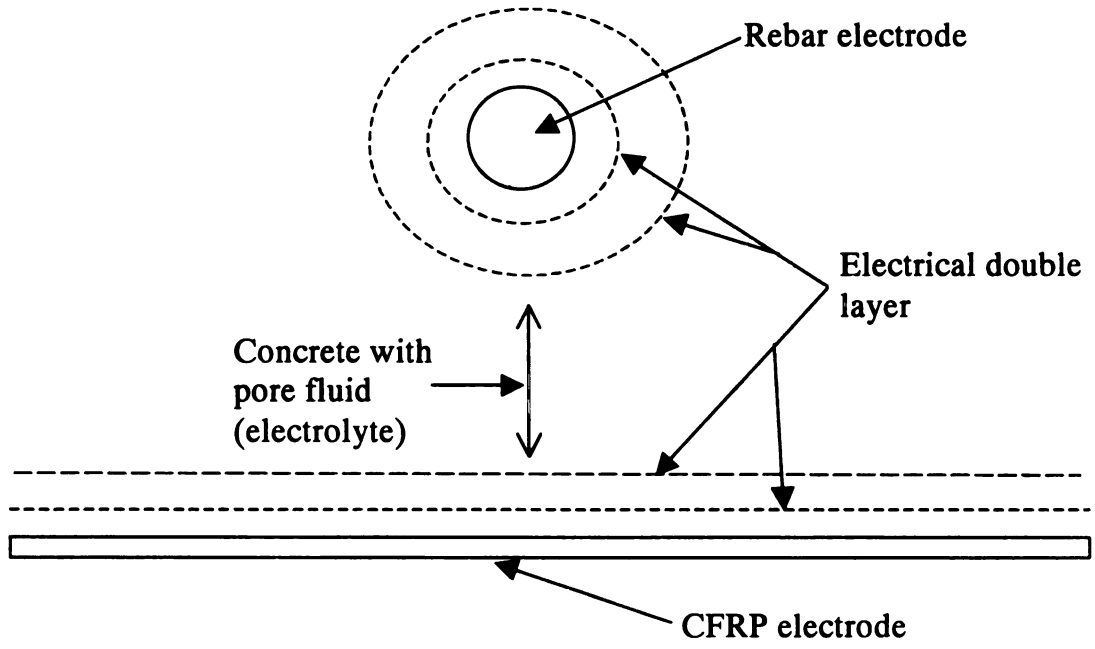

Figure 1-2 Model of the charge transfer process when the rebar and CFRP sheet (via external sensor) are used as electrodes

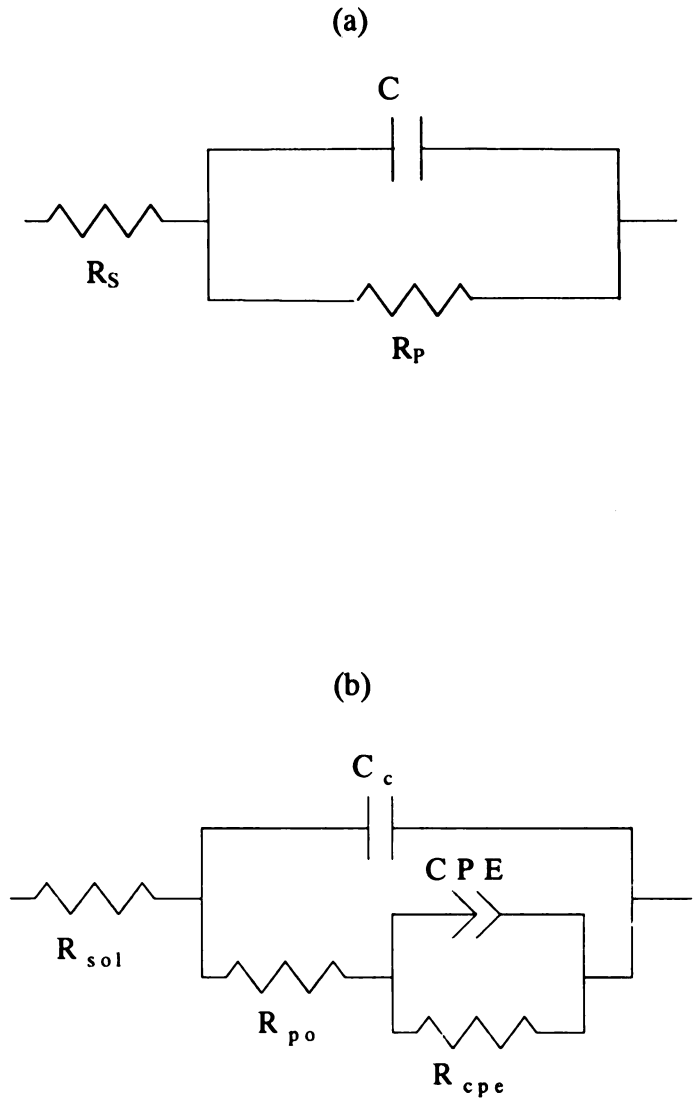

Figure 1-3 Equivalent circuit configurations — (a) simple circuit used for a corrosion reaction (Macdonald 1987) (b) circuit used to study an adhesive bond (Davis et al. 1999)

In the simplest method for analyzing the debonding effects, the impedance spectra can be compared directly (Figure 1-4). However, additional information can be obtained from the impedance spectra by using equivalent circuit analysis. Davis et al. (1999) conducted the wedge tests under dry and wet conditions. They used the equivalent circuit in Figure 1-3 (b), and found that the resistive components in the equivalent circuit they used were functions of moisture content and the capacitance parameter was a function of both moisture content and bonded area. The capacitance parameter from the equivalent circuit analysis varied linearly with the bonded area in the dry wedge test. However, the relationship was more complex when moisture was introduced during the wedge test. The resistance parameters from the equivalent circuit analysis correlated with moisture level in the electrochemical system. However, the resistance parameters did not show any correlation with bonded area. Figures 1-5 and 1-6 show the correlations between the parameters from the equivalent circuit analysis and the bonded area.

Davis et al. (1999) proposed the capacitance of an adhesive was influenced by the dielectric constant of the adhesive, the thickness of the adhesive and the bonded area. The capacitance may be expressed as

$$C = \frac{\varepsilon_o \varepsilon A}{d} \tag{1-9}$$

where C is the capacitance of the coating
ε_0 is the permitivity of free space,
ε is the dielectric constant of the adhesive (which is dependant on the moisture content)
A is the bonded area
d is the thickness of the adhesive

The dielectric constant increases as moisture ingresses into the adhesive. The relationship between the dielectric constant and moisture ingress is

$$\varepsilon = \varepsilon_{Ad} + M(\varepsilon_W - \varepsilon_{Ad}) \tag{1-10}$$

where ε_{Ad} is the dielectric constant of the epoxy adhesive
M is the moisture concentration in the adhesive
ε_w is the dielectric constant of water

By combining Eq (1-9) and Eq. (1-10), the moisture increase in the adhesive from one instart of measurement to another may be expressed as

$$M = \frac{\Delta C}{\alpha A}\left(\frac{\varepsilon_{Ad}}{\varepsilon_W - \varepsilon_{Ad}}\right) \tag{1-11}$$

where ΔC is the difference between the measured capacitance at two different times
α is the slope of the dry capacitance vs bonded area relationship

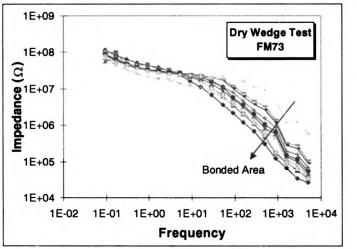

Figure 1-4 Typical impedance spectra taken from the wedge test (Source: Davis et al. 1999)

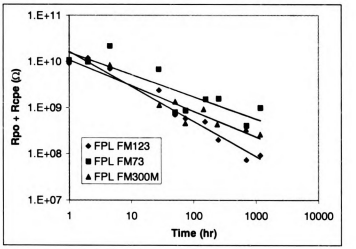

Figure 1-5 Resistance parameters from the equivalent circuit analysis as a function of time for the wedge tests under wet condition (Source: Davis et al. 1999)

(a)

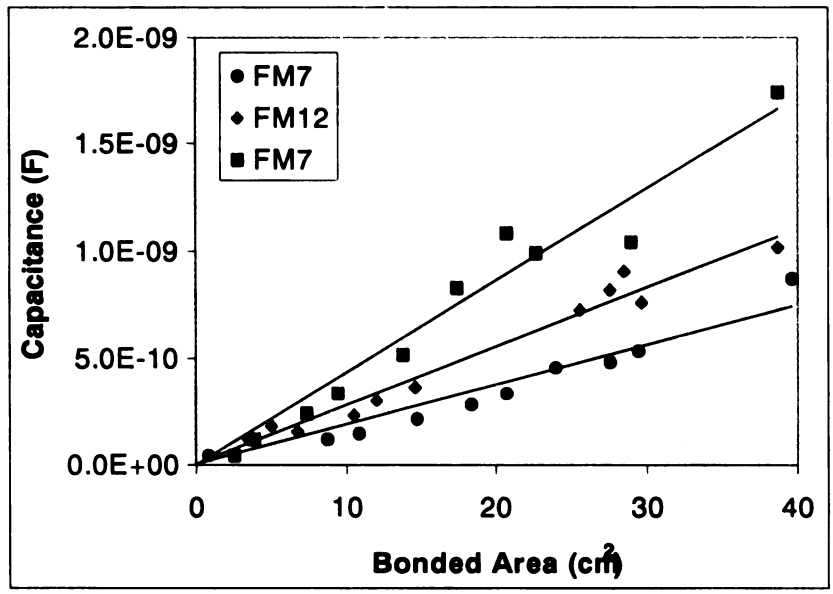

(b)

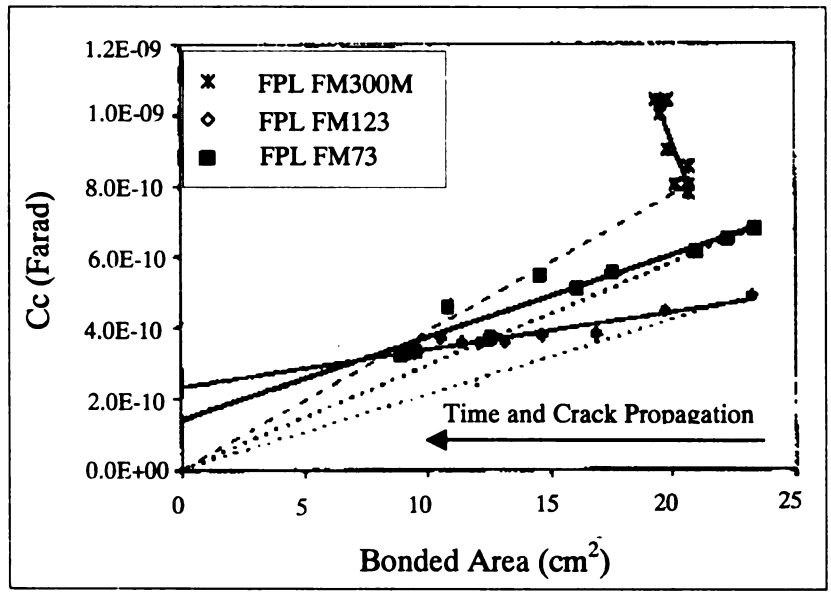

Figure 1-6 Variation of capacitance parameter from the equivalent circuit analysis as a function of bonded area for wedge tests under —(a) dry condition (b) wet condition (Source: Davis et al. 1999)

1.4 Hypothesis and Objectives

The hypothesis investigated in this research is that EIS can be used to detect debonding of CFRP reinforcement in concrete structures strengthened with CFRP. This hypothesis is based on the successful use of this method for glass-reinforced composite/composite bonds by Davis et al. (1999).

The objectives of the research are to:

- Develop effective sensor configurations, measurement schemes, and data interpretation techniques.
- Ascertain the effects of short-term environmental conditions such as temperature and humidity variations on the measurements and interpretations.
- Ascertain the effect of long term environmental conditions such as freeze-thaw cycles, wet-dry cycles and corrosion of reinforcement on the measurements and interpretations

Chapter 2

Experimental Design

Debonding of external CFRP reinforcement was investigated by using wedge tests. In these tests, the CFRP sheet is debonded by driving a thin wedge between it and the concrete substrate. Impedance measurements are taken periodically and the variation of impedance with the debonded length or area is studied.

Concrete structures rehabilitated with carbon fiber reinforced polymer (CFRP) are subjected to various environmental conditions. The environmental conditions can be divided into short-term and long-term conditions. Short-term environmental conditions represent the conditions at the time impedance measurement are taken. These conditions influence the impedance measurements, and include temperature variations, humidity variations and variations in chloride concentration caused by deicing agents.. The long-term environmental conditions include corrosion of reinforcing bars, freezing and thawing cycles and wetting and drying cycles. The impact of short term and long term environmental effects on impedance measurements must be well understood if the latter are to be used to detect debonding of the CFRP. It also is important to have durable and reliable sensors to obtain accurate impedance measurements during the service life time of rehabilitated structures.

Three different humidity levels and three different temperatures were applied to six reinforced-concrete specimens to study the sensitivity of sensor measurements on these short term environmental conditions. Of the six specimens, three were manufactured with chloride (18.6 lb NaCl per cubic yard of concrete) and three without chloride. Nine

reinforced concrete specimens with chloride were used to study the durability and reliability of installed sensors. Three specimens were subjected to 300 freeze-thaw cycles, three were subjected to 300 wet-dry cycles, and three were subjected to accelerated corrosion conditions to study effects of rebar corrosion.

The size of the concrete specimens and the effective electrode area of installed sensors can also affect impedance measurements. A large reinforced-concrete beam was fabricated and used to study size effects.

2.1 Specimen Preparation and Sensor Configuration

2.1.1 Specimen sizes and preparation

Three different sizes of reinforced concrete beams were manufactured and used in this research. Small reinforced-concrete prismatic beams (6 x 6 x 12 in.) with a #4 reinforcing bar were manufactured to study environmental effects on impedance measurements. Medium reinforced concrete beams (6 x 6 x 24 in.) with a #4 reinforcing bar were fabricated for conducting wedge tests to study the effect of CFRP debonding. Each #4 reinforcing bar was installed near the bottom surface (1.5 in. up from the bottom). A large reinforced concrete beam (1.5 x 2 x 8 ft) was fabricated to study the effect of CFRP debonding and specimen size. Figures 2-1 and 2-2 illustrate the size of the concrete beams and the location of the reinforcing bar.

One large reinforced concrete beam of dimension 8' x 1.5' x 2' was used to study size effects. The concrete beam had four 8-foot long #6 bars, one 8-foot long quarter inch by quarter inches square stainless steel bar, and number 3 stirrups at 10-inch spacing. Reinforcing bars were planned to be used as internal sensing elements. The stainless steel bar was included to eliminate the effect of corrosion which might affect measurements. In

the large beam, reinforcing bars as well as the stainless steel bar were to be used as internal sensing elements. Figure 2-3 shows the size of the large concrete beam and the location of sensors. Figure 2-4 shows the cross section of the large beam.

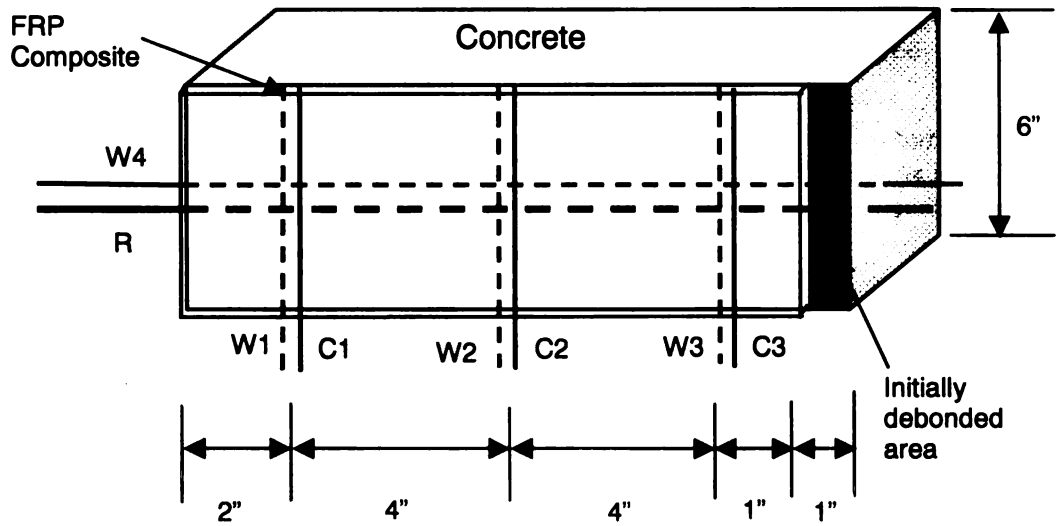

Figure 2-1 Small concrete beam configuration and sensor locations

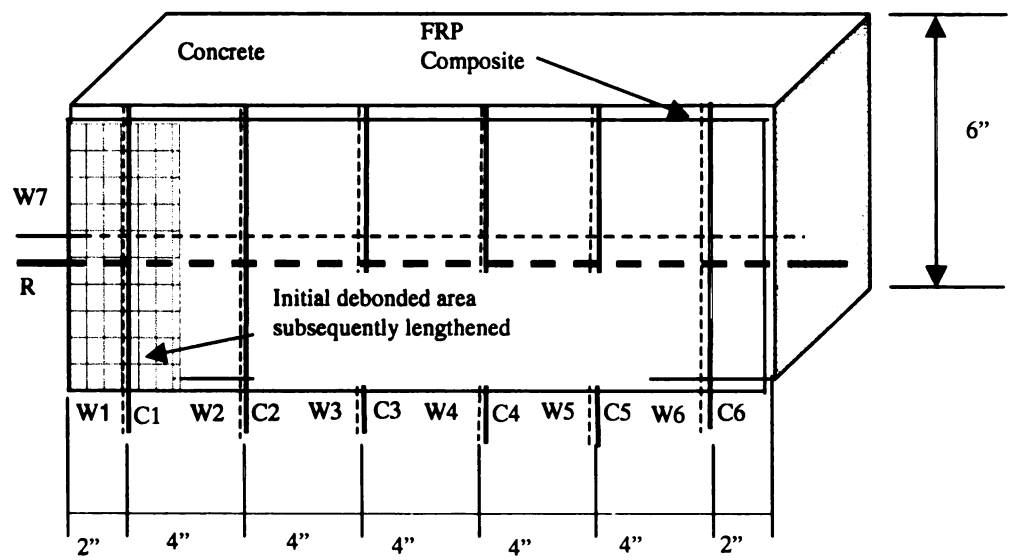

Figure 2-2 Medium concrete beam configuration and sensor locations

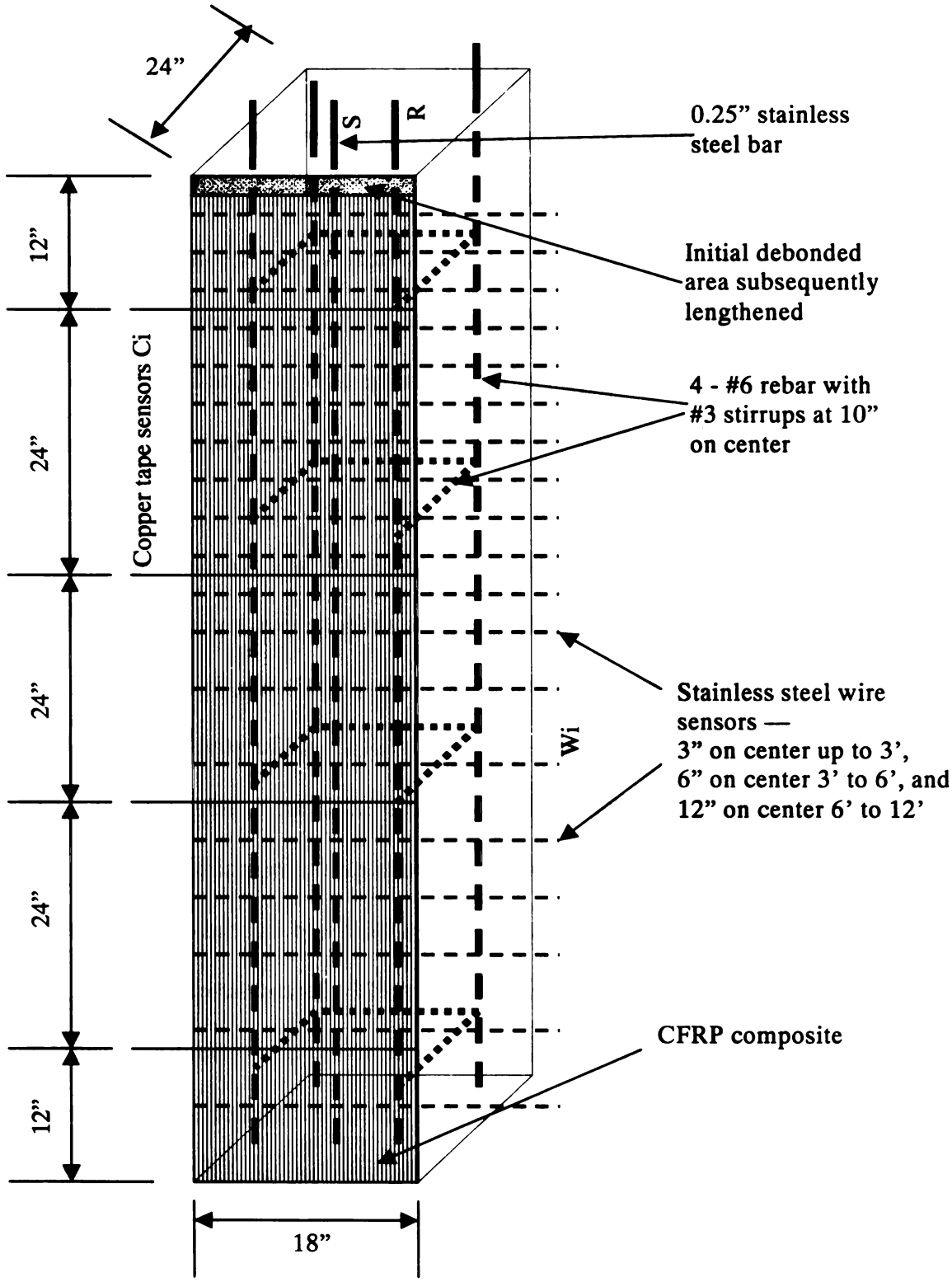

Figure 2-3 Large concrete beam configuration and sensor locations

2.1.2 Sensor configuration and installation

In the modified EIS technique, the impedance of an electrochemical cell is measured between two electrode sensors. Three different sensor elements were used in this research. These were the reinforcing bar, internal sensors and external sensors. Internal sensors (W_i) and external sensors (C_i) were installed after the reinforced concrete specimens were manufactured and grooved (0.25 inch deep) on the bottom surface using a concrete saw. The grooves were made in the longitudinal and transverse directions. Internal sensors consisted of 0.625 mm diameter stainless steel wire installed in the grooves.

External sensors consisted of copper tape with a conductive adhesive backing (Saint-Gobain, C665) placed over stainless steel wire. These were bonded directly to the carbon FRP prior to applying the last epoxy layer to create an embedded sensor because of the excellent conductivity of the CFRP. Initial investigations indicated that external sensors applied to the outside of the CFRP after the final protective epoxy layer was applied were ineffective. The thick protective epoxy layer yields impedances from the rebar to the external sensors that are beyond the range of what can be measured with the Gamry (PC4-300 Potentiostat board/11125) potentiostat. External sensors were installed only in the transverse direction on the outmost surface of the CFRP reinforcement. The carbon fibers are highly conductive in the longitudinal direction. However, because of gaps between adjacent fibers, the conductivity in the lateral direction is generally poor. By bonding the copper tape in the transverse direction across all the fibers in the carbon FRP, good electrical contact can be made with the carbon fibers. The entire FRP then acts as one of the electrodes in the cell. Since the copper tape is on the outside of the FRP, it does not affect the bond between the FRP and the concrete or between different FRP

layers, and will therefore not compromise the strength of the CFRP reinforcement. Figures 2-1, 2-2 and 2-3 show the configuration and direction of the sensors on the concrete beam specimens. Table 2-1 shows the number of sensors and their directions. For the large beam, the entire reinforcement cage (four longitudinal bars and stirrups) acts as an internal sensors and the stainless steel bar was a second internal sensor.

Installation of internal sensors must be done carefully so that the stainless steel wires do not touch the CFRP. A short circuit can be created between the copper tape on one side of the CFRP and the wires on the other side. Even though there may be more than one layer of CFRP used with a thin layer of epoxy between the layers, a short circuit can be created. A heat-shrinking insulator was used around the internal sensors in the transverse direction where they overlapped the internal sensors in the longitudinal directions so that electrical contact between the wire electrodes was avoided. A heat-shrinking insulator was also used on the internal sensors at the edge of the concrete specimens to avoid contact with exposed carbon fiber in the CFRP.

2.1.3 Sensor combinations for impedance measurements

Three different sensor combinations were used to measure the impedance. Combinations of internal sensors (stainless steel wires W_i) to external sensors (copper tapes C_i), rebar to external sensors, and internal sensors to internal sensors were used to measure the raw impedance data.

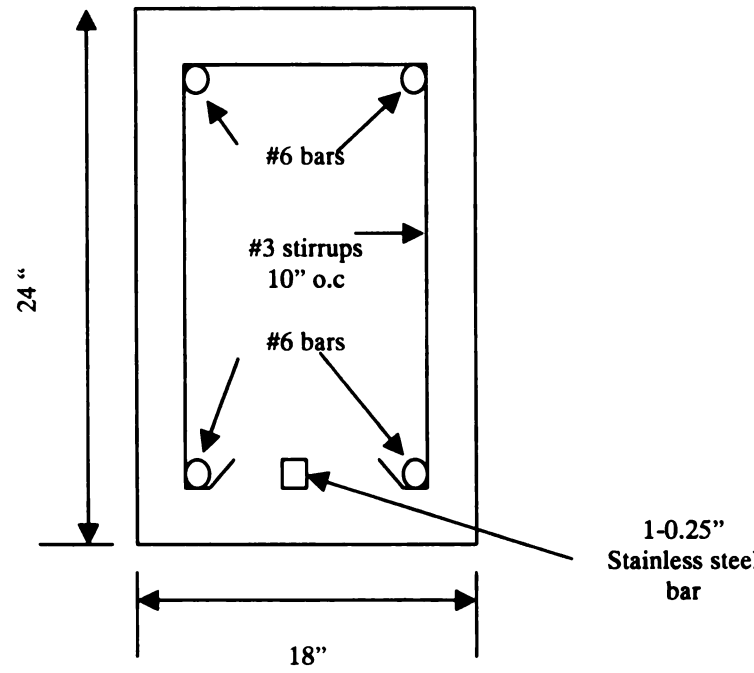

Figure 2-4 Cross-section of large beam

Table 2-1 Number of sensors and their orientation on the specimens

	Small size specimen		Medium size specimen		Large size specimen	
	Transverse	Longitudinal	Transverse	Longitudinal	Transverse	Longitudinal
Internal sensor	3	1	6	1	20	1
External sensor	3	0	6	0	4	0
Rebar	0	1	0	1	0	2

2.2 Detection of FRP Debonding

2.2.1 Two foot long specimens

Six 6"x 6" x 24" reinforced concrete specimens with chloride were prepared to determine whether impedance measurements could be used to detect the debonding of CFRP from concrete. Each specimen was prepared with an initial crack (4" in length) between the CFRP and concrete using a teflon insert. To propagate the interfacial crack between the CFRP sheet and the concrete substrate, a wedge (sharpened saw blade) was driven with a hammer. The crack was propagated by two to four inches each time. Impedance measurements were made at each extended crack states from the internal sensors (stainless steel wire or reinforcing bar) to each of the copper tape sensors.

Investigation of the debonding of CFRP reinforcement from concrete was conducted in two different environmental conditions. One was a controlled environment (in a refrigerator) with a temperature of about 42^0F and a constant relative humidity level of about 35% and the other was an ambient condition in the lab. It was noted during the study on temperature effects that at high temperatures relatively small variations in temperature caused significant variations in the impedance measurements. For this reason, a cold temperature was chosen to reduce the sensitivity of the impedance measurements to temperature fluctuations. Three concrete specimens were used in the controlled environment. The ambient condition represented a temperature of about 70^0F to 75^0F and a relative humidity that varied from 30% to 60%. Three concrete specimens were subjected to the wedge test in the ambient condition.

2.2.2 Large beam specimen

The effective electrode area of installed sensors and the size of the concrete specimen are expected to influence impedance measurements. Electrodes with larger effective surface areas in the electrochemical cell typically decrease the magnitude of impedance. A large reinforced-concrete beam was fabricated with external and internal sensor to study the impact of specimen size. The large specimen was prepared with an initial one-inch long crack by using a teflon insert. To create the interfacial crack between the FRP layer and the concrete substrate, a sharpened metal sheet (wedge) was driven with a hammer. The crack length was increased by two to four inches at each stage until the crack length was about 25% of the length of the entire beam. Impedance measurements were made at each extended crack state from internal sensors (stainless steel wire, stainless steel bar or reinforcing bar) to each of the copper tape sensors and between pairs of internal stainless steel wire sensors. The beam was constructed in the laboratory and after 28 days of curing it was moved outdoors. The beam was exposed to the winter climate from February 21 to April 2, 2003. The original intent was to conduct the wedge test in an outdoor environment when temperatures were in the 35-45^{0}F range. However, because of the unusually warm winter in 2003, temperature fluctuations were large. After obtaining impedance measurements at one crack stage (three-inch long crack) when the beam was outdoors, it was decided that the remainder of the test would be done indoors. The wedge test was therefore conducted in a normal ambient condition at temperatures between 65^{0}F and 75^{0}F and a relative humidity between 30% and 60%.

2.3 Assessment of the Sensitivity of Sensor Measurements to Environmental Effects

2.3.1 Humidity

Moisture in the concrete specimens is the medium for transporting charges between sensors. Since charge is carried in the electrochemical cell (concrete specimen) by the movement of ions, different levels of moisture should affect the capacity for transporting charges. Three different humidity levels were considered in the study to assess the sensitivity of sensor measurements to humidity.

Six small reinforced concrete specimens (6 x 6 x 12 in.) were subjected to relative humidity levels of 30 percent, 60 percent and 90 percent in a controlled environmental chamber, while the temperature was held constant at 72^0F (room temperature). The range of relative humidities from 30 to 90 percent covers a wide range from extremely dry air to highly saturated air.

Each of the six concrete specimens was subjected to the three different relative humidity level, until the weight of the specimens stabilized. Of the six specimens, three were manufactured with chloride (18.6 lb NaCl per cubic yard of concrete) and three without chloride. Impedance measurements were taken after this exposure.

2.3.2 Temperature

Temperature affects the rate of ion transfer in electrolytes and is therefore expected to influence the magnitude of impedance. In order to study temperature effects on the impedance measurements, six small concrete specimens (6 x 6 x 12 in.) were subjected to three different temperatures. The same six specimens used to study humidity effects were reused. The specimens were subjected to extreme cold (temperature of about 0^0F), a

moderate temperature (about 70^0F) and a typical hot summer temperature (about 100^0F). The humidity level was not controlled. For the cold condition, the specimens were kept in a freezer for a week at a temperature of 0^0F and the impedance measurements were taken while specimens were inside the freezer. For the hot summer temperature, the specimens were placed in an oven for a week at a temperature of 100^0F and the impedance measurements were taken while the specimens were inside the oven. For the moderate temperature, specimens were exposed to a room temperature of 70^0F and a relative humidity level of 60 percent.

2.3.3 Chloride content

Chloride ions can exist in concrete structures from the time the concrete is cast due to the use of chemical agents, and the concentration can change with time due to the diffusion of deicing agents through the concrete. The existence of chloride ions in concrete provides additional free ions for transport of charges in EIS and is expected to have an effect on the measurements. An experiment was setup to study the sensitivity of impedance measurements to the presence of chloride ions. The experiment to study chloride effects was conducted simultaneously with the experiment to study humidity and temperature effects. Six small reinforced concrete specimens (6 x 6 x12 in.) were used. Of the six specimens, three were manufactured with chloride (18.6 lb NaCl per cubic yard of concrete) and three without chloride. The specimens were subjected to relative humidity levels of 30 percent, 60 percent and 90 percent at a temperature of 70^0 F in a controlled environmental chamber and the same six reinforced concrete specimens were also subjected to temperatures of 100^0F and 0^0F without any humidity control. Figure 2-5 illustrates how the same specimens were re-used to study the effects of humidity, temperature and chloride content.

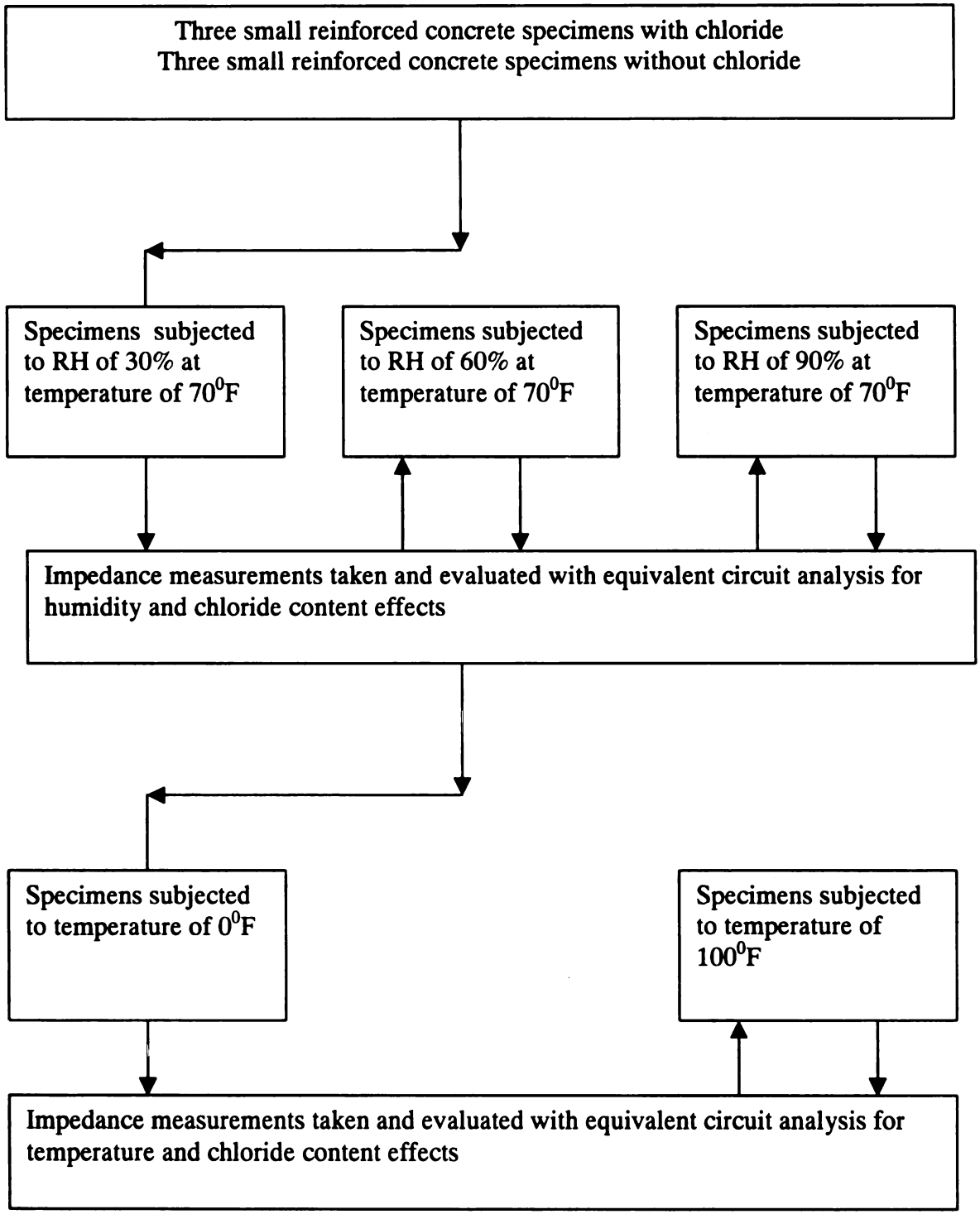

Figure 2-5 Experimental design flow chart for humidity, temperature and chloride content effects

2.3.4 Freeze – thaw

Concrete bridge structures in Michigan undergo freezing and thawing cycles in winter which promotes the growth of microcracks in the concrete. This is likely to change impedance measurements. A freeze-thaw test was setup to study the variability of sensor measurements. This experiment was setup to determine the change in impedance measurements before and after 300 freeze-thaw cycles. Three small concrete specimens (6 x 6 x 12 in.) with chloride (18.6 lb NaCl per cubic yard of concrete) were used to study freeze – thaw effects.

Initially, the concrete specimens were subjected to a temperature of about 70^0F and a humidity level of 60 percent until their weight stabilized. The baseline impedance measurements were then taken before the specimens were subjected to freeze-thaw cycles. The specimens were then subjected to 300 cycles of freeze-thaw. The ASTM C666 Procedure B was used in which each freeze –thaw cycle consisted of a two-hour freezing period and a four-hour thawing period in a freeze-thaw machine. After 300 cycles of freeze-thaw, the specimens were removed from the freeze-thaw machine and placed in an oven to dry out the excessive water absorbed during the freeze-thaw test. Once the specimens reached approximately the same weight as before the freeze-thaw test, they were conditioned at a temperature of about 70^0F and impedance measurements were taken again.

2.3.5 Wetting and drying

Concrete bridge structures experience cycles of wetting and drying on a continuous basis. The expansion and shrinkage resulting from wetting and drying cycles is likely to promote the growth of microcracks and cause impedance measurements to change. A wet-dry experiment was set up to study the changes in impedance measurements after

wet-dry cycles. Baseline impedance measurements were taken on three small concrete specimens (6 x 6 x 12 in.) with chloride at a temperature of about 70^0F and a humidity level of 60 percent. The specimens were then subjected to 300 wet-dry cycles. Each wet-dry cycle consisted of a two hour wet period followed by a ten hour dry period. A 2% NaCl solution was used to wet the specimens in order to increase the concentration of chloride ions. After 300 cycles of wetting and drying, the specimens were placed in an oven at a temperature of about 45^0C to dry out the excessive water absorbed during the experiment. Once the concrete specimens reached approximately the same water content at which the baseline measurement were taken, impedance measurements were retaken.

2.3.6 Corrosion of reinforcing bar

The reinforcing bar in the specimen was used as an internal sensor. The electrical properties of the reinforcing bar and surrounding concrete may change due to corrosion of the reinforcing bar and the presence of corrosion products in the concrete. Cracking of the concrete surrounding the reinforcement due to the volume expansion associated with corrosion also is likely to change impedance measurements. An accelerated corrosion experiment was used to study the effect of corrosion of the reinforcing bar on the impedance measurements.

For the corrosion study, small concrete specimens (6 x 6 x 12 in.) with two reinforcing bars, one near the bottom face and the other near the top face, were used. Baseline impedance measurements were taken at a temperature of 70^0F prior to the accelerated corrosion test. A constant voltage of 12 V was then supplied across the two reinforcing bars using an external power source. A 2 percent sodium chloride solution (by weight) was used to wet the concrete specimens for one hour in each 24 hour period. The moisture in the concrete specimens and the applied current induces corrosion in the

anodic reinforcing bar in an accelerated fashion. The anodic bar was located near the bottom face of the specimens on which the CFRP was bonded. Figure 2-6 shows the accelerated corrosion experimental setup. The three specimens were subjected to accelerated corrosion for three weeks (21 days). The applied current was monitored at an interval of two minutes with a voltage data-logging unit (Omega Engineering Inc., AD128-10T2), since this has a direct correlation with the total corrosion in the reinforcing bar. After 21 days of accelerated corrosion, the specimens were placed in an oven to dry out the excessive water absorbed during the wetting of the specimens. Impedance measurements were taken once the concrete specimens reached approximately the same water content at which the baseline measurement were taken.

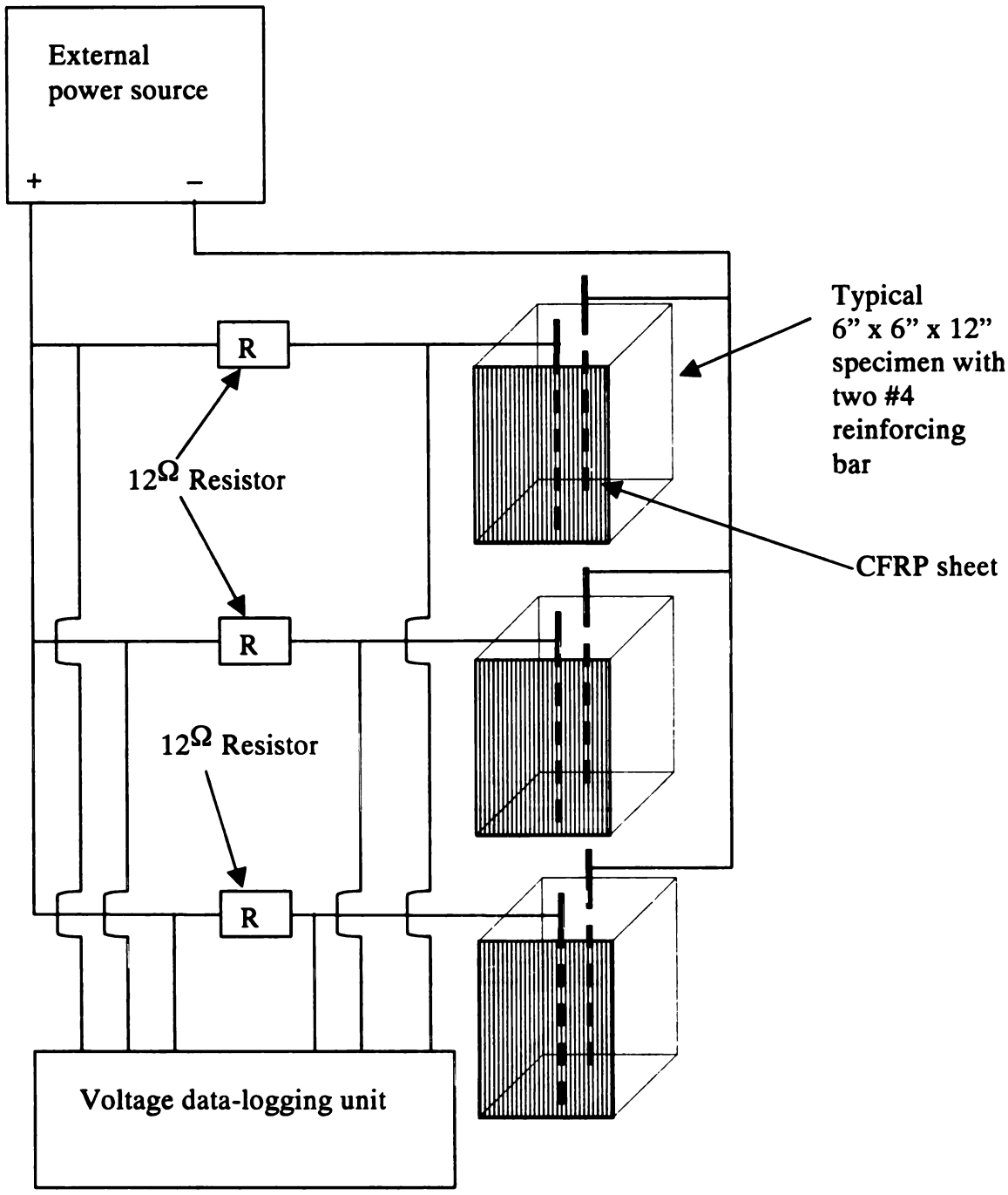

Figure 2-6 Experimental setup for accelerated corrosion

2.4 Electrode size effects

The electrode surface area of the sensors installed in concrete may influence impedance measurements. One reinforced concrete slab of dimension 6" x 2' x 1' was used to study the effect of different electrode sizes. Five steel sensors with diameters of 0.034", 0.25", 0.5", 0.59", and 0.75" were embedded in the slab. Two layers of CFRP sheets were bonded to the face of the slab closest to the embedded sensors. Figure 2-7 shows the concrete slab configuration.

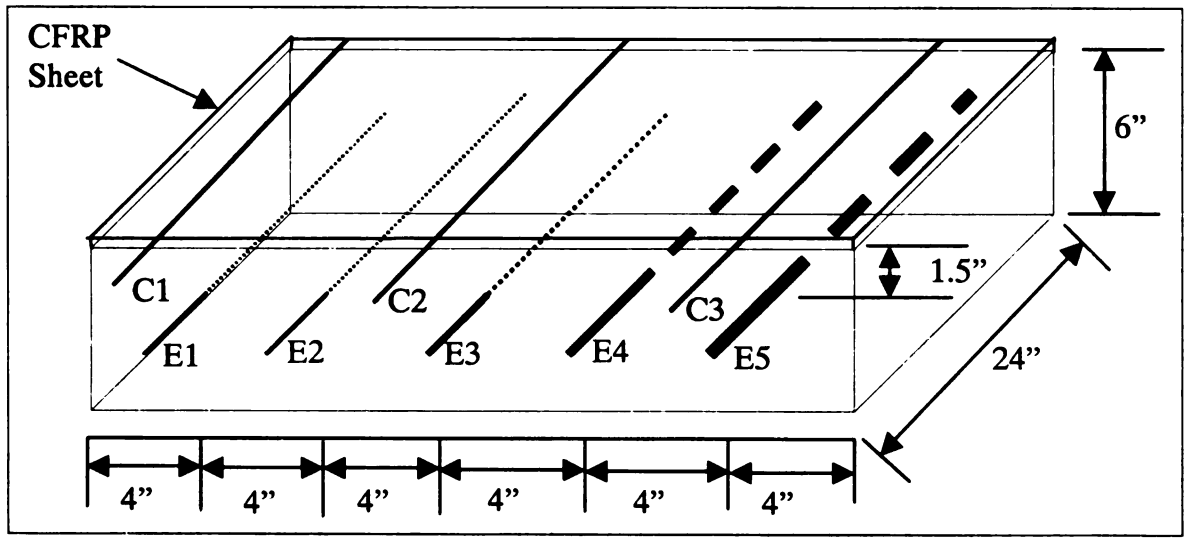

Figure 2-7 Concrete slab configuration and sensor locations

Chapter 3

Experimental Results, Equivalent Circuit Analysis, and Discussion

Three different sensor electrode combinations were used to measure the impedance. Combinations of internal sensors (stainless steel wires W_i) to external sensors (copper tapes C_i), rebar to external sensors and internal sensors to internal sensors were used to produce the impedance spectra. The interfacial debonding effects are best observed with the combinations of rebar to external sensors and internal sensors to internal sensors. These measurements and their interpretation are discussed in this chapter.

3.1 Equivalent circuit

Impedance spectra were measured between an internal and external sensor, the rebar and external sensor, and two internal sensors. Once the raw impedance data is obtained, then equivalent circuit analysis is performed by fitting the data to obtain the circuit element parameters. Finding an equivalent circuit approximate for the measured EIS spectra can be a challenge since each equivalent circuit has its own unique characteristics and impedance spectra. An equivalent circuit is composed of common electrical components such as resistors and capacitors. Sometimes, specialized elements such as a constant phase element are added to the equivalent circuit to describe the special characteristics of the electrochemical cell.

Different equivalent circuits were tried to obtain good fits to the measured impedance spectra. The circuit shown in Figure 1-2 (b) which was used by Davis et al. (1999) for studying composite/composite bonds was one of the first circuit tried. This

circuit fits spectra measured between the rebar and an external sensor reasonably well. However, it did not produce a good fit in the low-frequency range for impedance measurements between an internal and external sensor or between two internal sensors. A new equivalent circuit was developed to provide a better fit of the measured impedance spectra over the entire frequency range for all sensor combinations. Figure 3-1 shows the equivalent circuit configuration used in this research. Figure 3-2 shows the measured spectra between the rebar and an external sensor and the fit by the two circuits shown in Figures 1-2(b) and 3-1 on the Bode magnitude and phase angle plot. Figure 3-3 shows the impedance measured between two internal sensors and the fit obtained using the two equivalent circuits on the Bode magnitude and phase angle plots (Figure 3-3 (a)) and the Nyquist plot (Figure 3-3 (b)). It can be seen from the figures that the new circuit in Figure 3-1 yields very good fits for all measured spectra even though it is more complex than the one used by Davis (Figure 1-2(b)). The new circuit has eight independent parameters (one for each resistor and capacitor, and two for the CPE), and was used to analyze all the measurements obtained in this work.

In the equivalent circuit analysis, the R1, C1 and CPE parameters control the impedance in the low-frequency region (0.1 to 10 Hz) and characterize the diffusion process in the electrolyte (pore fluid in the concrete). The C2, C3, R2 and R3 parameters control the impedance in the mid- (10 to 1000 Hz) and high-frequency (1000 to 100,000 Hz) regions and characterize the charge transfer processes at the two electrode/electrolyte interfaces (see Figure 1-2). The impedance of the equivalent circuit in Figure 3-1 can be expressed analytically using Equations 1-7 and 1-8. The first loop has the equivalent impedance

$$Z_1 = \frac{PY + SQ}{P^2 + Q^2} - j\frac{SP + YQ}{P^2 + Q^2} \tag{3-1}$$

where

$$P = A * C1 * \omega^{1-\alpha} * \sin(\frac{\alpha\pi}{2}) + 1$$

$$Y = R1 + A * \omega^{-\alpha} * \cos(\frac{\alpha\pi}{2})$$

$$Q = C1 * R1 * \omega + A * C1 * \omega^{1-\alpha} * \cos(\frac{\alpha\pi}{2})$$

$$S = A * \omega^{-\alpha} * \sin(\frac{\alpha\pi}{2})$$

The second and third loops have the equivalent impedances

$$Z_2 = \frac{R2}{1 + \omega^2 * C2^2 * R2^2} - j\frac{\omega * C2 * R2^2}{1 + \omega^2 * C2^2 * R2^2} \tag{3-2}$$

$$Z_3 = \frac{R3}{1 + \omega^2 * C3^2 * R3^2} - j\frac{\omega * C3 * R3^2}{1 + \omega^2 * C3^2 * R3^2} \tag{3-3}$$

The impedance of the entire circuit is therefore

$$Z_{eq} = Z_1 + Z_2 + Z_3 \tag{3-4}$$

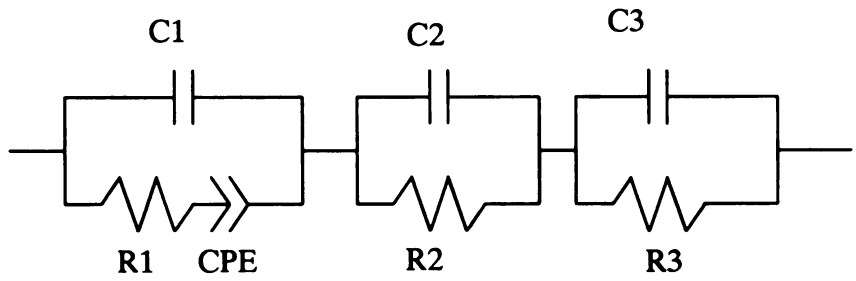

Figure 3-1 Equivalent circuit used to study CFRP debonding

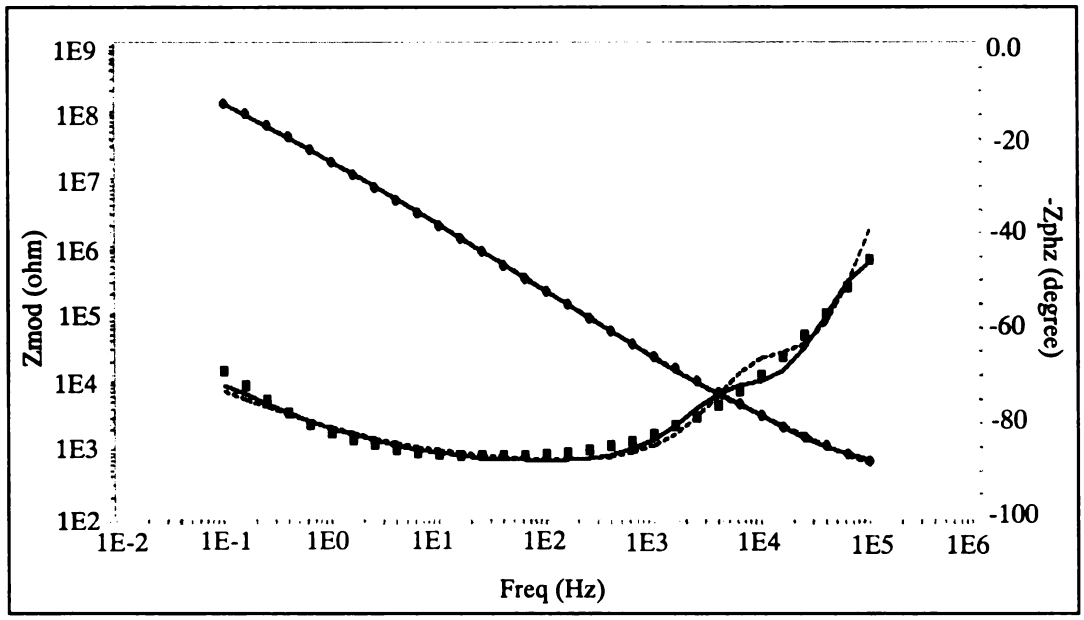

Figure 3-2 Fitted Bode magnitude and phase angle plots using the two equivalent circuits. Dots are the actual measured impedance from the rebar to an external sensor. Solid lines are the theoretical impedance using the equivalent circuit in Figure 3-1. The dotted lines are the theoretical impedance using the equivalent circuit in Figure 1-2 (b).

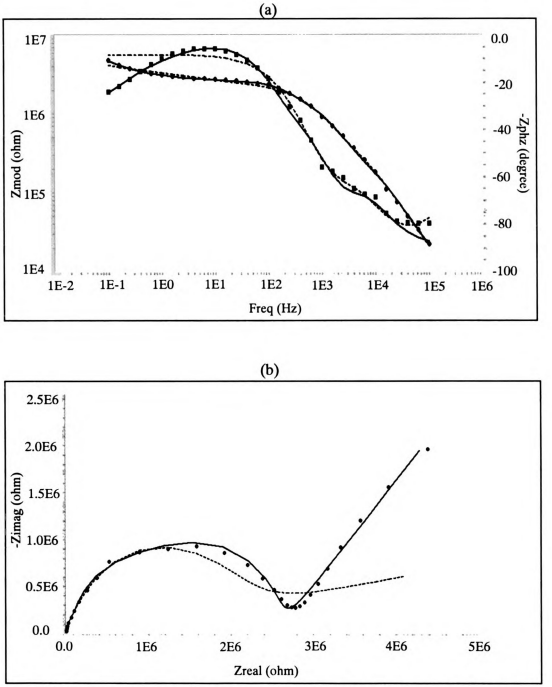

Figure 3-3 Fitting with the equivalent circuits. Dots are the actual measured impedances between two internal sensors. Solid lines are the theoretical impedances using the equivalent circuit in Figure 3-1. The dotted lines are the theoretical impedances using the equivalent circuit in Figure 1-2 (b). — (a) Bode magnitude and phase angle plot; (b) Nyquist plot.

3.2 CFRP Debonding

3.2.1 Results for 2-foot long specimens

Based on measurements from numerous pairs of sensors, it was found that measurements from the rebar to external sensors had the strongest promise for revealing a relationship between impedance measurements and the debonded area of CFRP. Figures 3-4 and 3-5 show the effect of CFRP debonding on the magnitude of the measured impedance in the controlled environment (in the refrigerator), and in the uncontrolled environment (ambient condition), respectively. These figures show that the measured impedance increases over all frequencies due to debonding of the CFRP. The effects of CFRP debonding on the measured impedance in the controlled environment also can be seen with the Nyquist plot in Figure 3-6. The radius of the arc in the Nyquist plot increases as the crack length increases. Figure 3-7 is an enlargement of Figure 3-5 in the low- to mid-frequency range and shows the interference of humidity and debonding effects on the measured impedance. The ambient relative humidity fluctuated from 30% to 60% when the crack lengths increased from 6 in. to 10 in. This increase in relative humidity caused the impedance magnitude at low frequencies to decrease even though the interfacial crack length increased. However, the increase in humidity did not cause a reversal in the measured impedance at mid- and high- frequencies. The interference of humidity and debonding effects on the measured impedance can be seen more clearly on the Nyquist plot shown in Figure 3-8. The radii of the arc in the Nyquist plot decreased significantly when the crack lengths were at 8 and 10 inches.

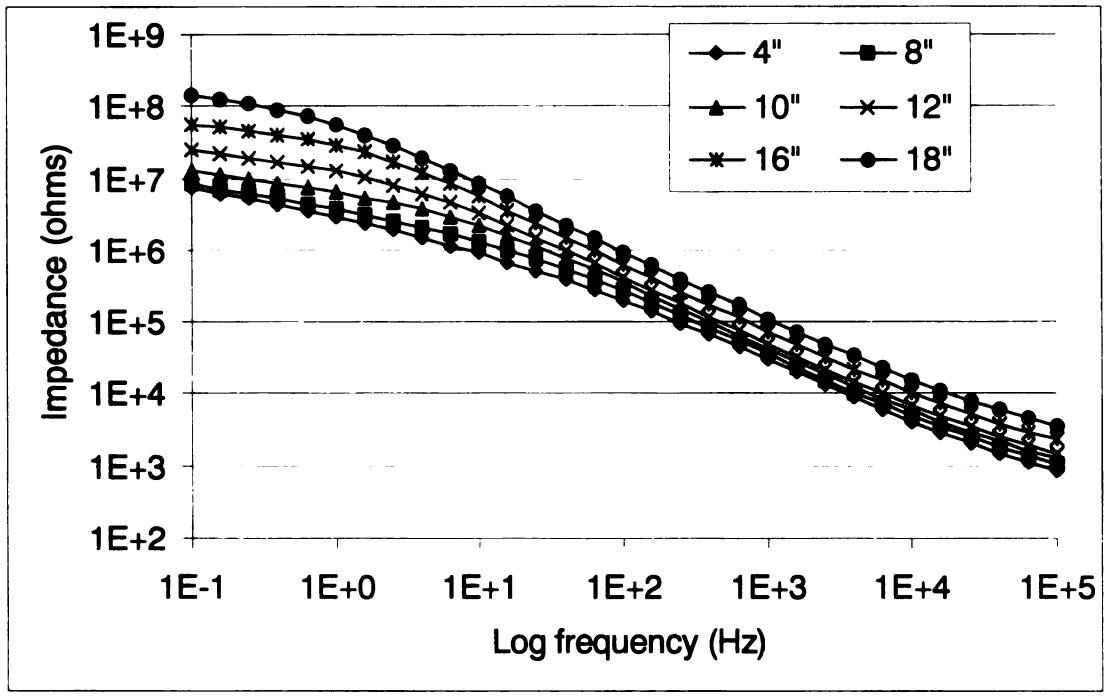

Figure 3-4 Bode magnitude plot of typical impedance spectra measured from the rebar to copper tape for wedge test in controlled environment (legend gives the crack length in inches)

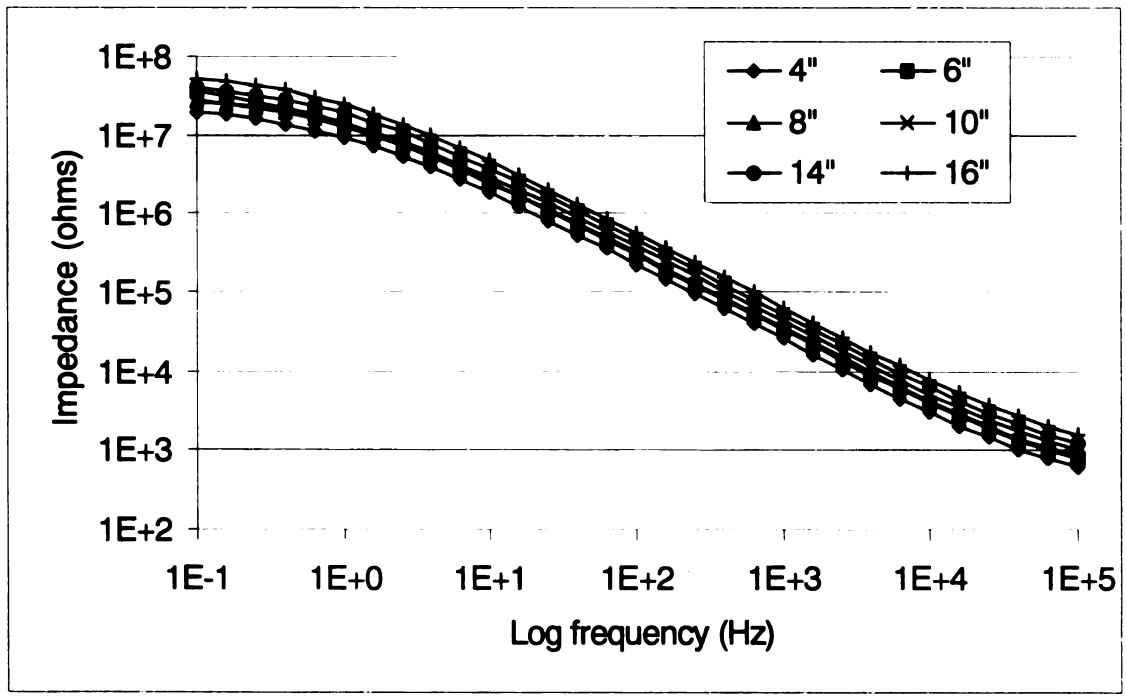

Figure 3-5 Bode magnitude plot of typical impedance spectra measured from the rebar to copper tape for wedge test in ambient environment (legend gives the crack length in inches)

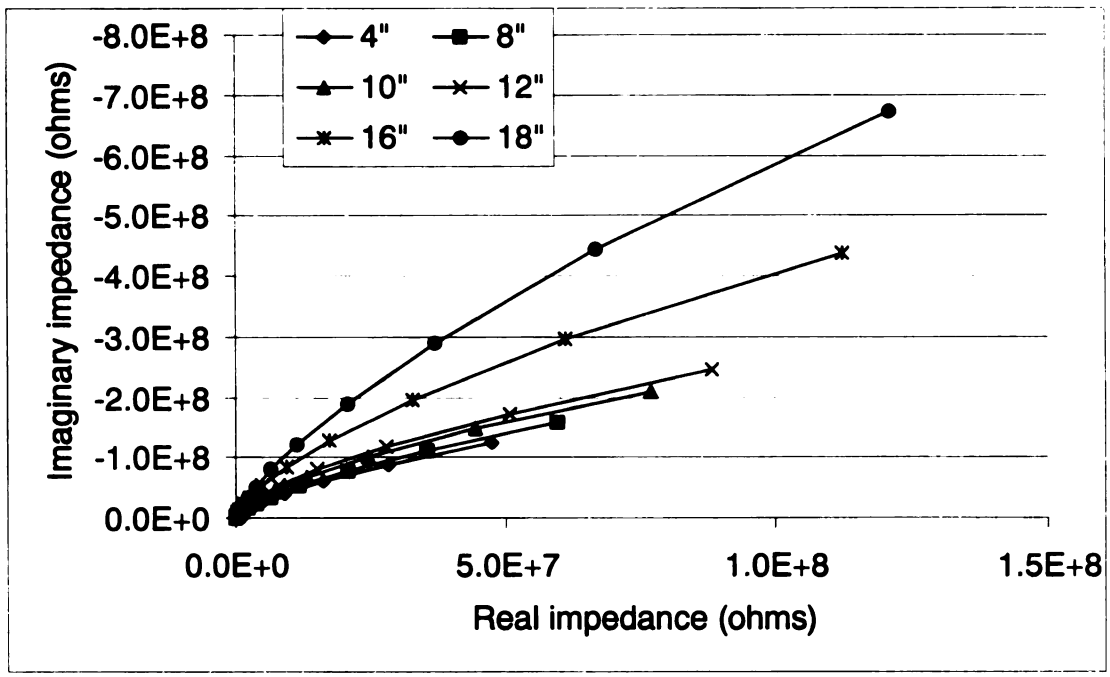

Figure 3-6 Nyquist plot of typical impedance spectra measured from the rebar to copper tape for wedge test in controlled environment (legend gives the crack length in inches)

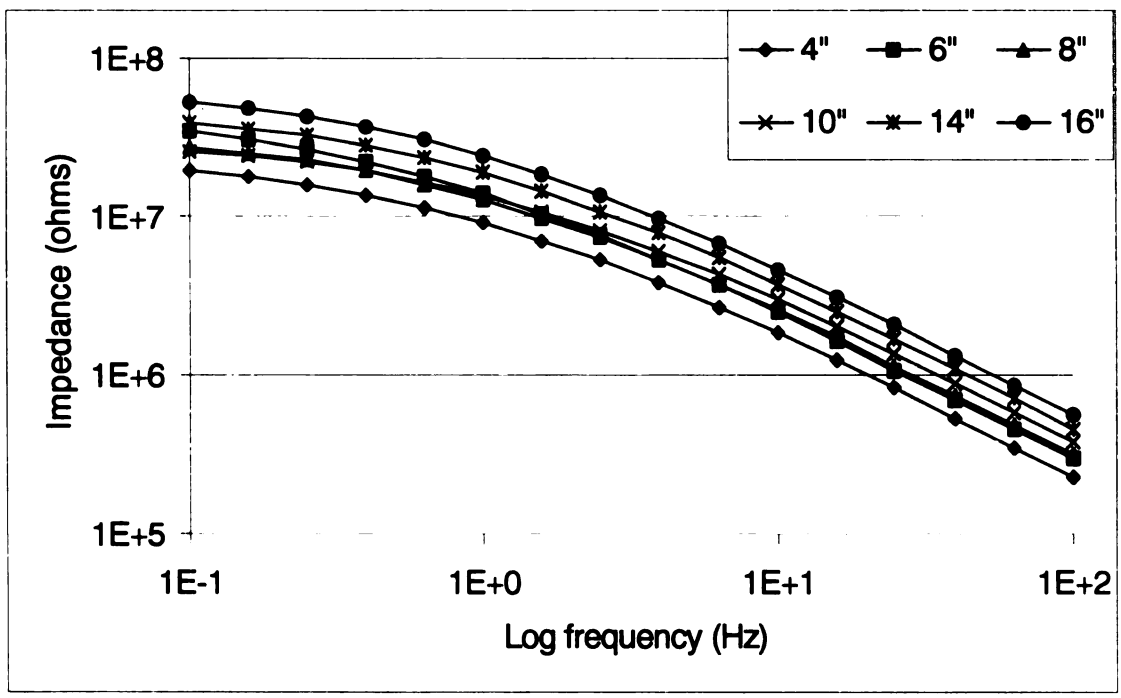

Figure 3-7 Enlargement of Figure 3-6, showing variation of measure impedance in the low to mid- frequency range (legend gives the crack length in inches)

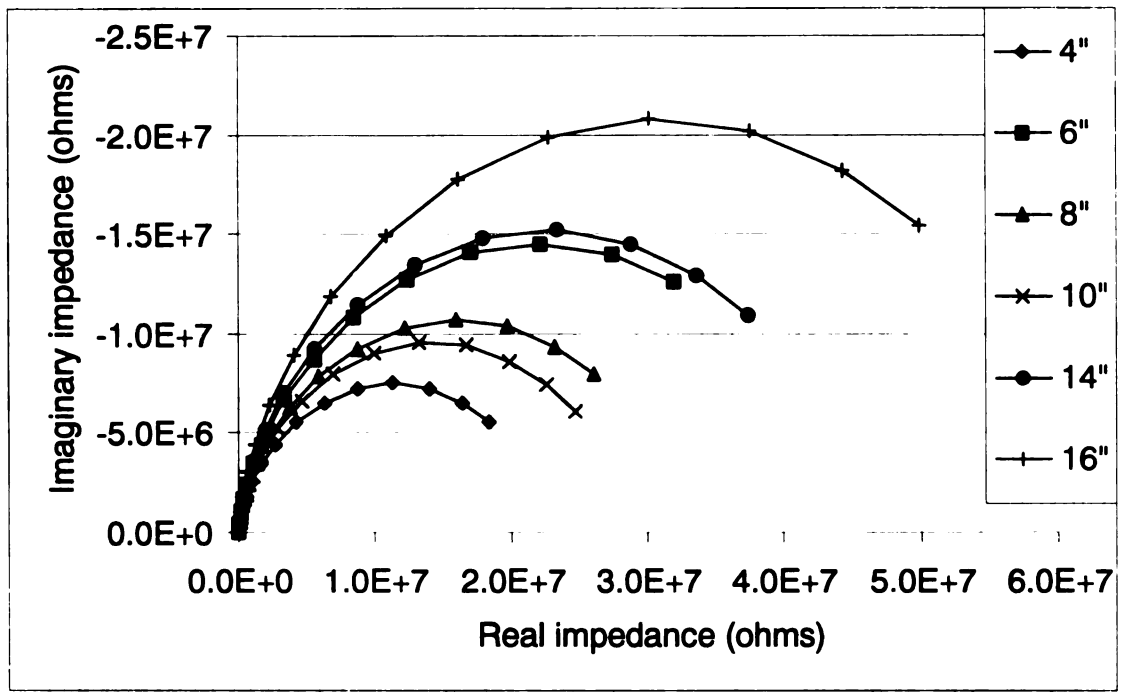

Figure 3-8 Nyquist plot of impedance spectra measured from the rebar to copper tape for wedge test in ambient environment (legend gives the crack length in inches)

3.2.1.1 Comparison of raw impedance spectra

Figures 3-9 to 3-11 show the variation of the measured impedance at 10,000 Hz, 100 Hz and 1 Hz as a function of the interfacial crack length. These frequencies are arbitrary representative of high, medium and low frequencies. The impedance magnitude vs. crack length curves are close together at 10,000 Hz, and spread further and further apart at 100 Hz and 1 Hz. The specimen-to-specimen variation in the measurements is therefore the least at high frequencies. In general, the measured impedance at a specific frequency increases exponentially as the crack length increases.

3.2.1.2 Results from equivalent circuit analysis

The variation of the CPE parameter with crack length is shown in Figures 3-12 and 3-13. Although the CPE parameter exhibits good correlation with the interfacial crack length it has high specimen-to-specimen variation and is also sensitive to temperature and humidity. The variations of the capacitance parameters with interfacial crack length are shown in Figures 3-14 to 3-16. The capacitance parameters exhibit a linear relation with the crack length and except for specimen 3, the C2+C3 and C1+C2+C3 values for the other four specimens are quite similar.

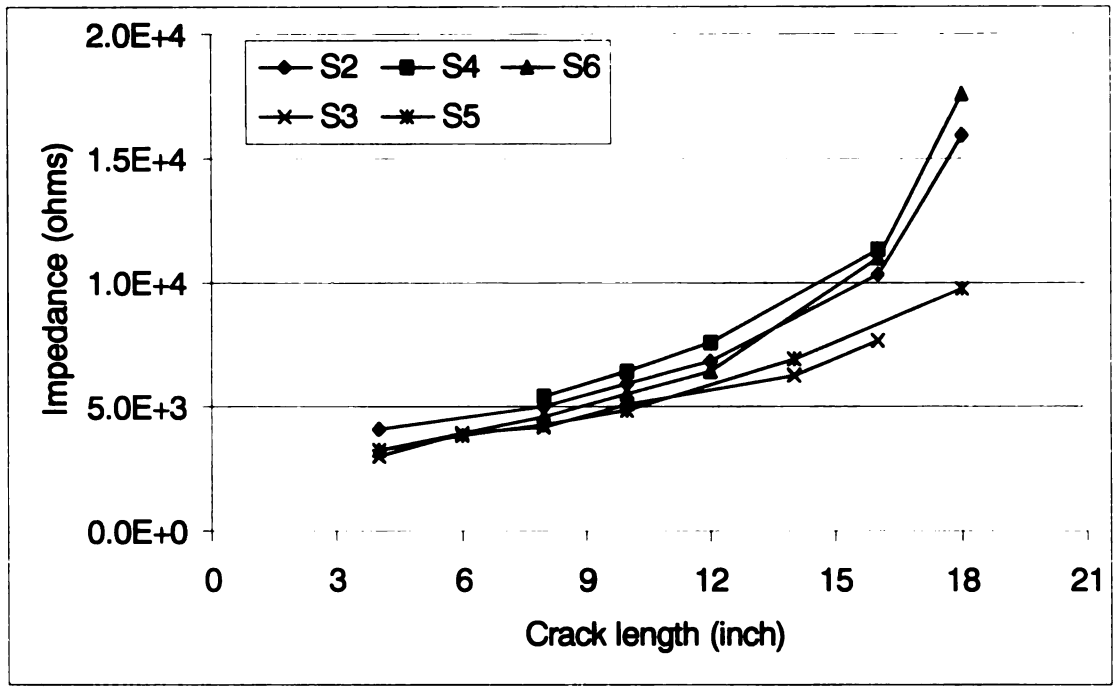

Figure 3-9 Variation of typical measured impedance from the rebar to copper tape for wedge test at 10,000 Hz

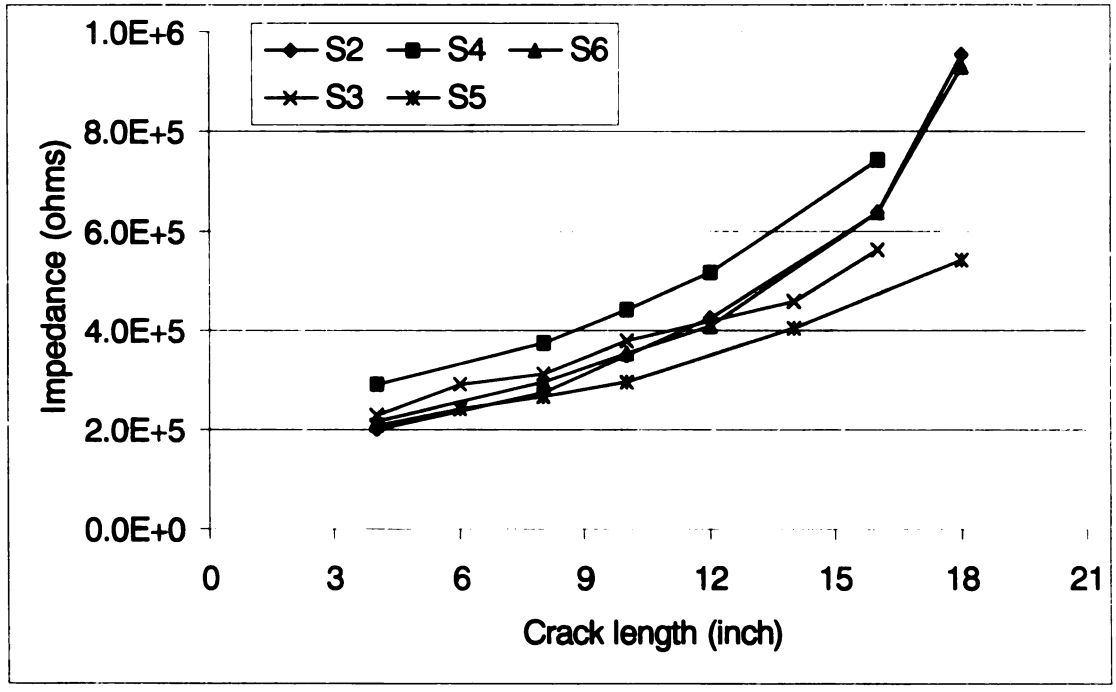

Figure 3-10 Variation of typical measured impedance from the rebar to copper tape for wedge test at 100 Hz

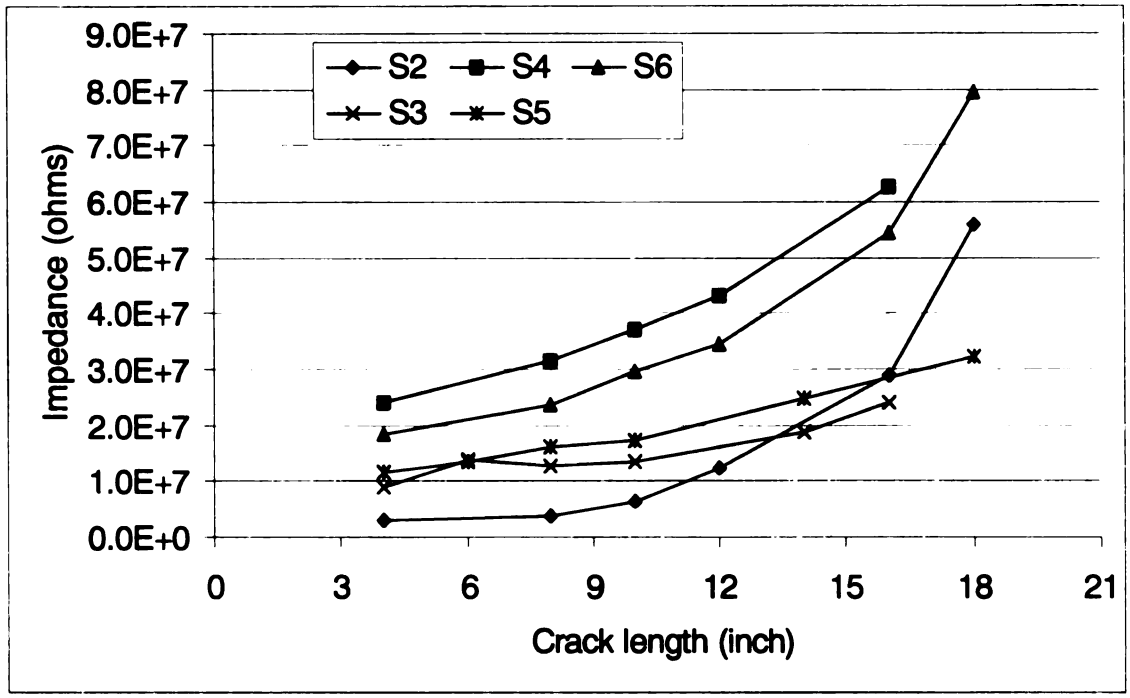

Figure 3-11 Variation of typical measured impedance from the rebar to copper tape for wedge test at 1 Hz

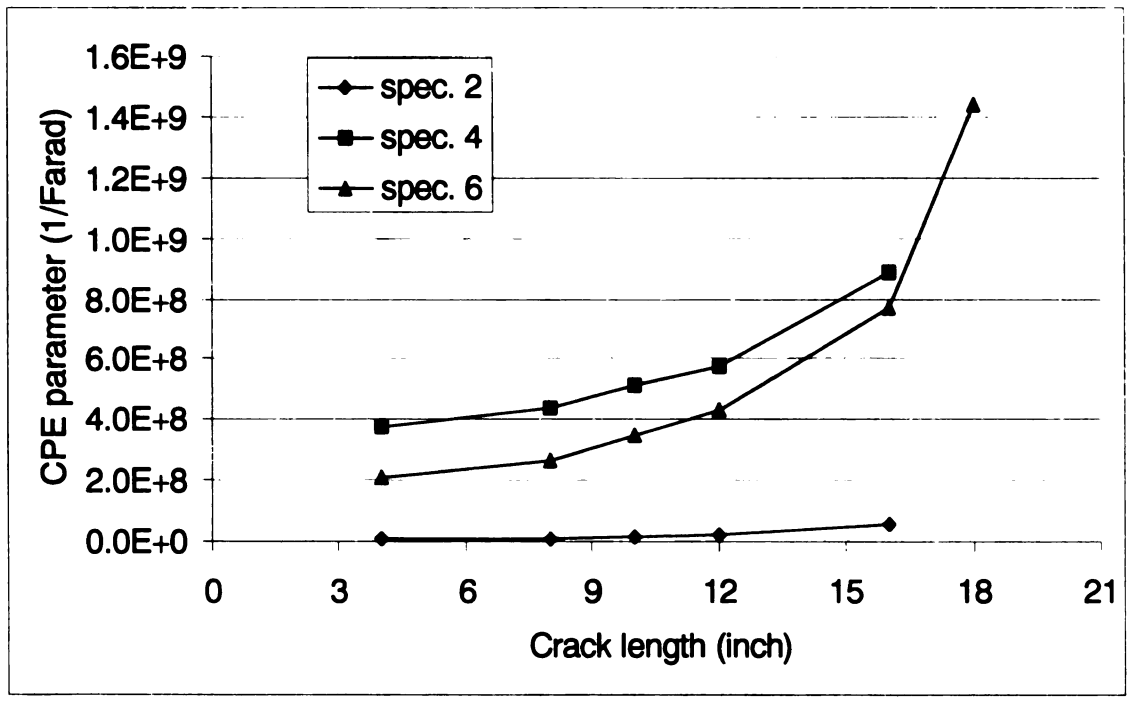

Figure 3-12 Variation of the CPE parameter for wedge test in the controlled environment for measurements from the rebar to external sensors

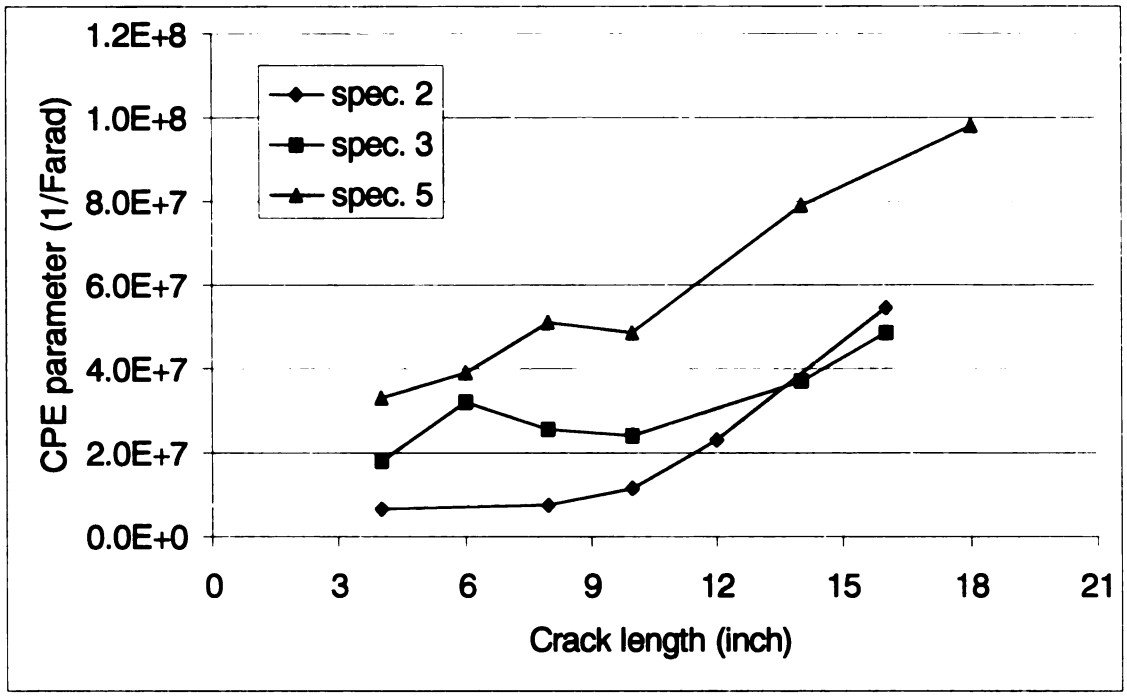

Figure 3-13 Variation of the CPE parameter for wedge test in ambient condition for measurements from the rebar to external sensors (Note: the CPE parameter for spec. 2 is measured in controlled environment)

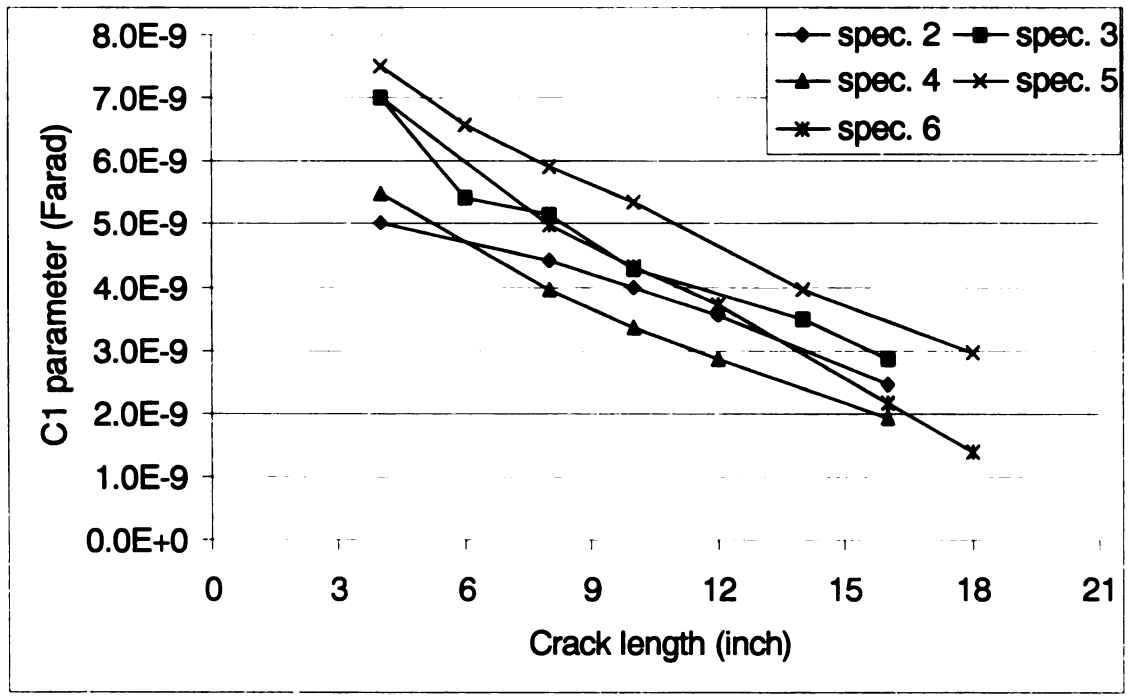

Figure 3-14 Variation of the C1 parameter from equivalent circuit analysis for wedge test from the rebar to external sensors

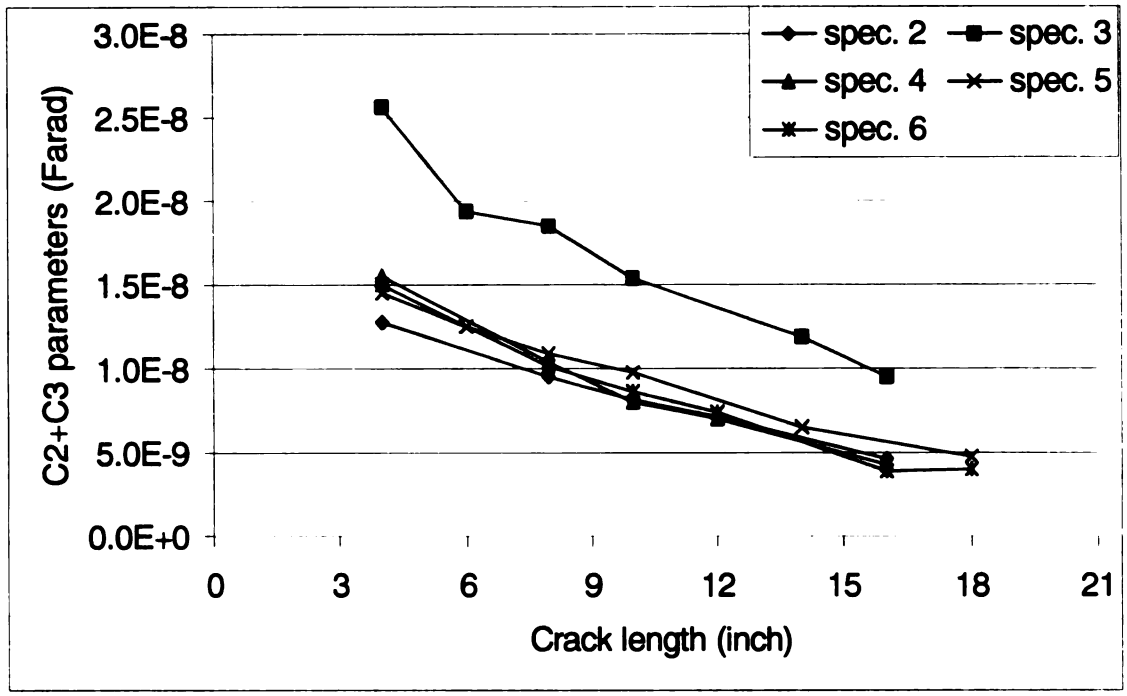

Figure 3-15 Variation of the C2+C3 parameter from equivalent circuit analysis for wedge test from the rebar to external sensors

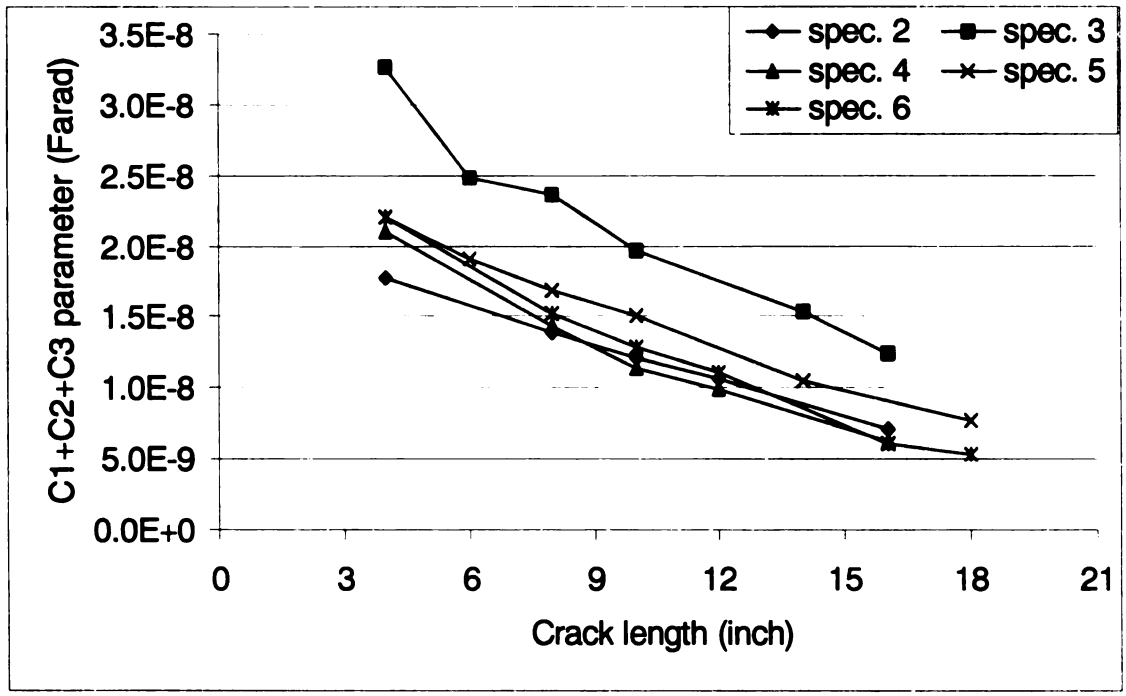

Figure 3-16 Variation of the C1+C2+C3 parameter from equivalent circuit analysis for wedge test from the rebar to external sensors

3.2.2 Results for 8-foot long specimen

The large concrete beam was studied in an ambient condition. Temperature fluctuated from about 65^0F to 75^0F and the relative humidity fluctuated from about 30% to 60%.

3.2.2.1 Comparison of raw impedance spectra

Figures 3-17 and 3-18 show typical measured impedance spectra for the large beam as a function of the debonded length of the CFRP reinforcement. The measured impedances for the large beam are about on order of magnitude lower than those for the two-foot long beams. This is believed to be due to the larger sensor surface areas in the beam (reinforcement cage and CFRP sheet). Figure 3-18 is an enlargement of Figure 3-17 in the low-frequency range and Figure 3-19 is the Nyquist plot over the entire frequency range. The study of the effect of CFRP debonding on the two-foot long specimens indicated that the radius of the arc in the Nyquist plot increases as the crack length increases. In Figure 3-19, however, the radius of the arc in the Nyquist plot decreases as the crack length increases. Figures 3-18 and 3-19 suggest that humidity and temperature variations interfere with the effect of CFRP debonding in the low-frequency range, and the impedance magnitude appears to decrease as the debonded length of the CFRP increases.

The large beam was initially placed outdoors from February to March 2003 and then moved indoors. It is very likely that the concrete dried out when it was outdoors at very cold temperatures. After it was moved indoors the concrete would begin absorbing moisture. Because of its large size, the beam is likely to have absorbed moisture gradually over a long period of time. The increased moisture would explain the reduction in impedance at low frequencies.

Figure 3-20 is an enlargement of Figure 3-17 in the high-frequency range. In the high frequency range the magnitude of the impedance increases with the debonded length of the CFRP although humidity and temperature fluctuated. Figure 3-21 shows typical measured impedance spectra from the rebar and the stainless steel bar to copper tape sensor. The measured impedance spectra from the stainless steel bar were very similar to the measurements from the rebar. Figure 3-22 shows the measured impedance at 100,000 Hz. At this frequency the impedance magnitude shows a linear relation with the debonded length of CFRP.

3.2.2.2 Results from equivalent circuit analysis

Figures 3-23 and 3-24 show the variation of the parameters from the equivalent circuit analysis due to CFRP debonding. The CPE parameter decreased as the crack was propagated. This is a direct result of the low–frequency behavior of the impedance (Figure 3-19) and is opposite to what is expected. The C1 parameter was almost constant during the CFRP debonding test. It is speculated that the effect of CFRP debonding on the C1 parameter was compensated by variations in humidity and temperature. The C2+C3 parameter and the C1+C2+C3 parameters decreased significantly during the initial debonding of the CFRP.

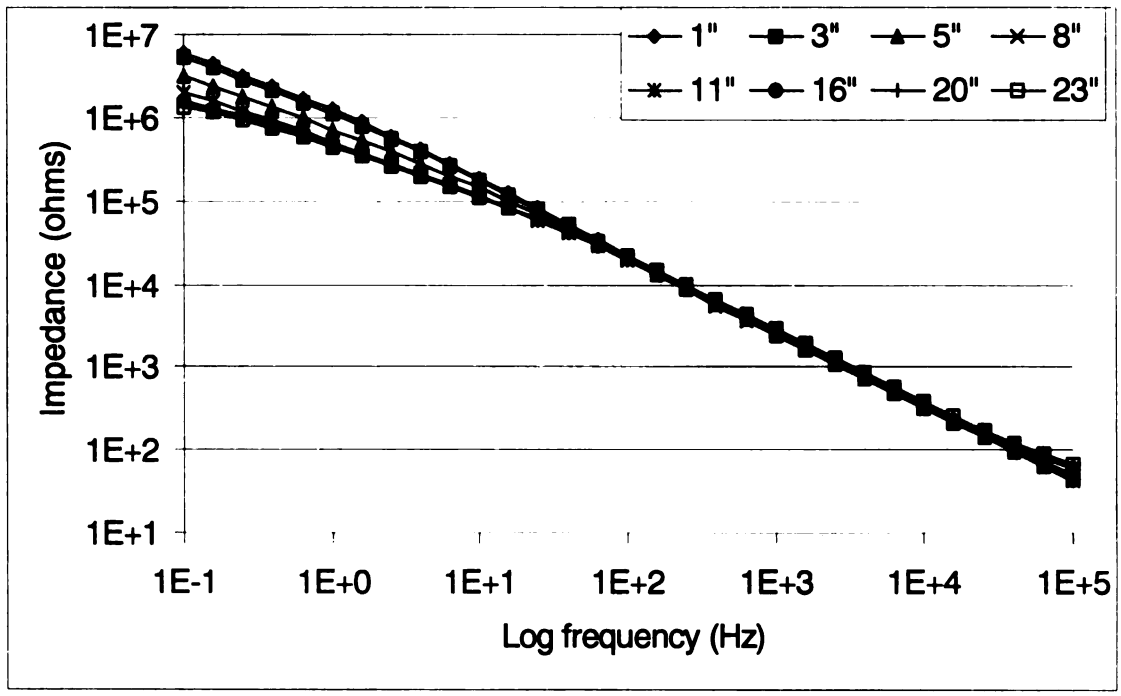

Figure 3-17 Bode magnitude plot of typical impedance spectra measured from the rebar to copper tape for wedge test of the large beam (legend gives the crack length in inches)

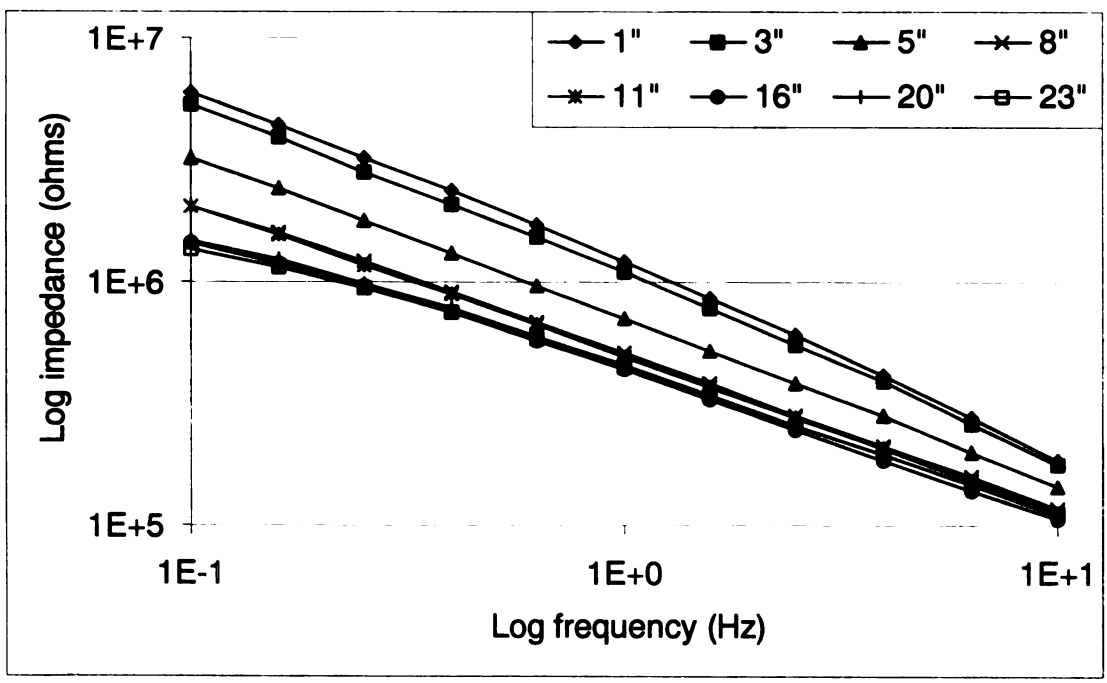

Figure 3-18 Enlargement of Figure 3-17, showing variation of measure impedance in the low-frequency range (legend gives the crack length in inches)

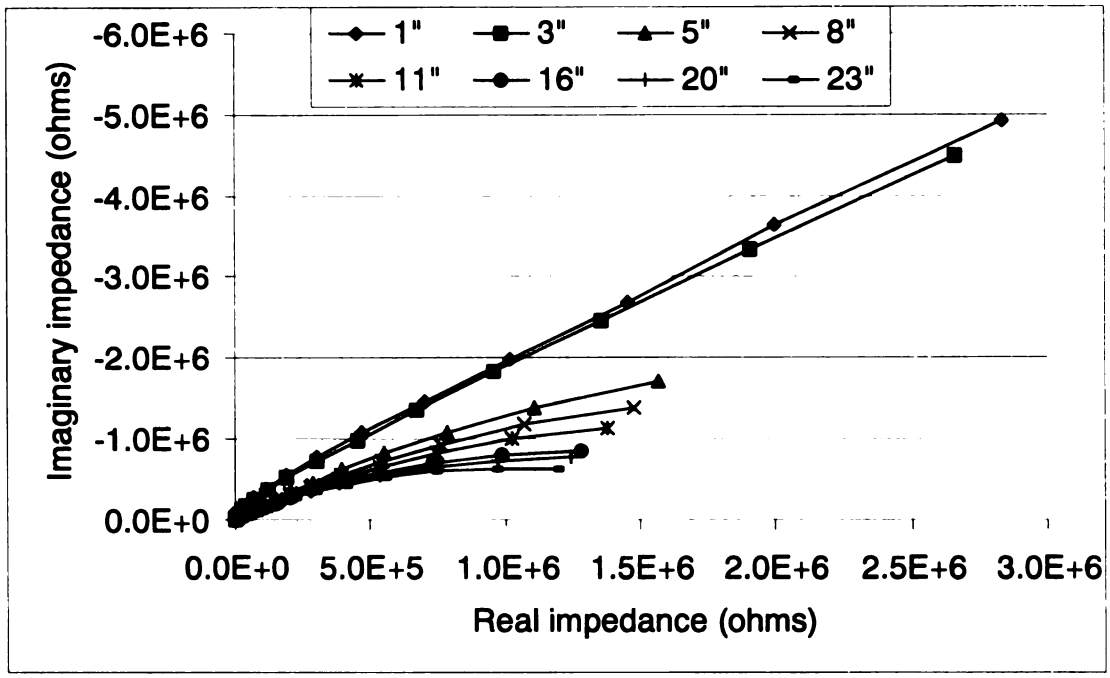

Figure 3-19 Nyquist plot of impedance spectra measured from the rebar to copper tape for wedge test of large beam in ambient environment (legend gives the crack length in inches)

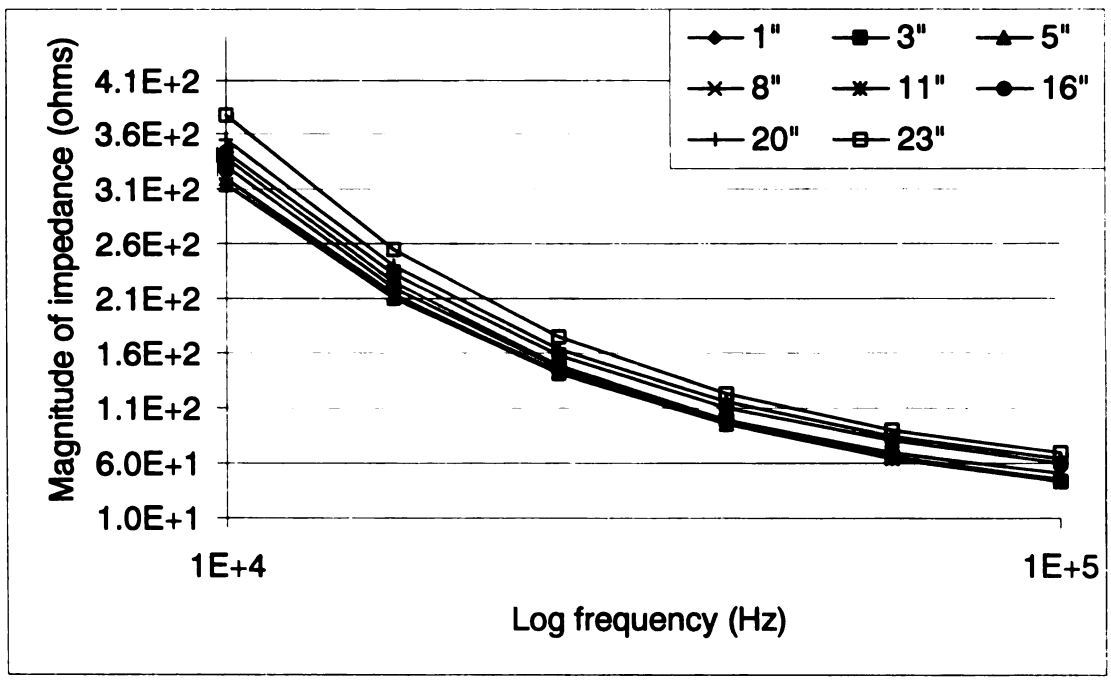

Figure 3-20 Enlargement of Figure 3-17 showing variation of measured impedance in the high-frequency range (legend gives the crack length in inches)

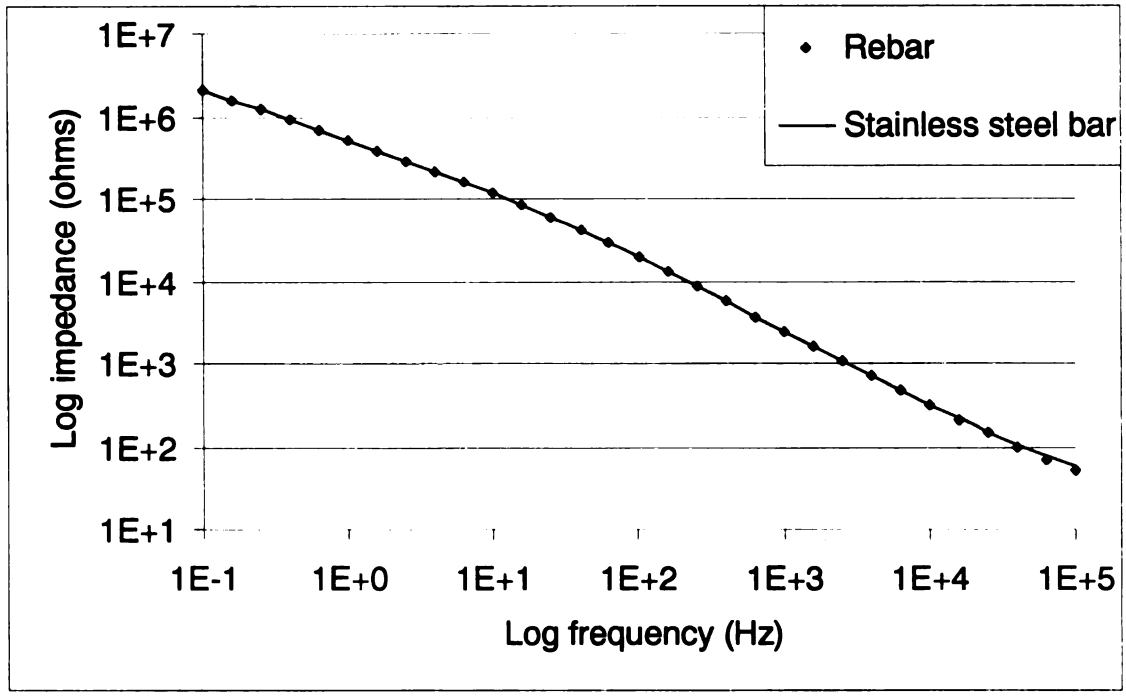

Figure 3-21 Bode magnitude plot of typical impedance spectra measured from the rebar to copper tape and the stainless steel bar to copper tape for wedge test of the large beam (legend gives the crack length in inches)

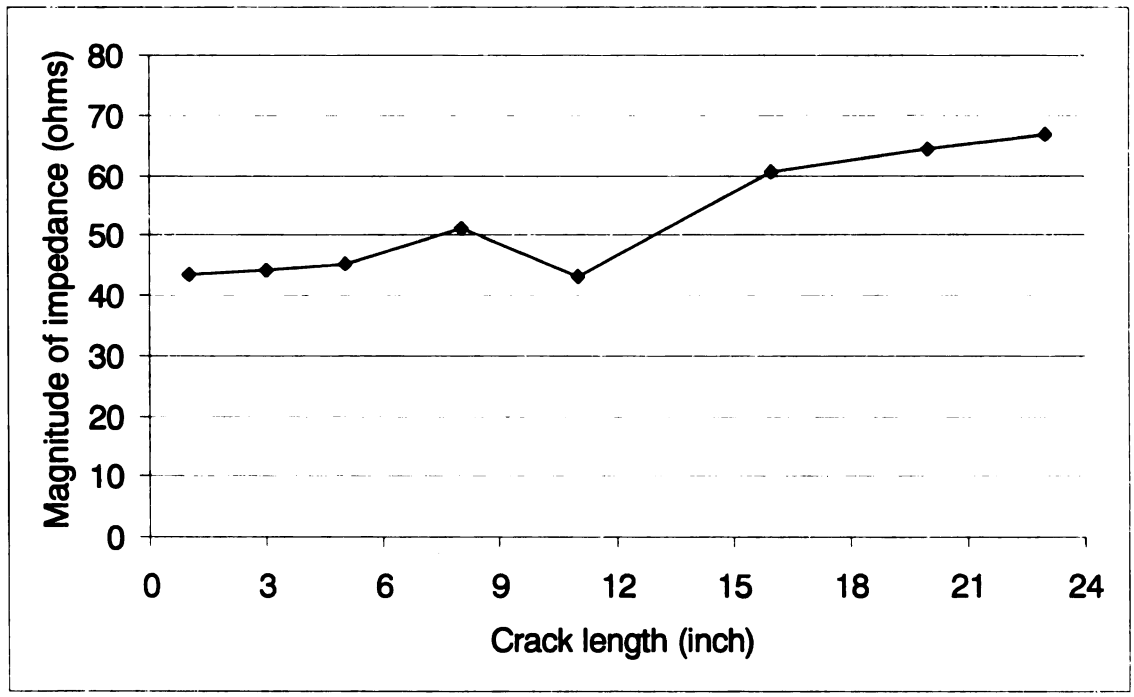

Figure 3-22 Variation of typical measured impedance from the rebar to copper tape for wedge test at 100,000 Hz

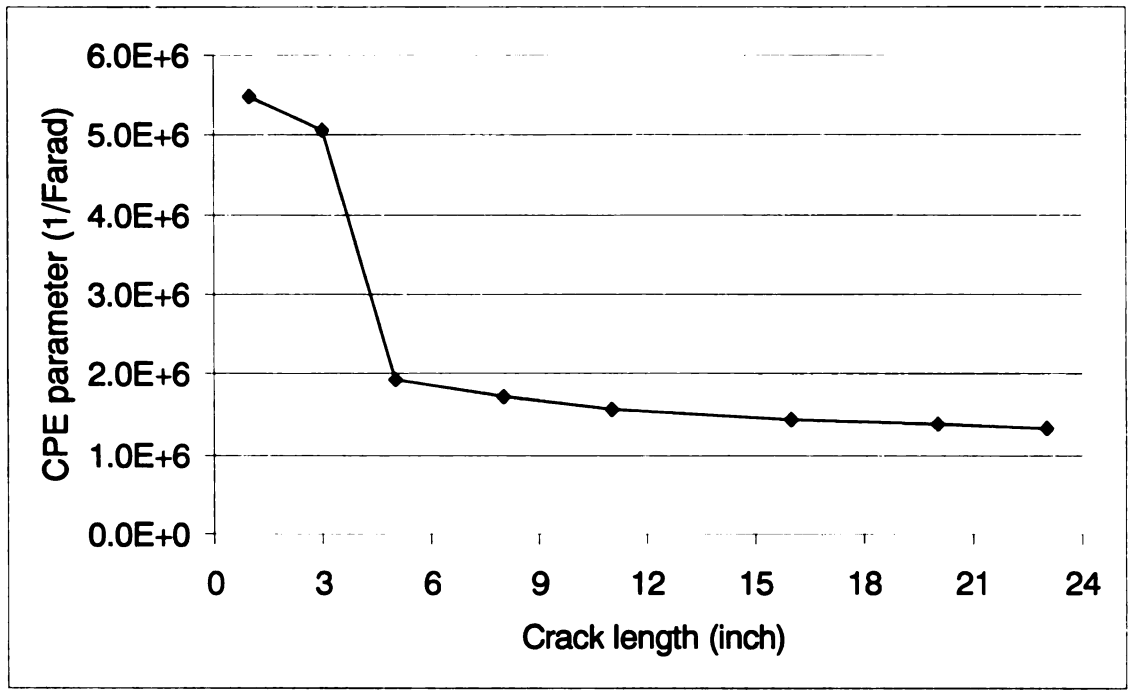

Figure 3-23 Variation of the CPE parameter from equivalent circuit analysis for the large specimen from the rebar to external sensor

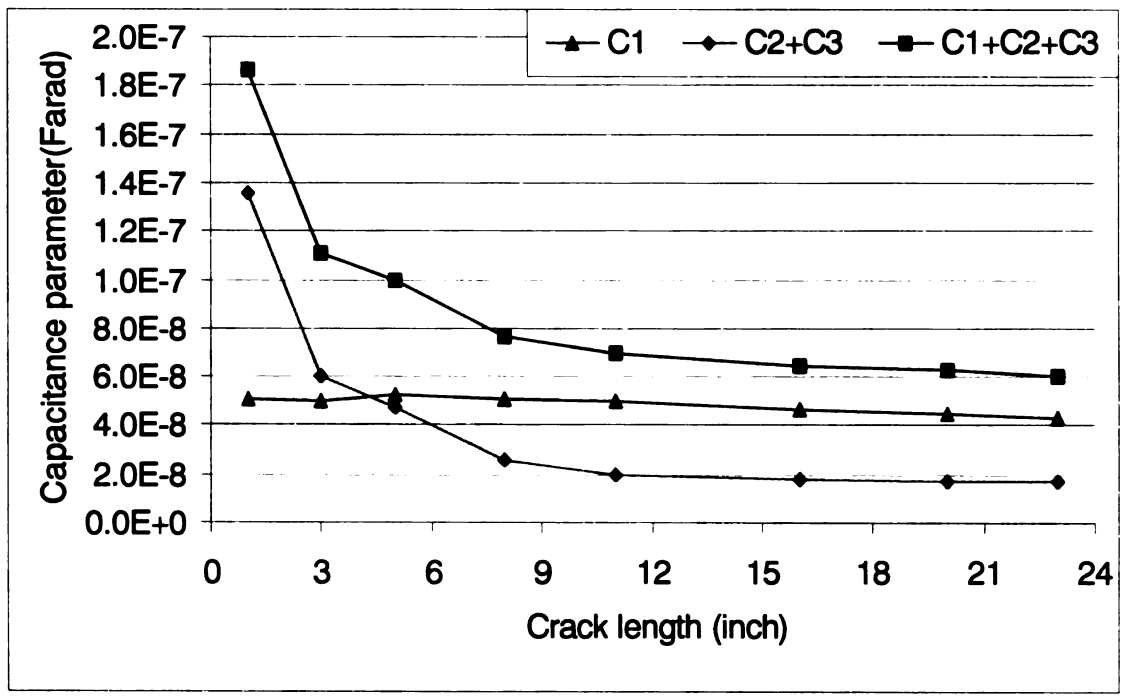

Figure 3-24 Variation of the capacitance parameters from equivalent circuit analysis for the large specimen from the rebar to external sensor

3.2.3 Detecting the location of debonded regions

While impedance measurements between the rebar and an external sensor provide a global assessment of the debonded area, they are incapable of revealing the location of debonded regions. However, impedance measurements between pairs of internal wire sensors (W_i) can be used to detect debonded regions. Measurements between internal sensors were taken for the large eight-foot long beam as well as for a two-foot long specimen as the internal crack between the CFRP and concrete was propagated.

3.2.3.1 Comparison of raw impedance spectra

Impedance measurements were made between adjacent sensors (such as W1 and W2, W2 and W3, and so on). Figures 3-25 to 3-28 show the variation of measured impedance at different crack states. Figure 3-25 shows the measured impedance from the eight-foot long specimen when the crack between the CFRP and concrete was about 8 inches long with the crack tip between sensors W2 and W3. At this crack length, W1 and W2 were in the debonded region and the remaining sensors were in the bonded region. The measured impedance between sensors in the debonded region (W1W2) had the highest magnitude especially in the low-frequency region. The measured impedances between sensors in the bonded region (W3W4, W4W5, and W5W6) had the lowest magnitudes. The same distinguishable trends on the impedance measurements were observed with a two-foot long specimen. Figure 3-26 shows the measured impedance from two-foot long specimen when the crack was about 12 inches long with the crack tip between sensor W3 and W4. At this crack length, W1, W2, and W3 were in the debonded region and W4, W5, and W6 were in the bonded region.

Measured impedances between a sensor in the debonded region and a sensor in the bonded region (eg., W1W4 and W2W3 from Figure 3-25 and W3W4 from Figure 3-26)

have magnitudes that fall inbetween those corresponding to sensors in the debonded region and those corresponding to sensors in the bonded region. Figure 3-27 shows the Nyquist plot corresponding to Figure 3-26. On the Nyquist plot, the impedance measurements from the sensors in the debonded region yield the largest arc radii while the impedance measurements from the sensors in the bonded region produce the smallest arc radii. When one sensor is in the bonded region and the other in the debonded region (W3W4), the arc radii is in between those for the other two cases.

Figure 3-28 shows the measured impedances for the two-foot long specimen when the CFRP was debonded to 16 inches with the crack tip between the W5 and W6 sensors. Again, impedance magnitudes between sensors in the debonded region (W1W2, W2W3, W3W4, and W4W5) are much higher than those in the bonded region (W6W7, W7W8, and W8W9), especially at low frequencies.

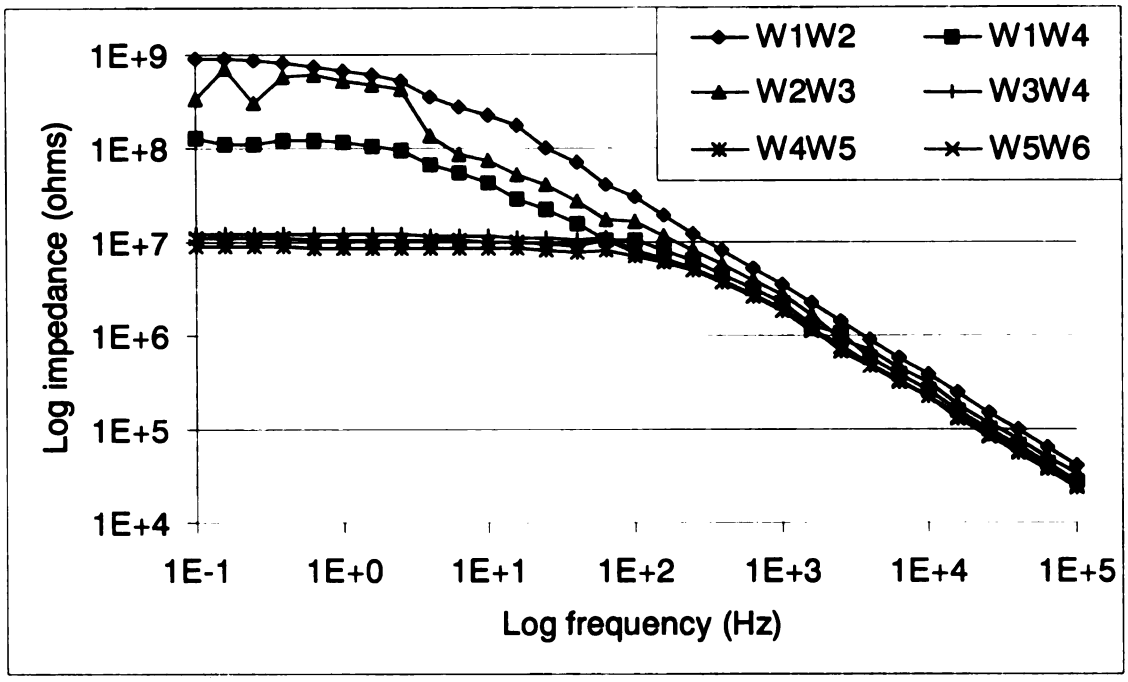

Figure 3-25 Bode magnitude plot of impedance spectra measured between pairs of internal sensors for eight-foot specimen in ambient condition when crack tip was between sensors W2 and W3 (legend shows the internal sensors used)

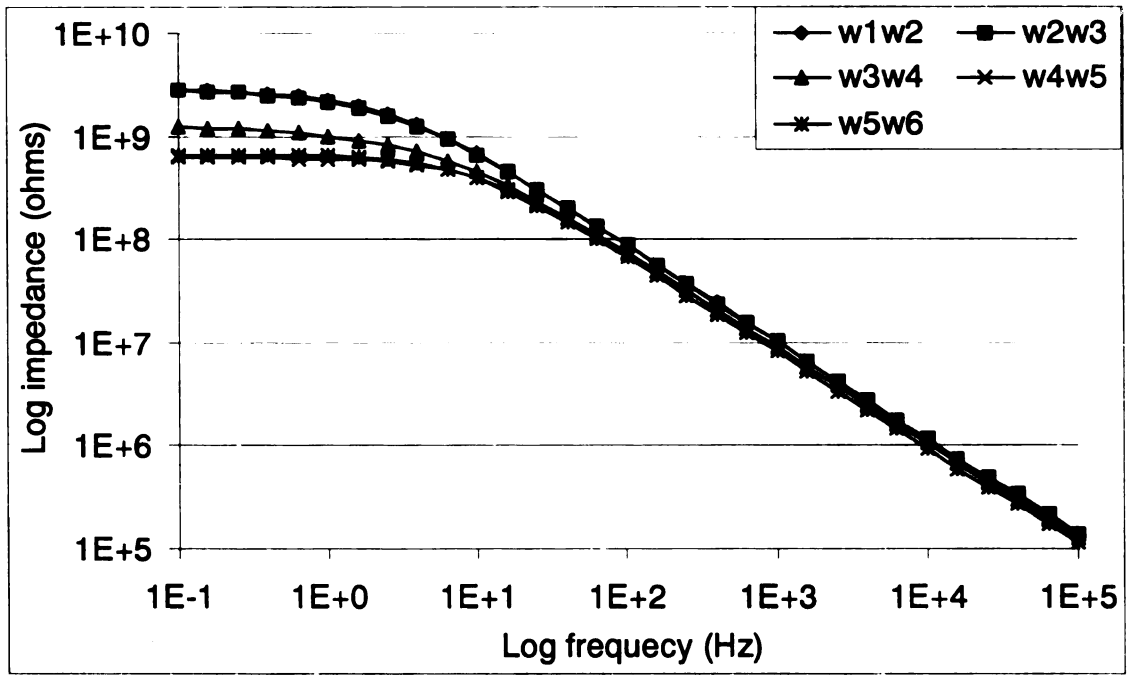

Figure 3-26 Bode magnitude plot of impedance spectra measured between pairs of internal sensors for two-foot specimen in ambient condition when crack tip was between sensors W3 and W4 (legend shows the internal sensors used)

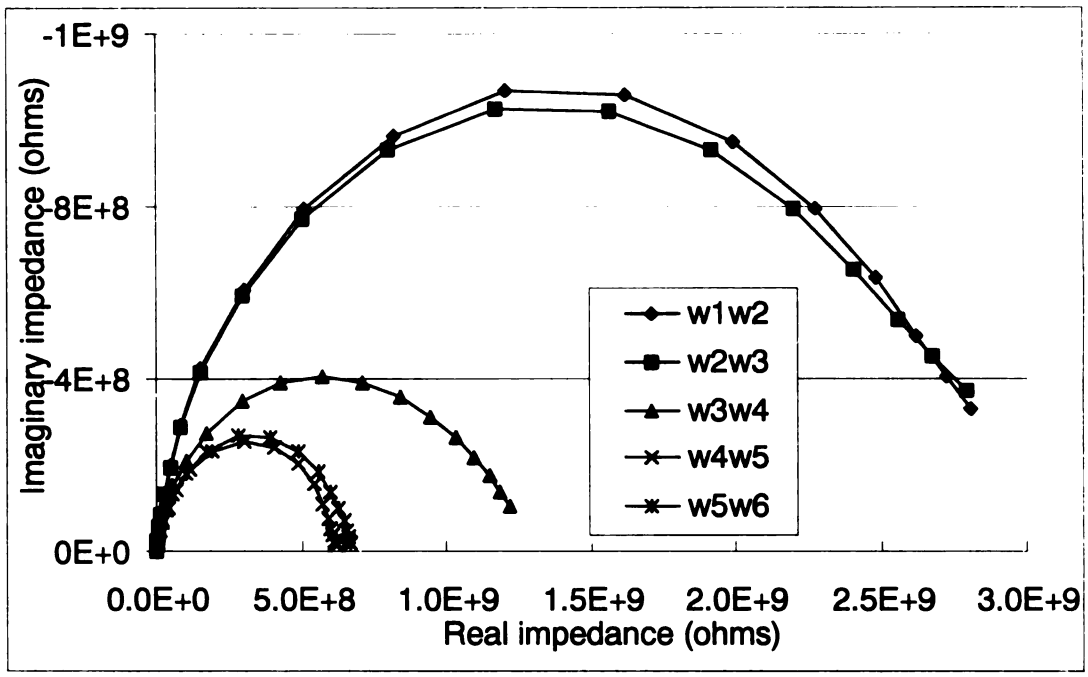

Figure 3-27 Nyquist plot of impedance spectra measured between pairs of internal sensors for two-foot specimen in ambient condition when crack tip was between sensors W3 and W4 (legend shows the internal sensors used)

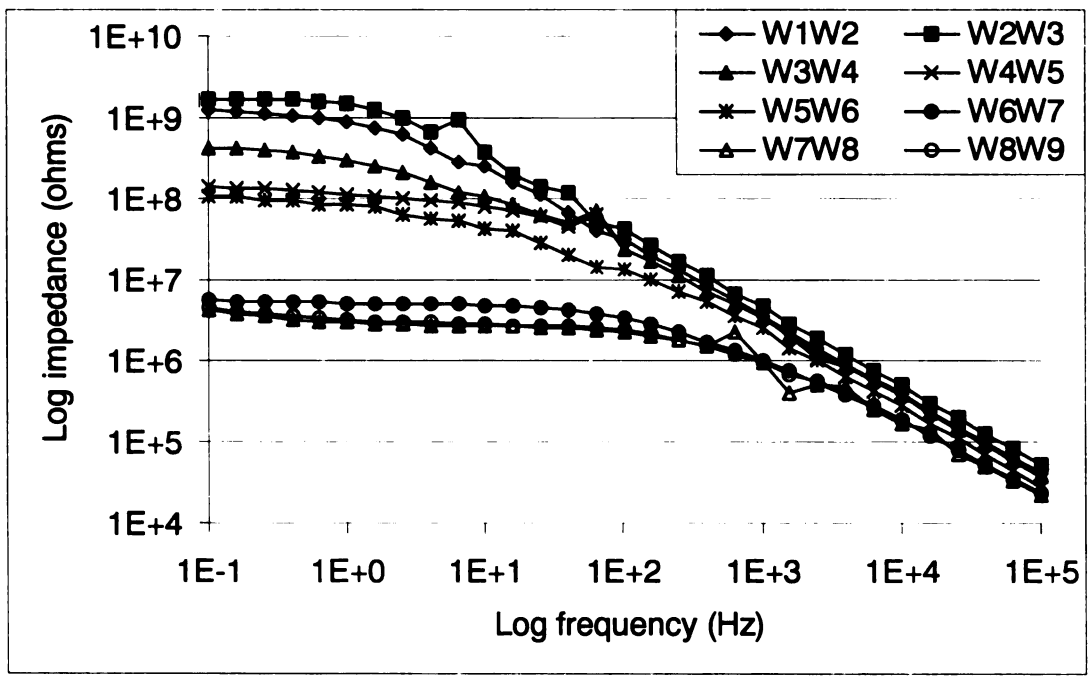

Figure 3-28 Bode magnitude plot of impedance spectra measured between pairs of internal sensors for eight-foot specimen in ambient condition when crack tip was between sensors W5 and W6 (legend shows the internal sensors used)

3.2.3.2 Results from equivalent circuit analysis

While raw impedance measurements are sufficient to detect debonded regions, equivalent circuit analysis also can be used. The effect of debonding on the impedances measured between internal sensors is best observed with the CPE parameter which characterizes the low-frequency behavior of the impedance spectrum. The variation of the CPE values corresponding to the spectra in Figure 3-25 are shown in Figure 3-29 (crack tip was between the W2 and W3 sensors). Figure 3-30 shows the variation of the CPE values corresponding to the spectra in Figure 3-26 (crack tip between the W3 and W4 sensors). The magnitude of the CPE parameter corresponding to measurements between pairs of sensors in the debonded region are about two orders of magnitude higher than those corresponding to pairs of sensors in the bonded region.

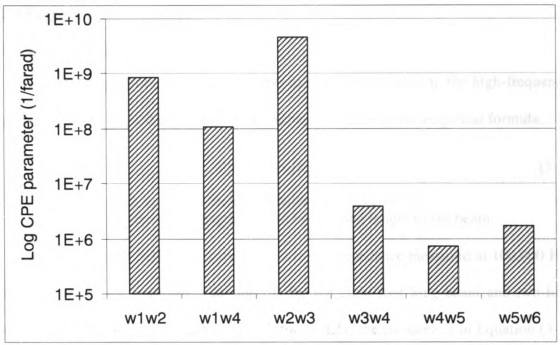

Figure 3-29 Variation of the CPE parameter for pairs of internal sensors for the 8-foot beam when crack tip was between sensors W2 and W3 (name of the bar shows the internal sensors used)

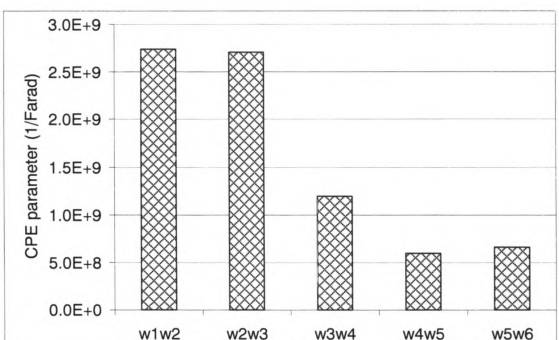

Figure 3-30 Variation of the CPE parameter for pairs of internal sensors for the 2-foot long beam when crack tip was between sensors W3 and W4 (name of the bar shows the internal sensors used)

3.2.4 Empirical Relationships

3.2.4.1 Raw impedance spectra

Measured impedances between the rebar to an external sensor in the high-frequency region (100,000 – 10,000 Hz) show a remarkable good fit with the empirical formula.

$$|Z| = a_1 \exp(\beta x) + a_2 \tag{3-5}$$

where a_1, β, a_2 are coefficients obtained by curve fitting
x is the crack length divided by the total length of the beam

Figures 3-31 and 3-32 show curves fitted to the impedance measured at 100,000 Hz. Table 3-1 shows the parameters for the fits for the eight-foot long beam and two-foot long beams in the high-frequency range. Unfortunately, the parameters in Equation (3-5) vary considerably from one fit to another and hence it is difficult to recommend values that can be used for diagnosis purposes.

Table 3-1 Parameters of the curve fitted to measured impedance in the high-frequency range

Frequency (KHz)	a_1	β	a_2	a_1	β	a_2
	Eight-foot specimen			Two-foot specimen 2		
100	10.25	5.29	32.02	26.94	6.09	840.00
64	4.13	8.06	60.07	30.98	6.24	1098.00
40	1.78	11.38	94.56	37.34	6.35	1484.00
25	0.94	14.54	143.16	47.67	6.43	2056.00
16	0.79	16.31	214.78	63.75	6.47	2914.00
10	0.76	17.82	322.67	89.42	6.48	4197.00
	Two-foot specimen 4			Two-foot specimen 6		
100	1034.00	1.78	-583.00	28.36	6.26	705.29
64	700.00	2.39	45.00	30.39	6.54	928.79
40	619.00	2.79	483.00	36.49	6.68	1257.00
25	661.00	3.01	927.00	49.16	6.68	1729.00
16	815.00	3.11	1483.00	71.00	6.60	2424.50
10	1109.00	3.14	2257.00	109.62	6.46	3443.00
	Two-foot specimen 3			Two-foot specimen 5		
100	272.00	2.26	263.00	219.00	2.89	369.00
64	389.00	2.17	275.00	294.00	2.85	448.00
40	600.00	2.03	258.00	405.00	2.79	570.10
25	638.00	2.30	606.00	566.00	2.73	763.60
16	1544.00	1.76	101.00	817.13	2.65	1040.00
10	2328.00	1.73	104.00	1157.00	2.62	1509.00

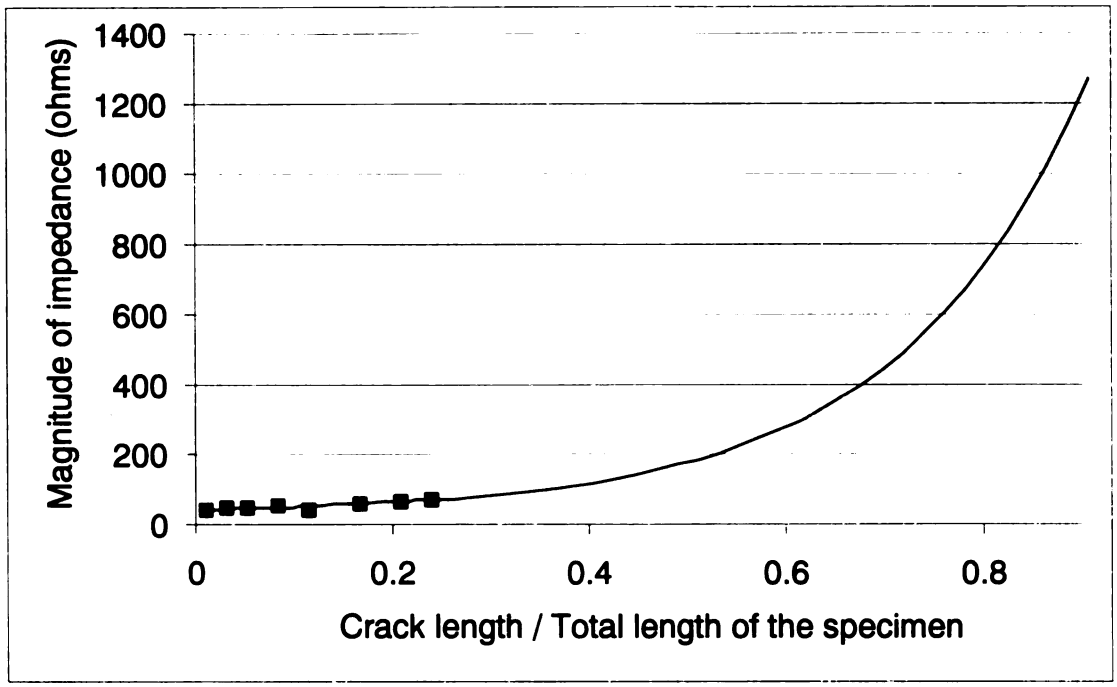

Figure 3-31 Fit of the measured impedance for 8-foot long beam from rebar to external sensors at 100,000 Hz: Dots are the measured data and the solid line is the fitted curve.

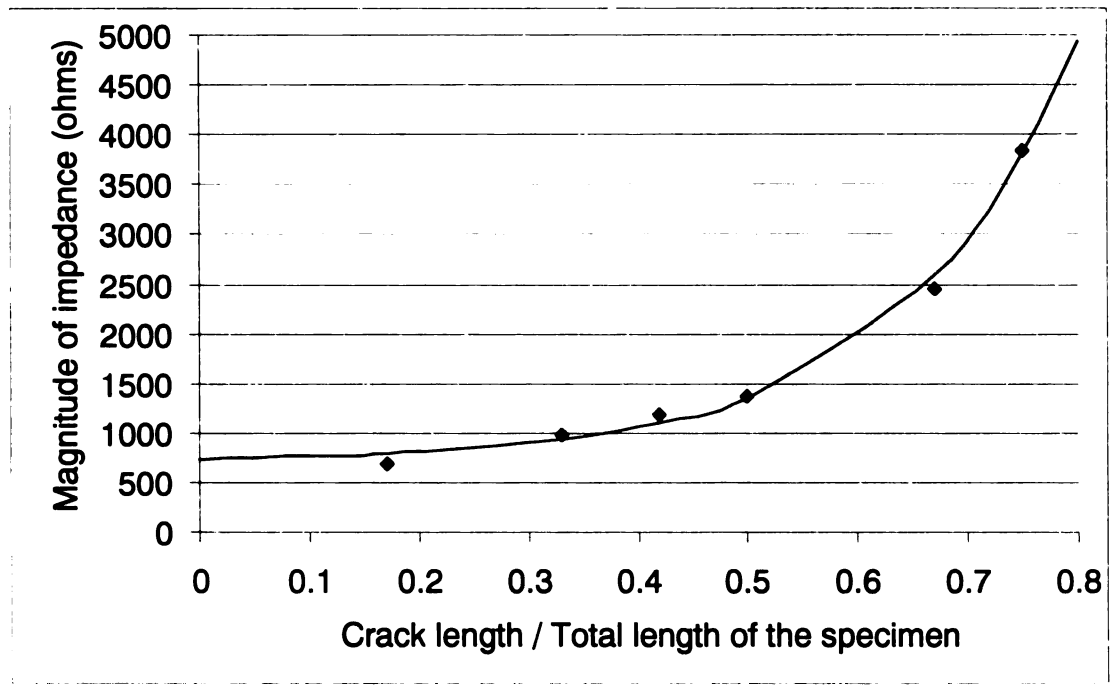

Figure 3-32 Typical fit of the measured impedance for two-foot long beam from rebar to external sensors at 100,000 Hz: Dots are the measured data and the solid line is the fitted curve.

3.2.4.2 Equivalent circuit analysis

The C1+C2+C3 parameter from equivalent circuit analysis is also fitted with Eq. 3-5 and the fits are shown in Figures 3-33 and 3-34. Table 3-2 shows the parameters in Eq. 3-5 for the fitted curves for the eight-foot beam and the two-foot beams.

Table 3-2 Parameters of the curve fitted to (C1+C2+C3) from equivalent circuit analysis

Specimen	a_1	β	a_2
Large	1.75E-07	-39.083	2.43E-08
S2	6.44E-08	-0.384	-4.26E-08
S4	3.16E-08	-2.228	-8.39E-10
S6	3.70E-08	1.507	-6.90E-09
S5	3.72E-08	-1.056	-9.28E-09
S3	3.87E-08	-3.135	8.96E-09

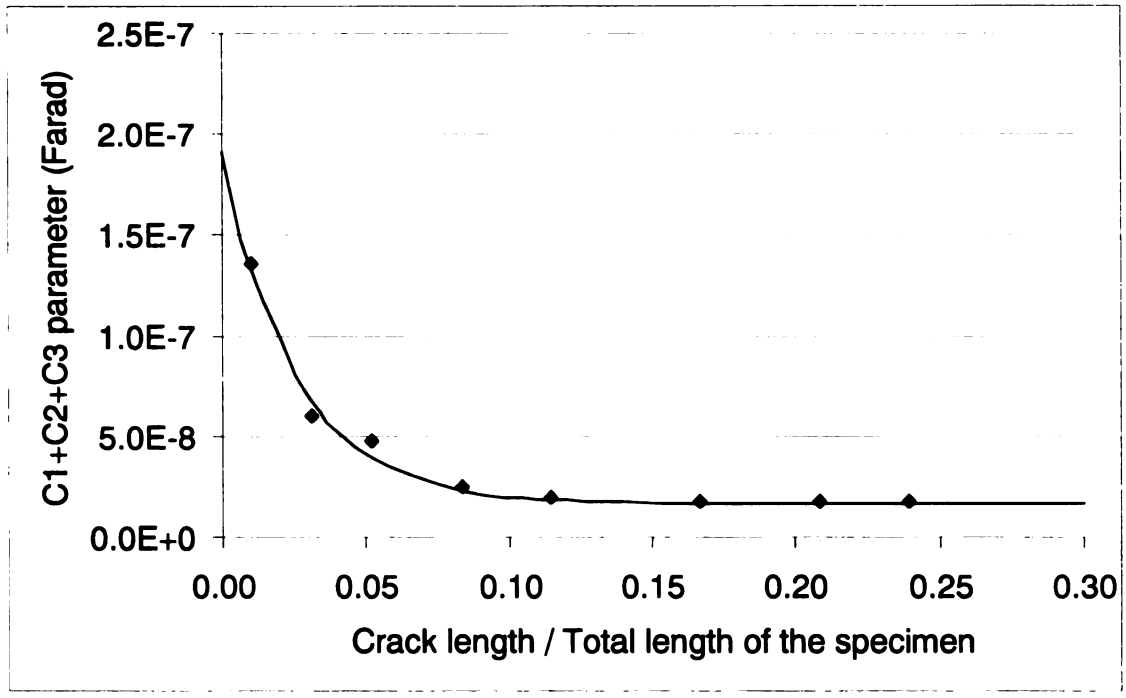

Figure 3-33 Fit for (C1+C2+C3) parameters for 8-foot beam: Dots are the measured data and the solid line is the fitted curve.

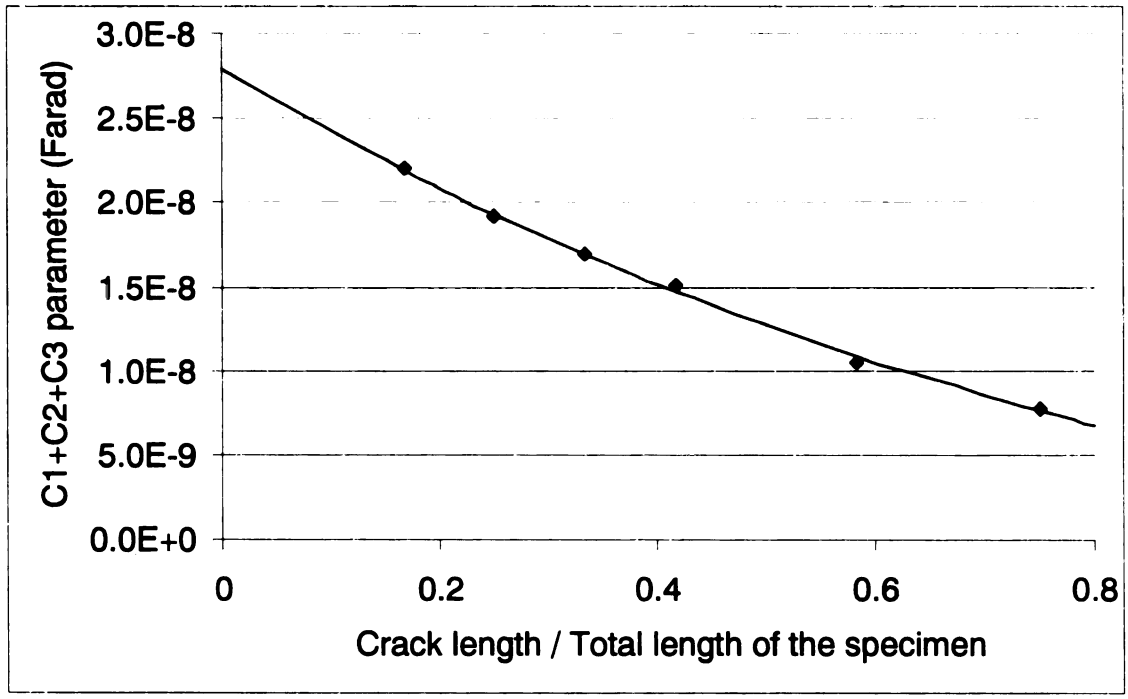

Figure 3-34 Typical fit for (C1+C2+C3) parameters for two-foot beam: Dots are the measured data and the solid line is the fitted curve.

3.2.5 Summary and Discussion

The effect of CFRP debonding was studied using impedance measurements from the rebar (R) to the copper tape sensors (C_i), and from the internal wire sensors (W_i) to the copper tape sensors. Impedances from two-foot (medium) concrete specimens were measured in a refrigerator and in an ambient condition at the initial crack state (4" crack length) and at extended crack states. The large concrete beam was subjected to an ambient condition and the crack was propagated in the ambient environment. The global effect of interfacial cracking is best observed with the impedance measured from the rebar to the external sensor (copper tape). The impedances measured between internal sensors (stainless steel wires) are used to detect the location of debonded regions. Impedance measurements at high frequencies (100,000 - 1000 Hz) yield data that have the least sample to sample variation, and display an exponential variation with the debonded area of CFRP.

Equivalent circuit analysis also is effective in studying CFRP debonding. The capacitance parameters correlate best with the debonded area of CFRP. It is found that the CPE, C1, C2+C3 and C1+C2+C3 values from equivalent circuit analysis all correlate well with the crack length. The relationship between the C2+C3 and C1+C2+C3 values and the debonded area of CFRP are approximately linear and show low sample-to-sample variation. These measures have the most promise for detecting the extent of CFRP debonding. The CPE parameter increases and the capacitance parameters decrease as the crack is propagated.

Impedance measurements taken between pairs of internal sensors are capable of revealing the location of regions where the CFRP is debonded from the concrete. Measurements between pairs of sensors in debonded regions yield high impedances in the

low-frequency region, while those between pairs of sensors in bonded regions yield low impedances. The CPE parameter from equivalent circuit analysis also is a strong indicator. The CPE value corresponding to measurements between pairs of sensors in the debonded region is about two orders of magnitude higher than that corresponding to pairs of sensors in the bonded region. It is postulated that the reason for this distinctive difference in the magnitude of impedance is the path of current flow in each case. When the impedance measurement is made between sensors in the debonded area, current must flow through the concrete, and the impedance is high. On the other hand, when measurements are made between sensors in the bonded area, current probably flows predominantly through the highly conductive CFRP sheet, with charge transfer between the internal sensors and the CFRP sheet, resulting in lower impedances.

The impedance in the high-frequency range for measurements from the rebar to external sensors and the C1+C2+C3 values are also fitted with the exponential empirical equation in Equation (3-5). Although this equation provides an excellent fit to the data, the parameters of the fitted equation vary widely from specimen-to-specimen and between the two-foot and eight-foot specimens. therefore, it is difficult to recommend parameter values that might used for diagnosis of the debonded length without first having historical data as the debonded progresses.

3.3 Sensitivity of Sensor Measurements to Environmental Effects

In Section 3.2 it was demonstrated that the measured impedances in the high frequency range and the C1+C2+C3 parameter from the equivalent circuit analysis correlate well with debonding between the CFRP reinforcement and the concrete substrate. In order to use these as indicators of the extent of debonding, environmental effects on the measured impedance were studied.

3.3.1 Humidity

Experiments were performed to determine the effect of humidity on the measured impedance over the frequency range from 0.1 Hz to 100 kHz.

3.3.1.1 Comparison of raw impedance spectra

Figures 3-35 and 3-36 show typical impedance spectra (log frequency vs log impedance) at different humidity levels. Different humidity levels affect the magnitude of the impedance in the low frequency region regardless of the chloride content. It should be noted that the magnitude of impedance at a relative humidity of 60% is lower than the magnitude of impedance at a relative humidity of 90% for the samples with chloride (Figure 3-35). The reason for this was that the controlled environmental chamber was malfunctioning at the time of these measurements.

Different humidity levels have a significant influence on the impedance measurements in the low-frequency region (0.1-10 Hz). Moisture in the concrete specimen serves as an electrolytic medium for transporting charges between sensors. At low excitation frequencies, the current flow in the electrochemical cell (concrete specimen) is dominated by the movement of ions (diffusion controlled), and different

moisture levels affects the rate of ion transport. However, it is found that different humidity levels have less of an influence on the impedance measurements in the high-frequency region (1000-100 kHz). The impedance is governed by the kinetics of the charge transfer processes at the electrode-electrolyte interface at high frequencies. This charge transfer process is influenced less by environmental conditions. The impedance measurements from the mid-frequency range (10-1000 Hz) are somewhat sensitive to moisture effects because at these frequencies charge transfer occurs both by diffusion and kinetics at the interfaces.

3.3.1.2 Results from equivalent circuit analysis

The changes of moisture content in the concrete specimen influence the CPE, C1 and C2+C3 parameters from the equivalent circuit analysis. The variation of the C1, CPE, C2+C3 and C1+C2+C3 parameters are shown in Figures 3-37 to 3-40. Different humidity levels have a significant influence on the CPE parameter and have less influence on the C1 and C2+C3 parameters in the equivalent circuit analysis. Although both the C1 and CPE parameters represent the changes of measured impedance in the low-frequency range, it is found that the C1 parameter is less sensitive and the CPE parameter is more sensitive to humidity variation. The value of the CPE parameter decreases with increasing water content in the concrete specimens and the value of capacitance parameters (C1, C2+C3, and C1+C2+C3) increase with increasing water content. The C1+C2+C3 parameter also increases slightly as the humidity level increases.

3.3.1.3 Summary and Discussion

A change in humidity over a period of time results in a change in the water content in the concrete specimens. Higher levels of water content lower the magnitude of impedance, and lower levels of water content increase the magnitude of impedance in the

concrete specimen. Since the impedance measurements at low frequencies are governed by the diffusion of ions which is affected by the water content, the water content in the concrete specimen most strongly influences the measured impedance in the low-frequency range.

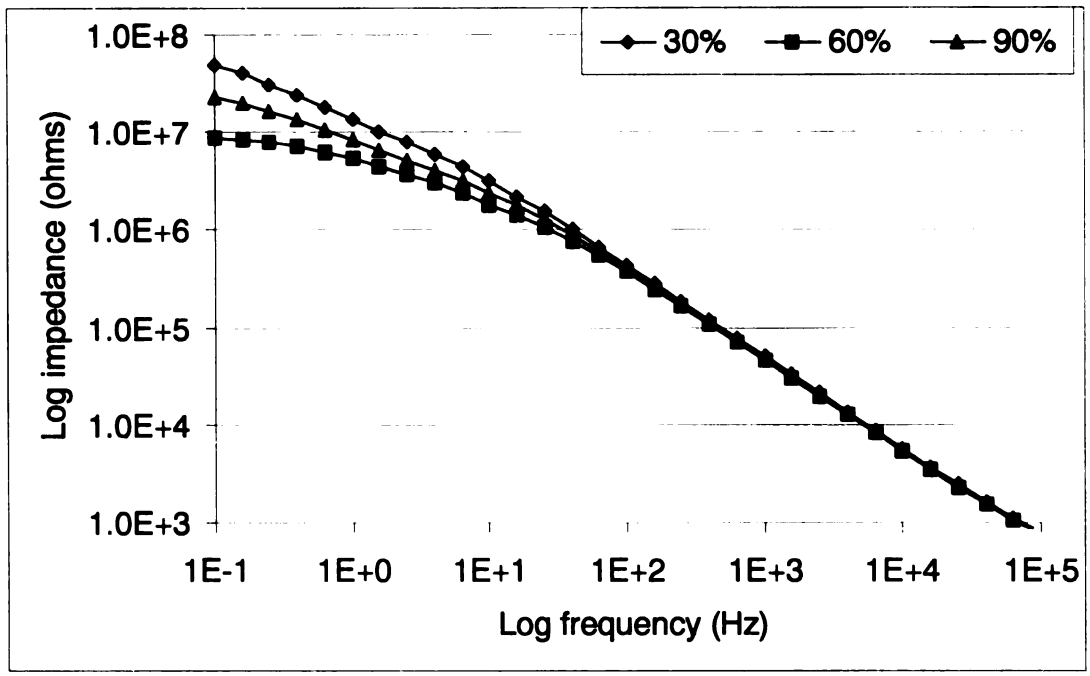

Figure 3-35 Bode magnitude plot of typical impedance spectra for specimens with chloride at different humidity levels

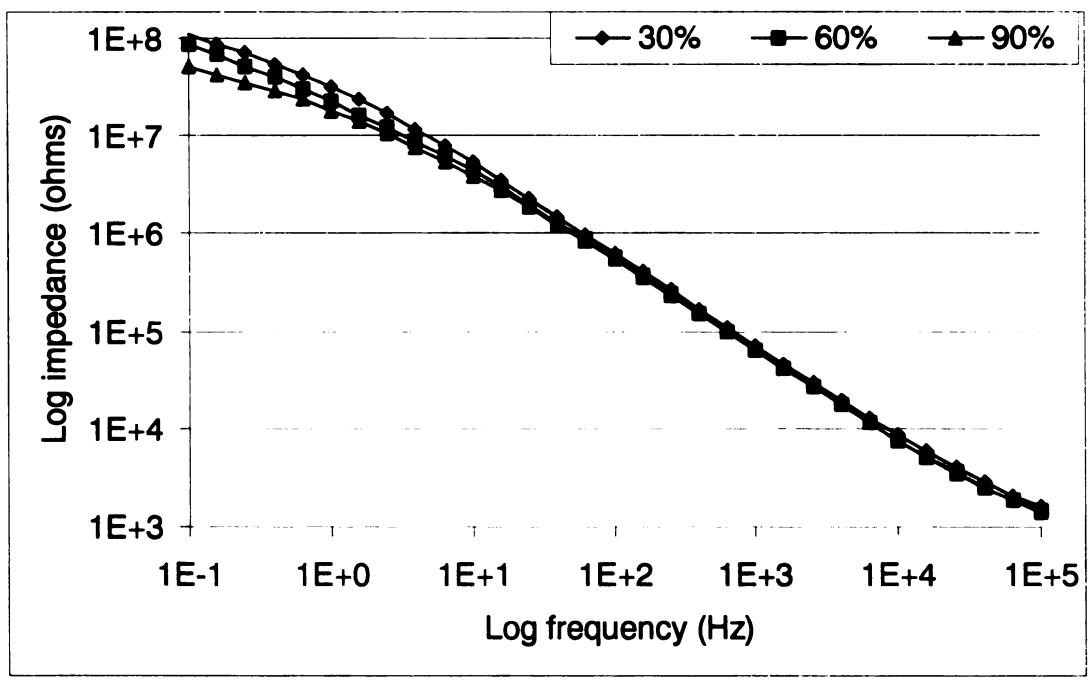

Figure 3-36 Bode magnitude plot of typical impedance spectra for specimens without chloride at different humidity levels

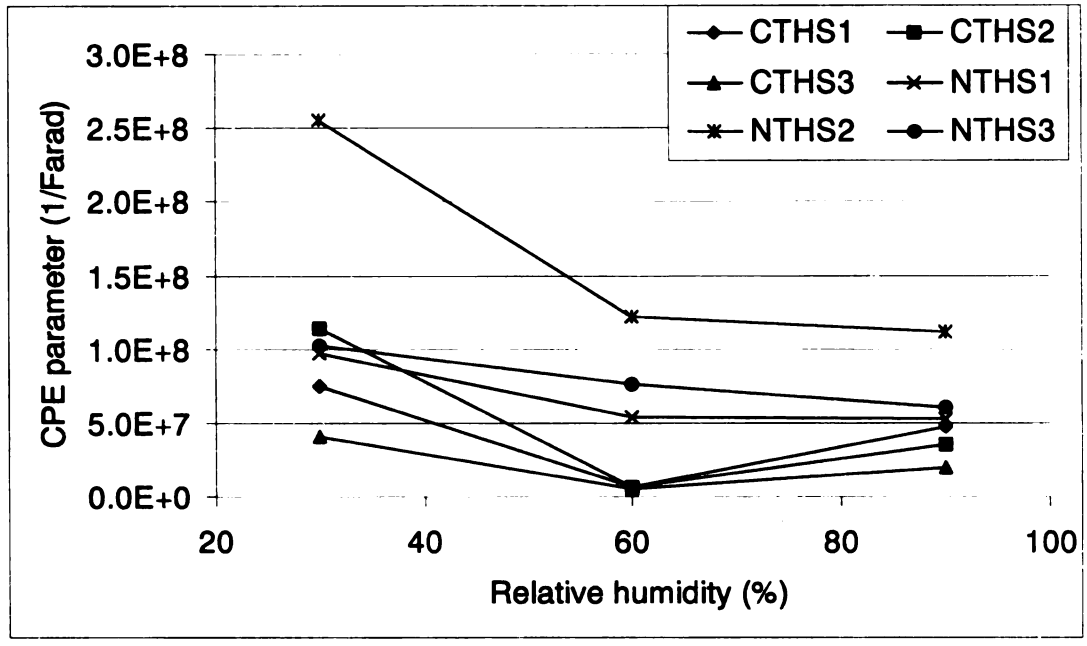

Figure 3-37 Variation of the CPE parameter from equivalent circuit analysis due to different humidity levels for measurements from the rebar to external sensors (legend gives the name of the specimen: C-chloride, N-non-chloride, T-temperature, H-humidity, Sn-specimen number)

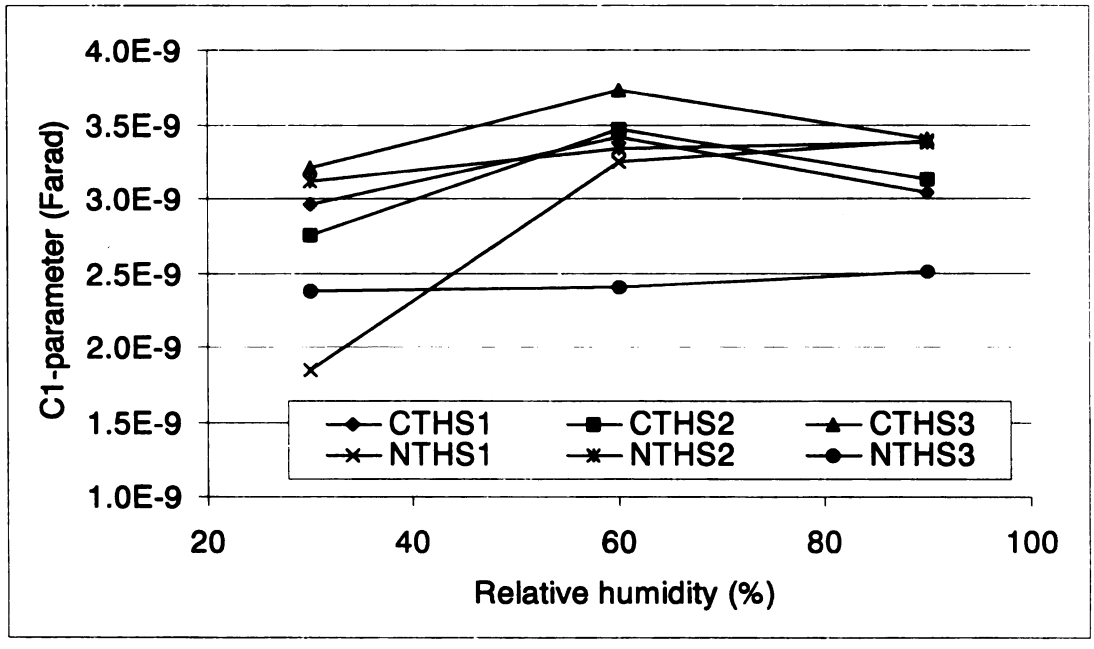

Figure 3-38 Variation of the C1 parameter from equivalent circuit analysis due to different humidity levels for measurements from the rebar to external sensors (legend gives the name of the specimen: C-chloride, N-non-chloride, T-temperature, H-humidity, Sn-specimen number)

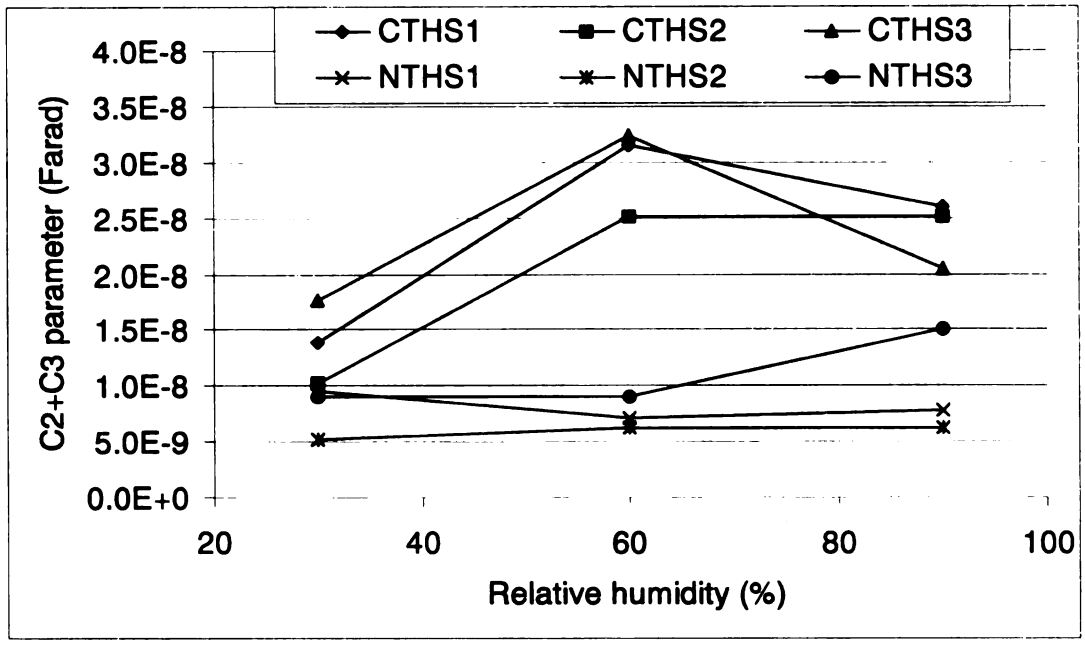

Figure 3-39 Variation of the C2+C3 parameter from equivalent circuit analysis due to different humidity levels for measurements from the rebar to external sensors (legend gives the name of the specimen: C-chloride, N-non-chloride, T-temperature, H-humidity, Sn-specimen number)

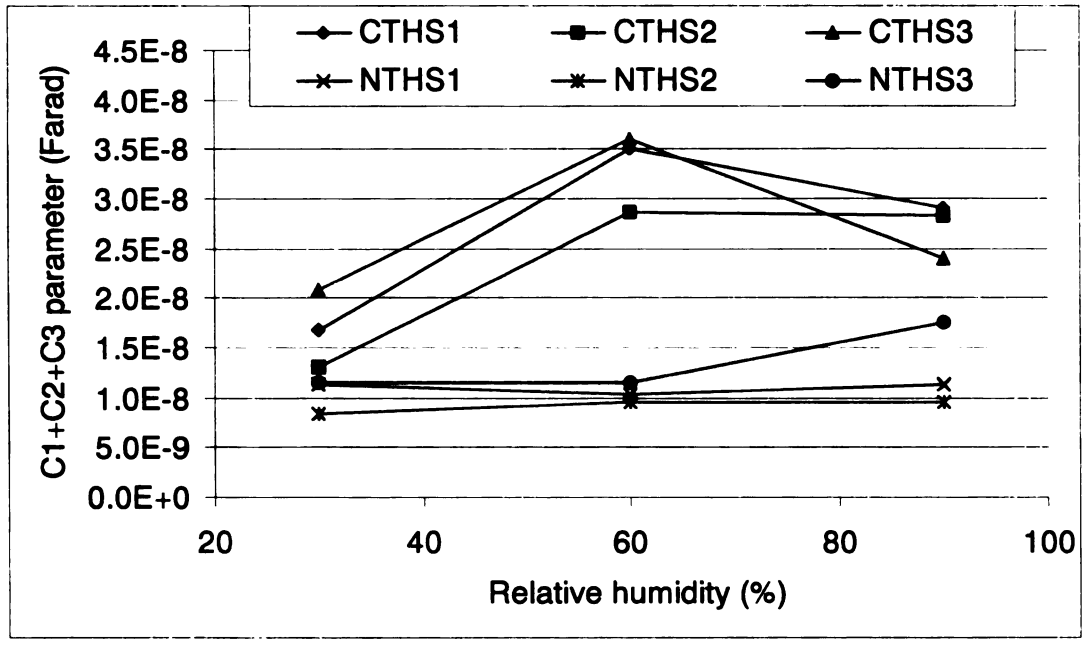

Figure 3-40 Variation of the C1+C2+C3 parameter from equivalent circuit analysis due to different humidity levels for measurements from the rebar to external sensors (legend gives the name of the specimen: C-chloride, N-non-chloride, T-temperature, H-humidity, Sn-specimen number)

3.3.2 Temperature

Experiments were performed to determine the influence of temperature effects on the measured impedance over the frequency range from 0.1 Hz to 100 kHz. Note, however, that the humidity level was not kept constant so the moisture content in the specimens are likely to have been different at the different temperatures.

3.3.2.1 Comparison of raw impedance spectra

Figures 3-41 and 4-42 show typical impedance spectra at different temperatures. The slope of the impedance magnitude changes at frequencies below 1000 Hz and becomes zero in the mid- and low-frequency region at the high temperature of 100^0F. At 70^0F, the slope of measured impedance becomes smaller at frequencies below 10 Hz compared to the measured impedance at 100^0F. The impedance measurements are affected in the low- and mid-frequency regions as the temperature varies from 70 ^{0}F to 100 ^{0}F.

Measured impedances are also analyzed at specific frequencies. Figures 3-43 to 3-45 show the variation of measured impedance at different temperatures at frequencies of 10,000 Hz, 100Hz, and 1 Hz. 10,000 Hz, 100 Hz, and 1 Hz are arbitrary representative frequencies for high-(100,000 – 1000Hz), mid- (1000 – 10 Hz), and low-frequency (10 – 0.1 Hz) ranges, respectively. The log of the magnitude at 10,000 Hz and 1 Hz show a reasonably linear trend with increasing temperature, but the trend is more nonlinear at 100 Hz. At 100 Hz the change in temperature from 0^0F to 70^0F has a much smaller influence of the impedance magnitude than the change in temperature from 70^0F to 100^0F.

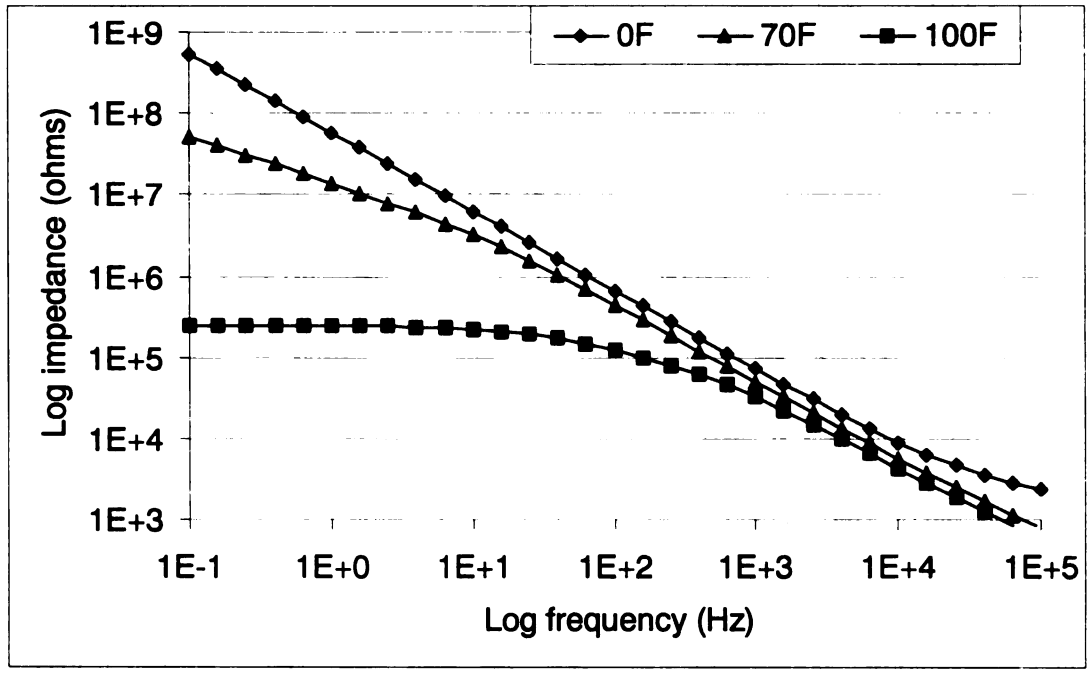

Figure 3-41 Bode magnitude plot of typical impedance spectra for specimens with chloride at different temperature levels

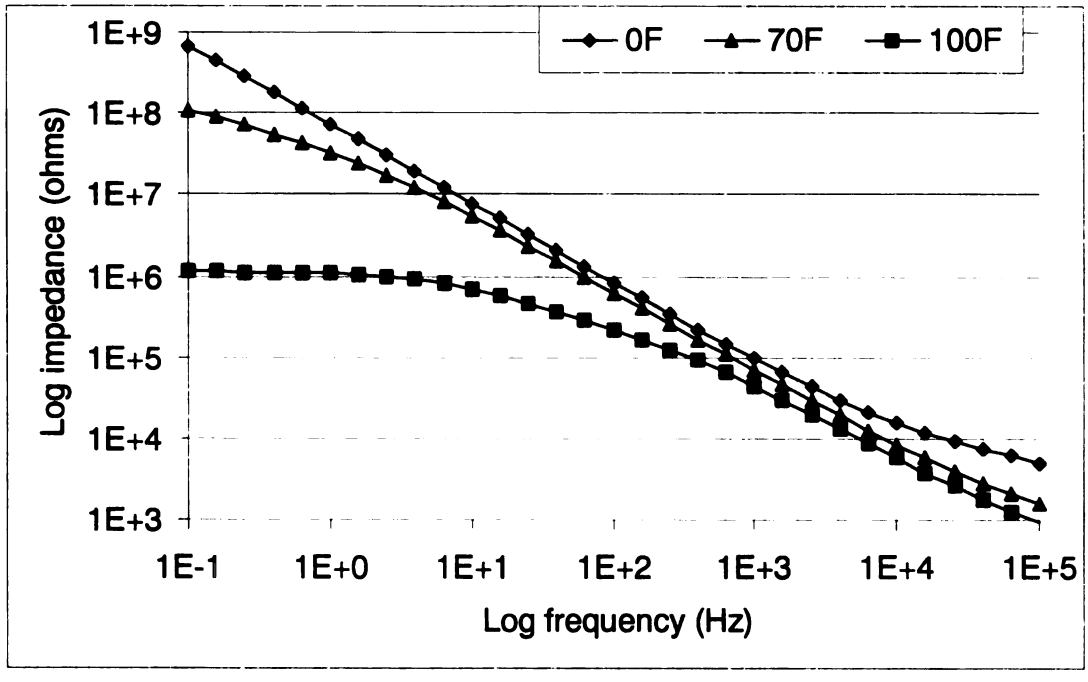

Figure 3-42 Bode magnitude plot of typical impedance spectra for specimens without chloride at different temperature levels

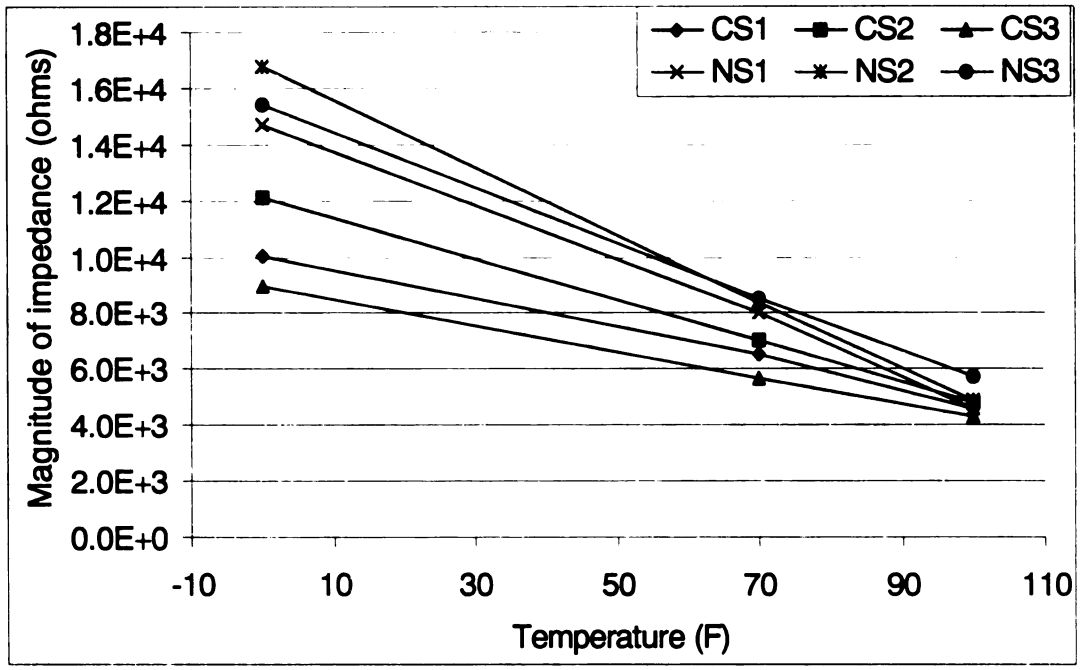

Figure 3-43 Variation of typical measured impedance in the high-frequency range at different temperature levels at 10,000 Hz (legend gives the name of the specimen: C-chloride, N-non-chloride, Sn-specimen number)

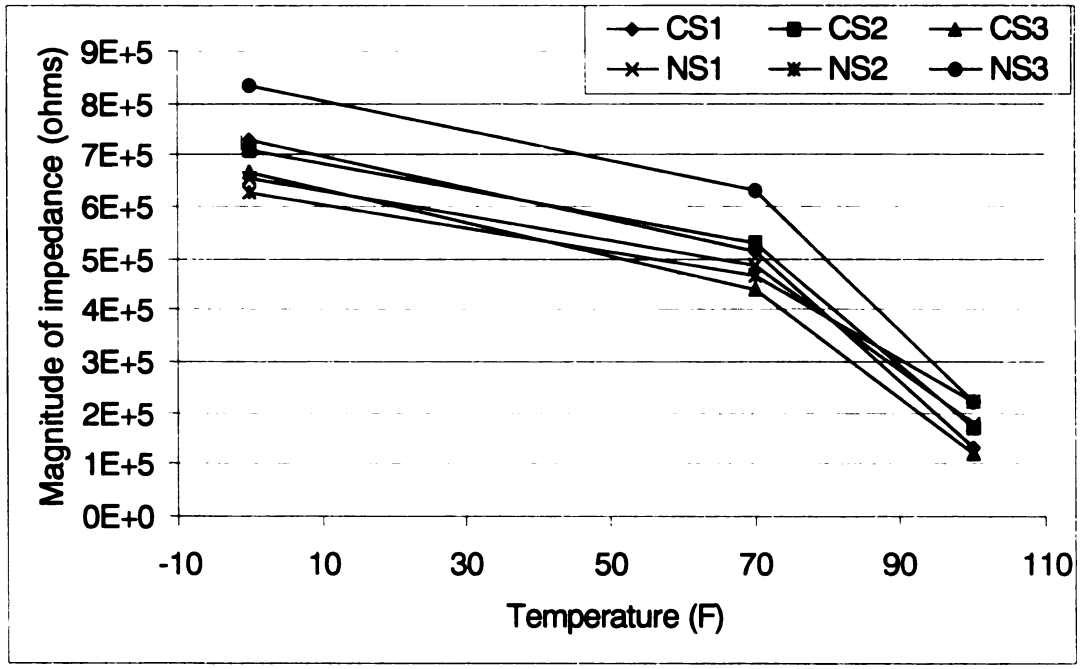

Figure 3-44 Variation of typical measured impedance in the mid-frequency range at different temperature levels at 100 Hz (legend gives the name of the specimen: C-chloride, N-non-chloride, Sn-specimen number)

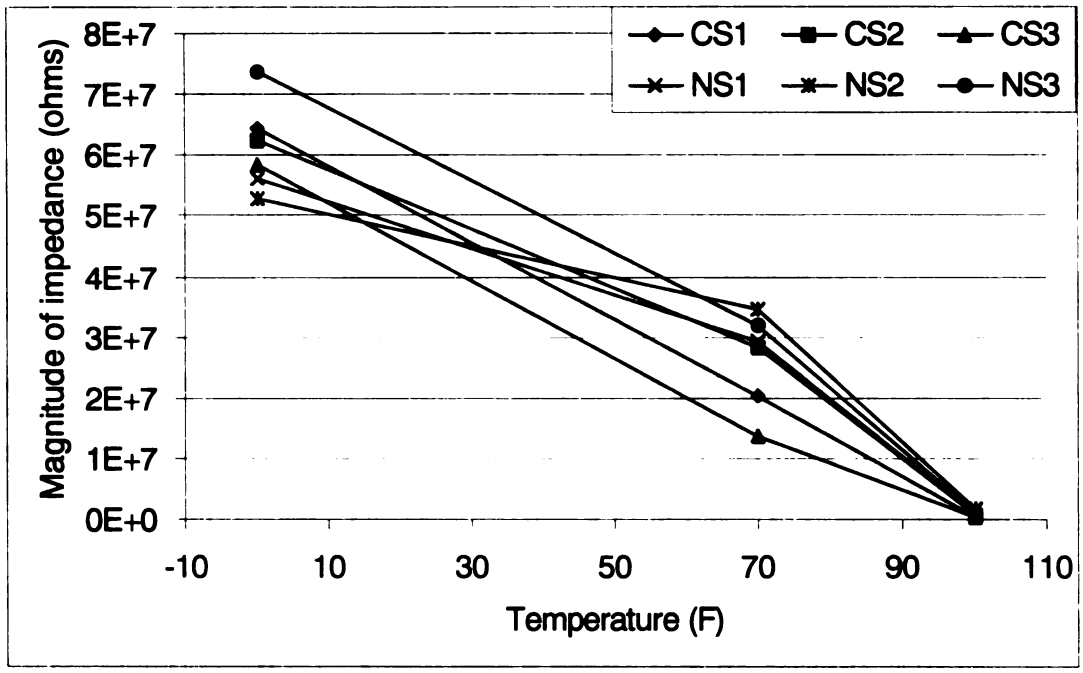

Figure 3-45 Variation of typical measured impedance in the low-frequency range at different temperature levels at 1 Hz (legend gives the name of the specimen: C-chloride, N-non-chloride, Sn-specimen number)

3.3.2.2 Results from equivalent circuit analysis

The variation of the CPE, C1, the C2+C3 and the C1+C2+C3 parameters with temperature are shown in Figures 3-46 to 3-49. It should be noted that the change in temperature from 0^0F to 70^0F has a smaller influence than the change in temperature from 70^0F to 100^0F on all the capacitance parameters. On the other hand, the change in temperature from 0^0F to 70^0F has a larger influence on the CPE parameter than the change in temperature from 70^0F to 100^0F. In general, different temperatures have a significant influence on the CPE parameter and have less influence on the C1, and the C2+C3 and C1+C2+C3 parameters in the equivalent circuit analysis. The value of the CPE parameter decreases with increasing temperature in the concrete specimens and the value of capacitance parameters (C1, C2+C3) increase with increasing temperature. The C1+C2+C3 parameter also increases slightly as the humidity level increases.

3.3.2.3 Summary and Discussion

Change in temperature in the concrete specimen has a significant influence on the impedance measurements. At very low temperatures 0^0F, water in the concrete is usually in a super-cooled state significantly slows down the diffusion of ions. This results in the magnitude of impedance being very high. On the other hand, high temperatures increase the mobility of ions and lower the magnitude of impedance.

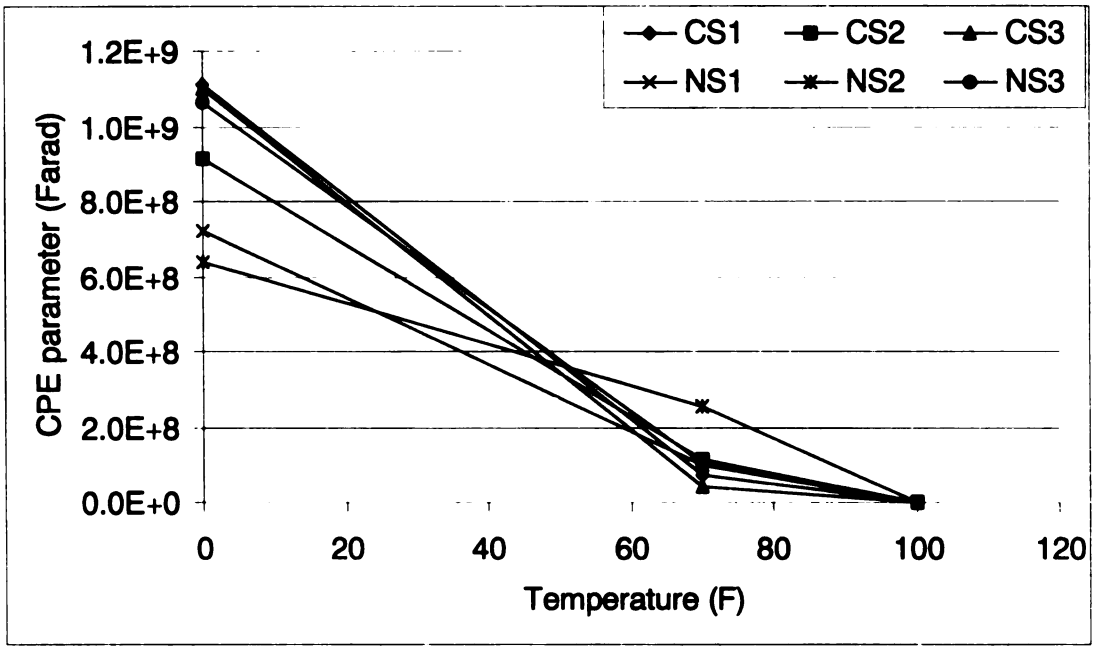

Figure 3-46 Variation of the CPE parameter from equivalent circuit analysis at different temperature levels for measurements from the rebar to external sensors (legend gives the name of the specimen: C-chloride, N-non-chloride, Sn-specimen number)

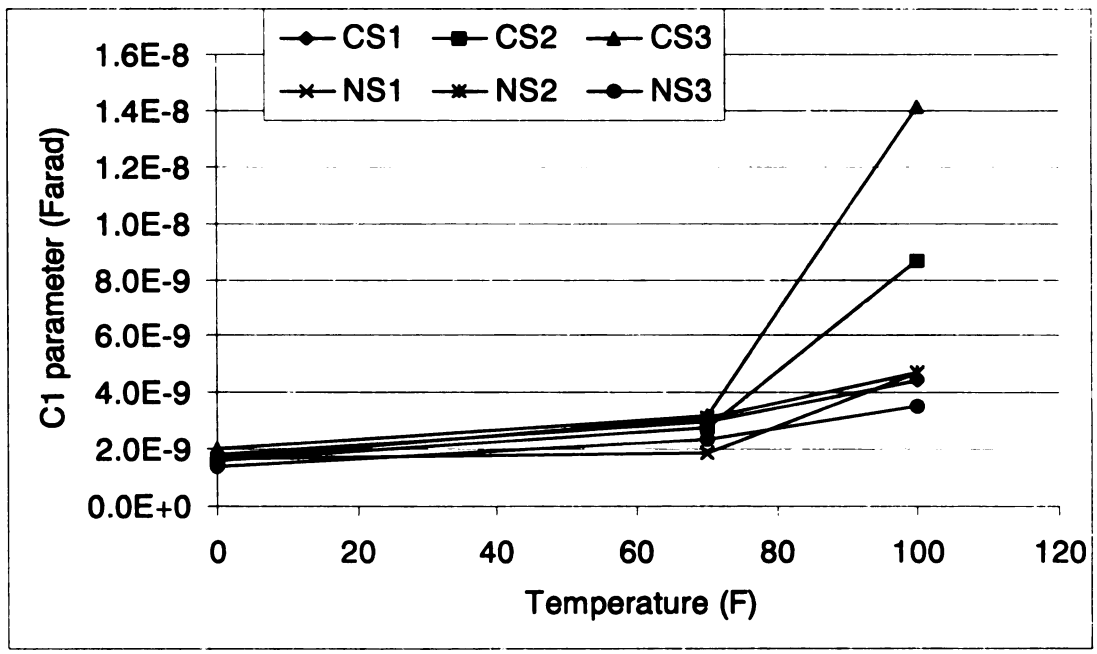

Figure 3-47 Variation of the C1 parameter from equivalent circuit analysis at different temperature levels for measurements from the rebar to external sensors (legend gives the name of the specimen: C-chloride, N-non-chloride, Sn-specimen number)

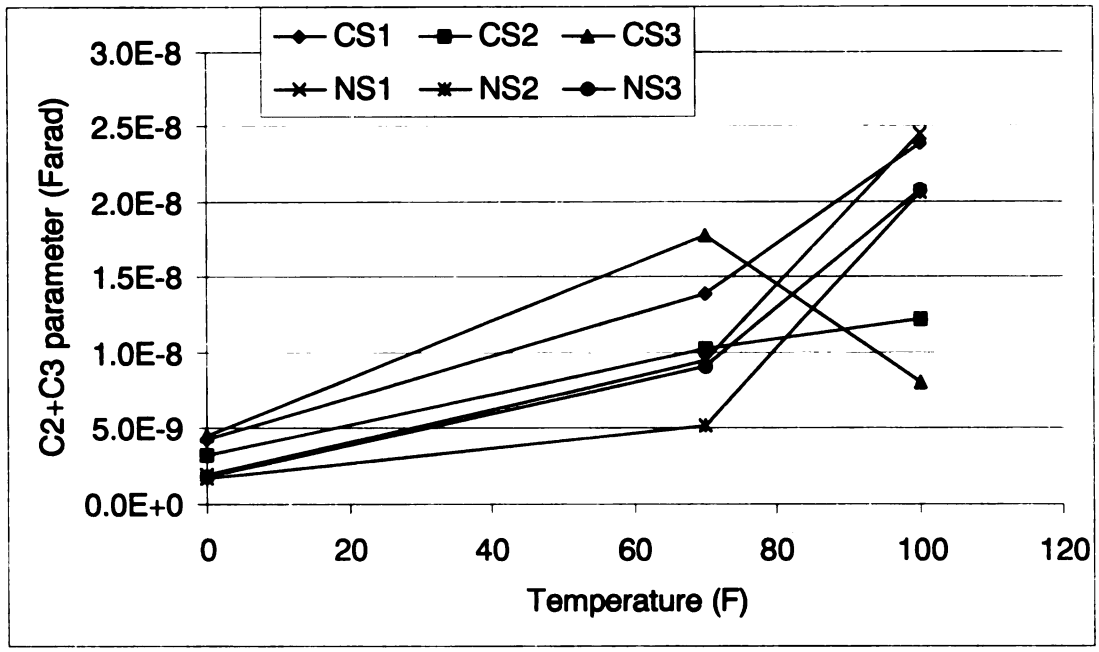

Figure 3-48 Variation of the C2+C3 parameter from equivalent circuit analysis at different temperature levels for measurements from the rebar to external sensors (legend gives the name of the specimen: C-chloride, N-non-chloride, Sn-specimen number)

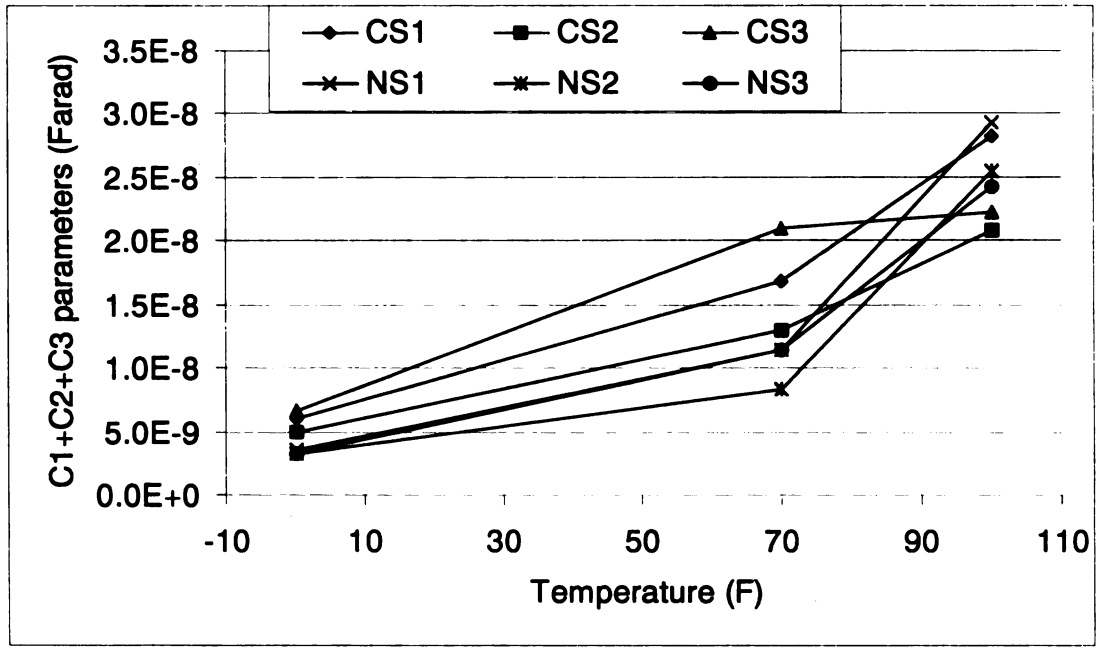

Figure 3-49 Variation of the C1+C2+C3 parameter from equivalent circuit analysis at different temperature levels for measurements from the rebar to external sensors (legend gives the name of the specimen: C-chloride, N-non-chloride, Sn-specimen number)

3.3.3 Chloride content

The experiment to study the impact of chloride content was conducted simultaneously with the experiment to study humidity and temperature effects.

3.1.3.1 Comparison of raw impedance spectra

Figures 3-50 to 3-52 show the measured impedance spectra over the entire frequency range at different humidity levels. Figures 3-53 to 3-55 show the impact of chloride content at different humidity levels on the measured impedance at specific frequencies. 10,000 Hz, 100 Hz, and 1 Hz are arbitrary frequencies that represent high-(100,000 – 1000 Hz), mid- (1000 – 10 Hz), and low-frequency (10 – 0.1 Hz) ranges, respectively. The lowering of the magnitude of impedance in the presence of chloride was observed in the high- and low-frequency range at all three different humidity levels (30, 60 and 90%). However, in the mid-frequency range, the presence of chloride ions has a smaller influence on the measured impedance at the three humidity levels.

The combination of chloride content and different temperatures has less influence on the measured impedance. Figures 3-56 to 3-58 show the measured impedance spectra over the entire frequency range at different temperature levels. Figures 3-43 to 3-45 show the impact of chloride content on the measured impedance at three temperatures at specific frequencies. The presence of chloride shows a clear influence on impedance only in the high frequency range at 0^0F and 70^0F. Nevertheless, the effect of chloride content on the measured impedance at different temperatures is relatively minor

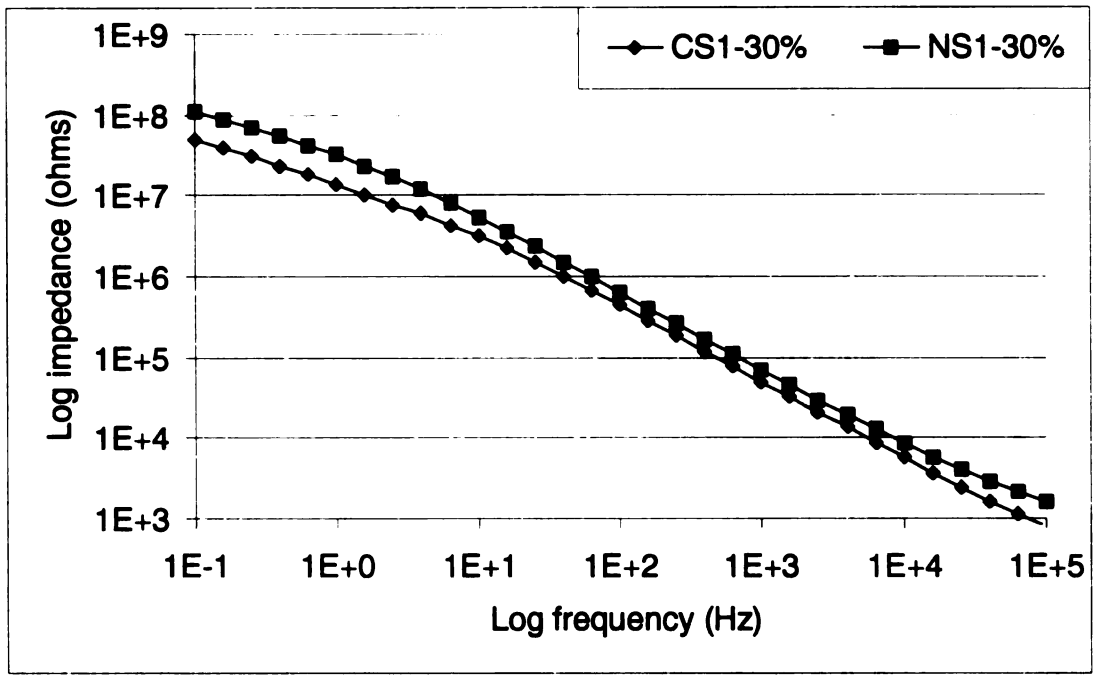

Figure 3-50 Bode magnitude plot of typical impedance spectra for specimens with/without chloride at a relative humidity of 30% (legend gives the name of the specimen: C-chloride, N-non-chloride, Sn-specimen number)

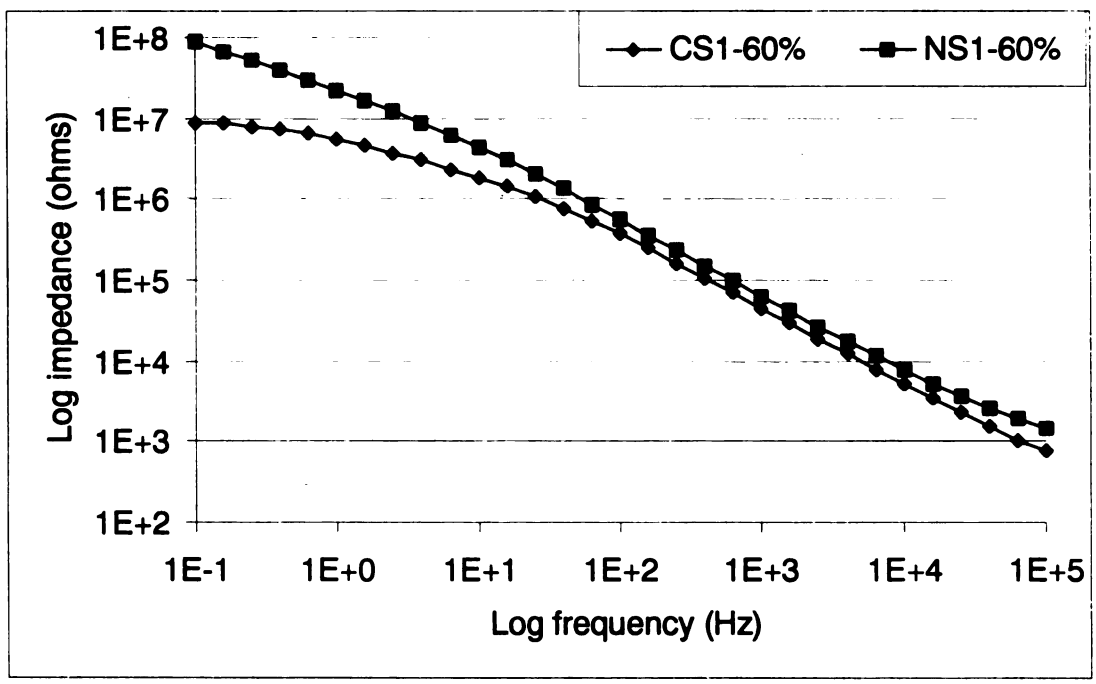

Figure 3-51 Bode magnitude plot of typical impedance spectra for specimens with/without chloride at a relative humidity of 60% (legend gives the name of the specimen: C-chloride, N-non-chloride, Sn-specimen number)

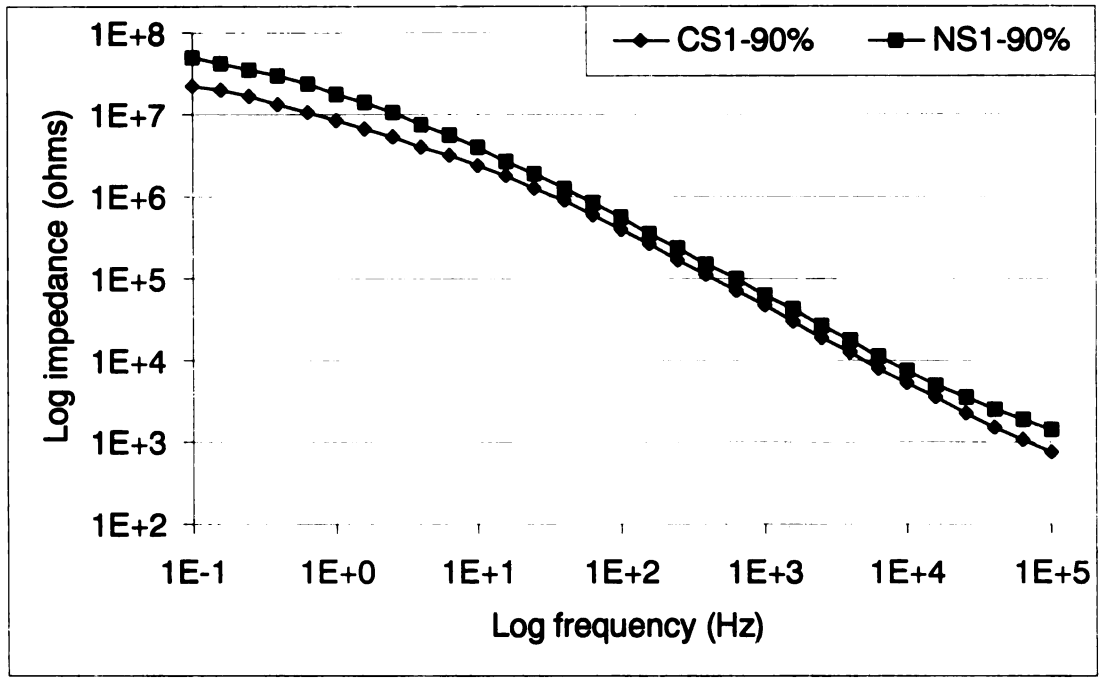

Figure 3-52 Bode magnitude plot of typical impedance spectra for specimens with/without chloride at a relative humidity of 90% (legend gives the name of the specimen: C-chloride, N-non-chloride, Sn-specimen number)

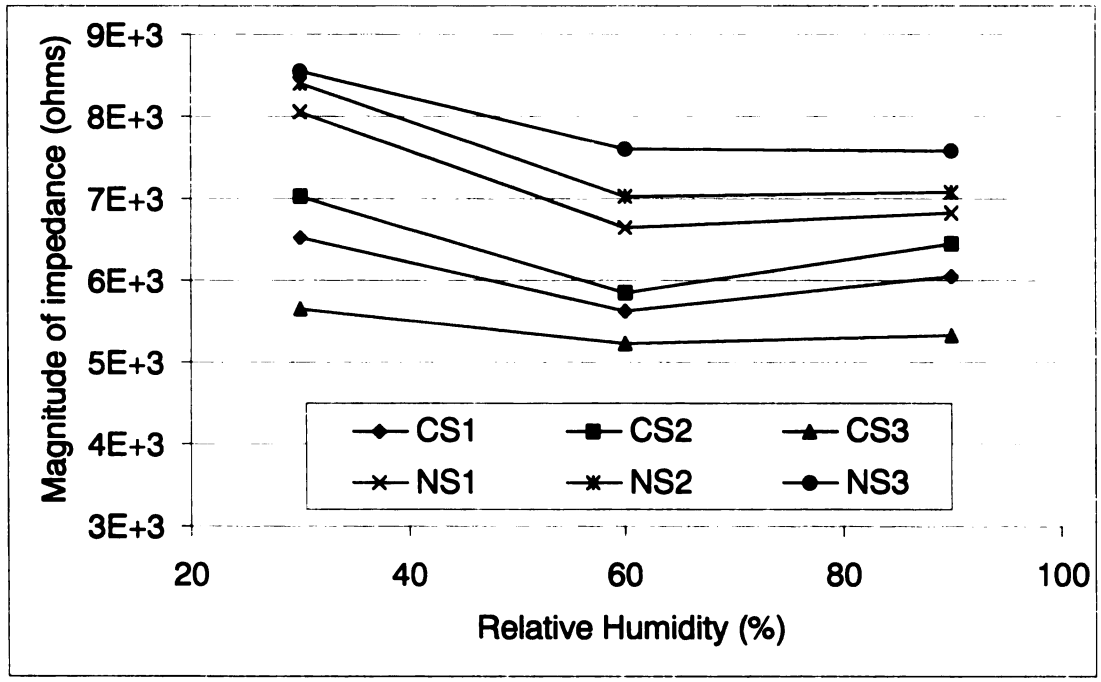

Figure 3-53 Variation of typical measured impedance in the high-frequency range at different humidity levels at 10,000 Hz (legend gives the name of the specimen: C-chloride, N-non-chloride, Sn-specimen number)

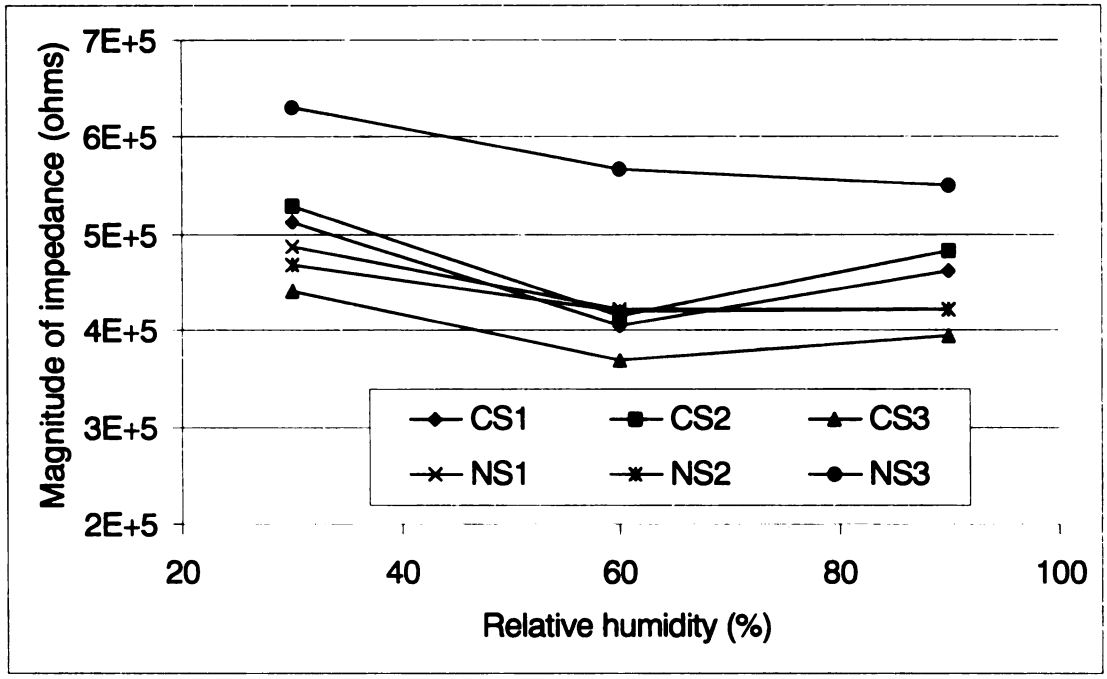

Figure 3-54 Variation of typical measured impedance in the mid-frequency range at different humidity levels at 100 Hz (legend gives the name of the specimen: C-chloride, N-non-chloride, Sn-specimen number)

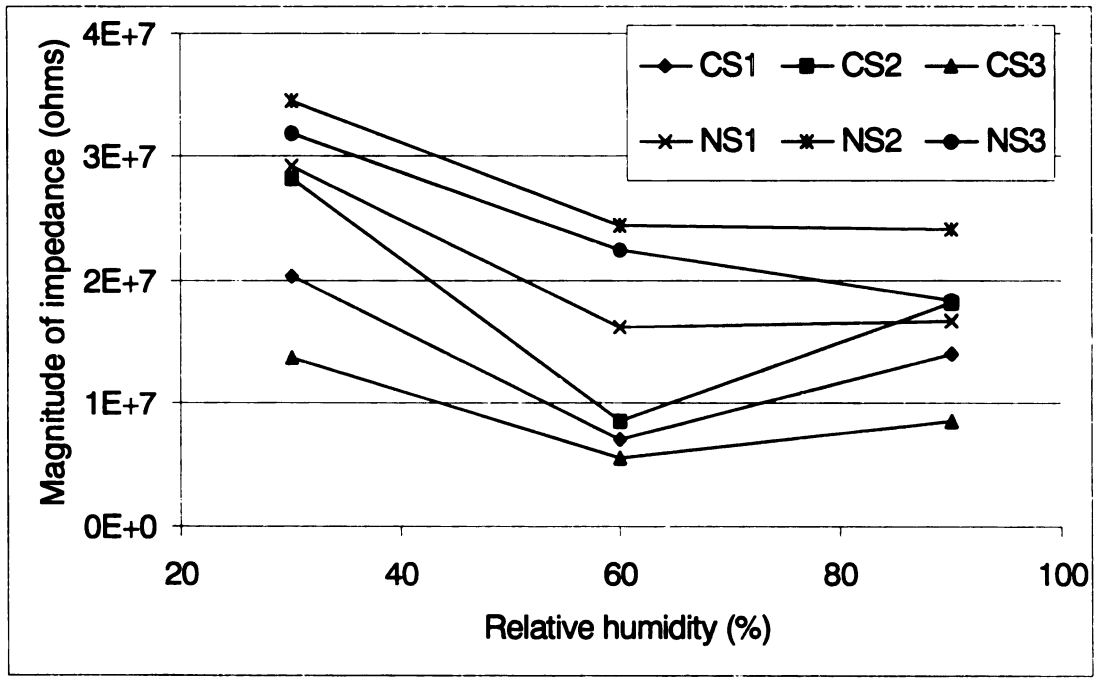

Figure 3-55 Variation of typical measured impedance in the low-frequency range at different humidity levels at 1 Hz (legend gives the name of the specimen: C-chloride, N-non-chloride, Sn-specimen number)

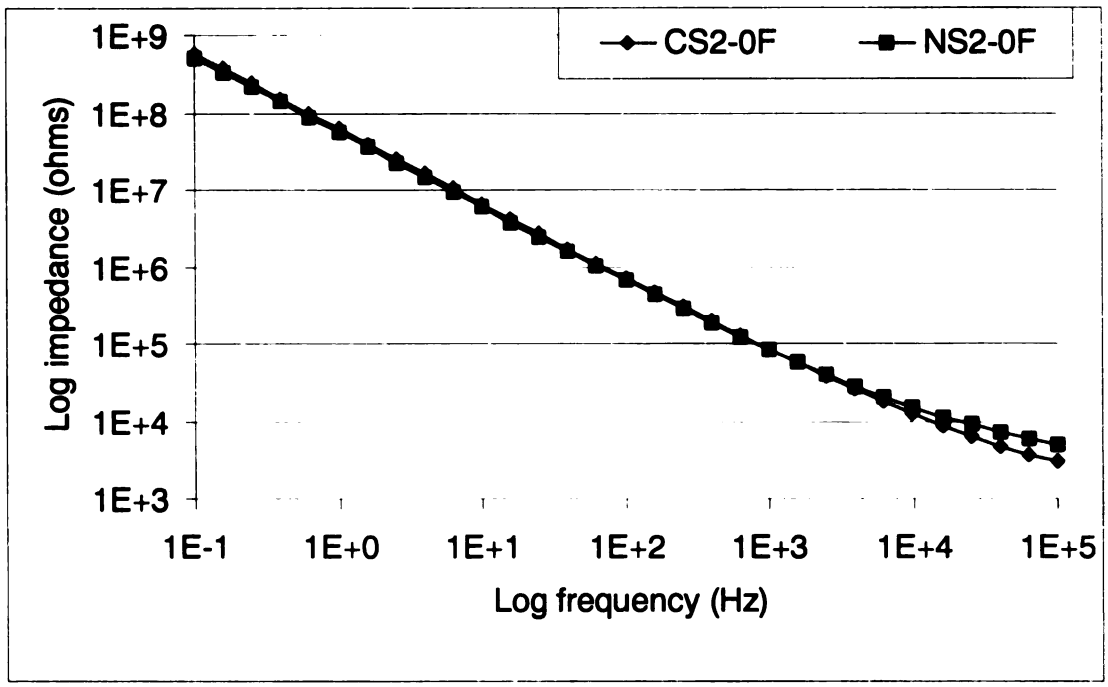

Figure 3-56 Bode magnitude plot of typical impedance spectra for specimens with/without chloride at a temperature of 0^0F (legend gives the name of the specimen: C-chloride, N-non-chloride, Sn-specimen number)

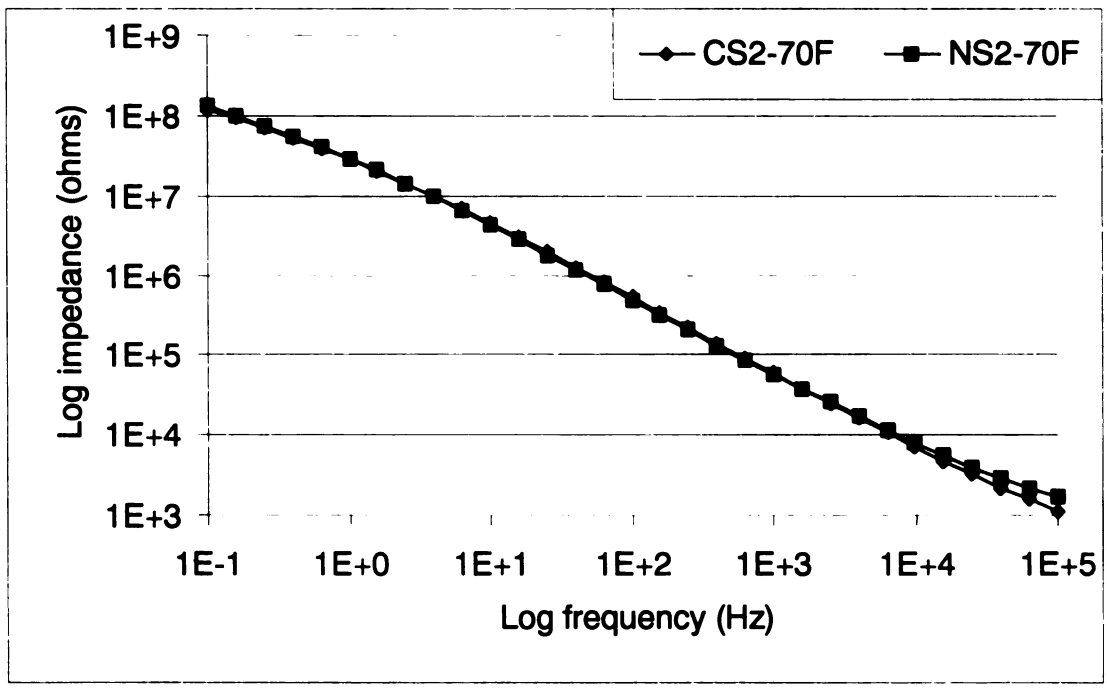

Figure 3-57 Bode magnitude plot of typical impedance spectra for specimens with/without chloride at a temperature of 70^0F (legend gives the name of the specimen: C-chloride, N-non-chloride, Sn-specimen number)

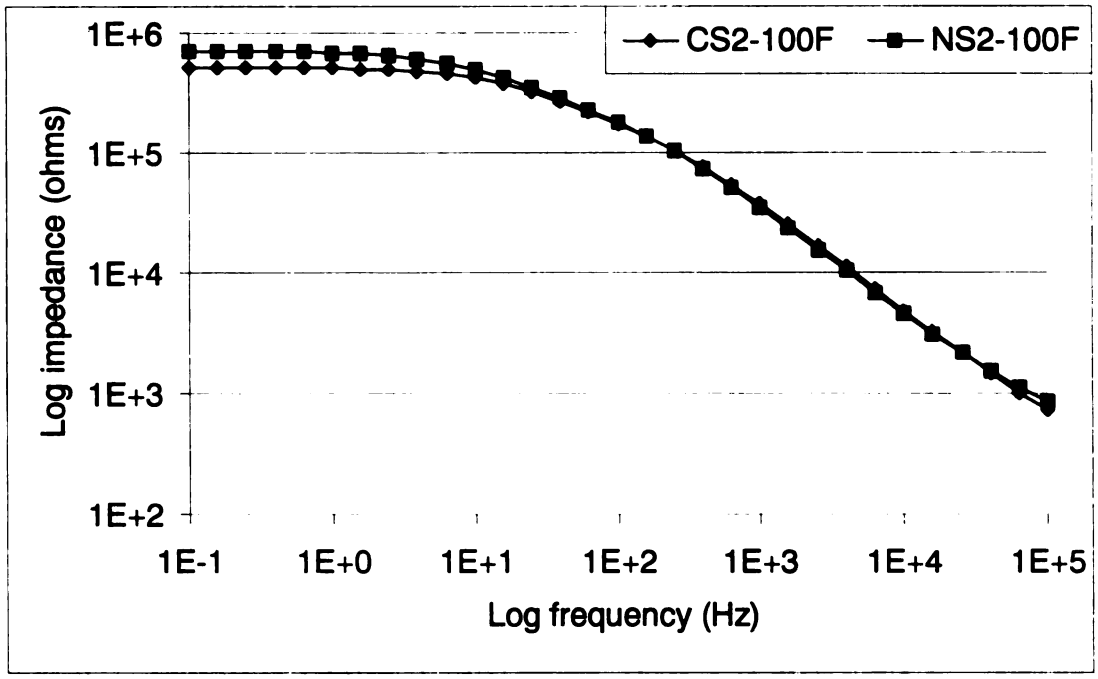

Figure 3-58 Bode magnitude plot of typical impedance spectra for specimens with/without chloride at a temperature of 100^0F (legend gives the name of the specimen: C-chloride, N-non-chloride, Sn-specimen number)

3.3.3.2 Results from equivalent circuit analysis

Figures 3-37 to 3-40 show the effect of chloride content on the equivalent circuit parameters at different humidity levels. The value of the CPE parameter is decreased by the presence of chloride ions in the concrete specimens and the value of the capacitance parameters (C2+C3) is increased. However, there is no clear effect of the presence of chloride ions on the C1 parameter at different humidity levels. In general, chloride content decreases the CPE parameter and increases the C2+C3 parameter in the equivalent circuit analysis.

Figures 3-46 to 3-49 show the variation of the equivalent circuit element parameters due to chloride content at different temperatures. There is no discernible difference in the equivalent circuit parameters due to the presence of chloride. The general scatter in the parameters is within the specimen-to-specimen variation of the parameter values.

3.3.3.3 Summary and Discussion

The chloride ion content in the concrete specimen has a minor influence on the impedance measurements. The existence of chloride ions in the concrete specimens affects the mobility of ions. The combination of chloride ions and humidity variation has a greater impact on the measured impedance than the combination of chloride ions and temperature variations. In general, the presence chloride ions in the concrete specimens lowers the magnitude of measured impedance at any humidity level and decreases the magnitude of the impedance slightly.

3.3.4 Freeze – thaw

3.3.4.1 Comparison of raw impedance spectra

The magnitude of impedance before and after 300 freeze-thaw cycles is plotted in Figure 3-59. The impedance is reduced over the entire frequency range regardless of the water content in the concrete specimens. However, the differences are most significant in the low- and mid-frequency ranges. The differences in the weight of the freeze-thaw specimens before and after freeze-thaw exposure are shown in Table 3-3. The concrete specimens were put in an oven to dry out the excessive water from the freeze-thaw experiment. Specimens 1 and 2 contained slightly less water and Specimen 3 contained slightly more water compared to the time when baseline measurements were taken.

3.3.4.2 Results from equivalent circuit analysis

Figures 3-60 to 3-63 show the variation of the equivalent circuit parameters following freeze-thaw exposure. After 300 cycles of freeze-thaw the CPE parameter dropped significantly. The C1 parameter increased, the C2+C3 parameter decreased, and the C1+C2+C3 parameter showed little change. The variation on the capacitance parameters from the freeze-thaw exposure is bigger than that from the short term environmental conditions (temperature and humidity). In general, 300 cycles of freeze-thaw have a significant influence on the CPE parameter and much smaller influences on the C1, the C2+C3 and the C1+C2+C3 parameter obtained from the equivalent circuit analysis.

3.3.4.3 Summary and Discussion

Freeze-thaw cycles generally tend to deteriorate the concrete and increase the width and density of microcracks. This increases the mobility of ions within the concrete and hence reduces the magnitude of impedance. The results indicate that the reduction in

impedance is most significant in the low- to mid-frequency regions. While the CPE, C1 and C2+C3 parameters from the equivalent circuit analysis display significant changes following freeze-thaw exposure, C1+C2+C3 is generally unchanged.

Table 3-3 Specimen weights before and after freeze-thaw testing

	Weight changes (gram)		
	Specimen 1	Specimen 2	Specimen 3
Before testing	16724	17938	17117
After testing	16674	17922	17123
Differences	-50	-16	6

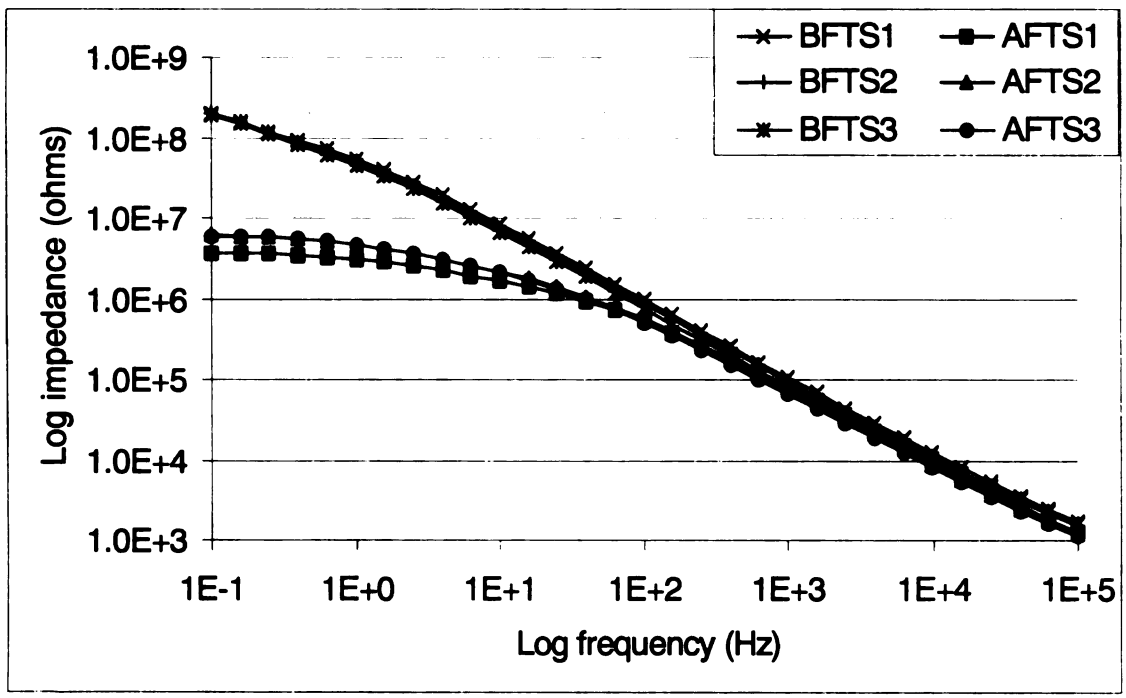

Figure 3-59 Bode magnitude plot of typical impedance spectra from the specimens with chloride for 300 cycles of freeze-thaw (legend gives the name of the specimen: B-before, A-after, FT-freeze-thaw, Sn-specimen number)

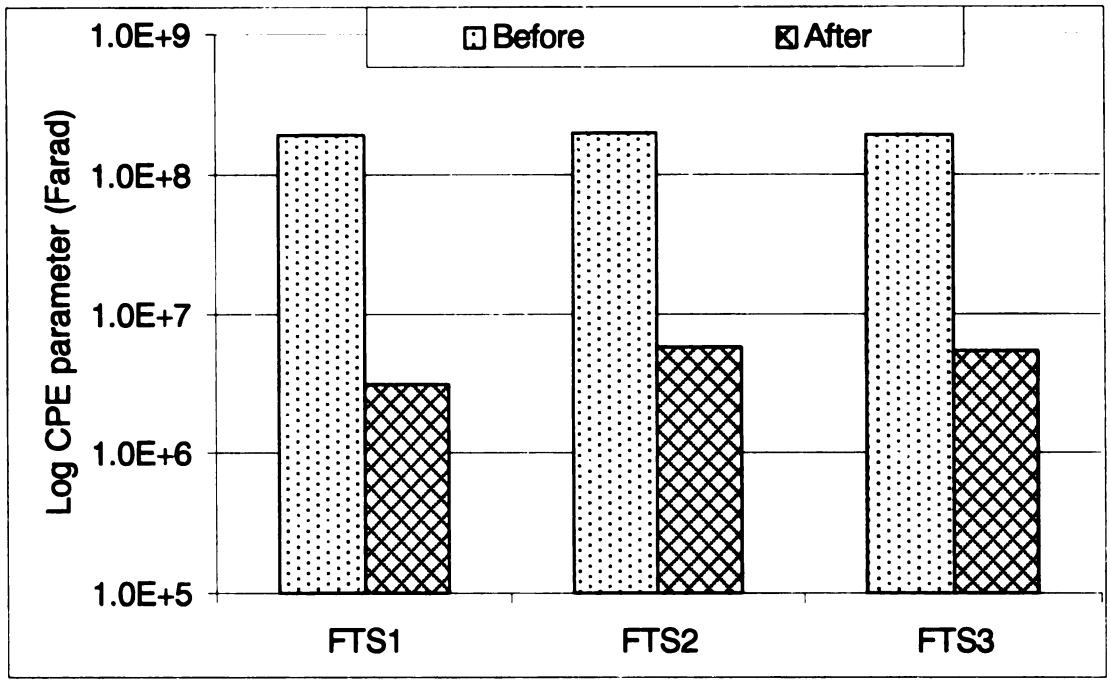

Figure 3-60 Variation of the CPE parameter from before and after 300 cycles of freeze-thaw for measurements from the rebar to external sensors (legend gives the name of the specimen: FT-freeze-thaw, Sn-specimen number)

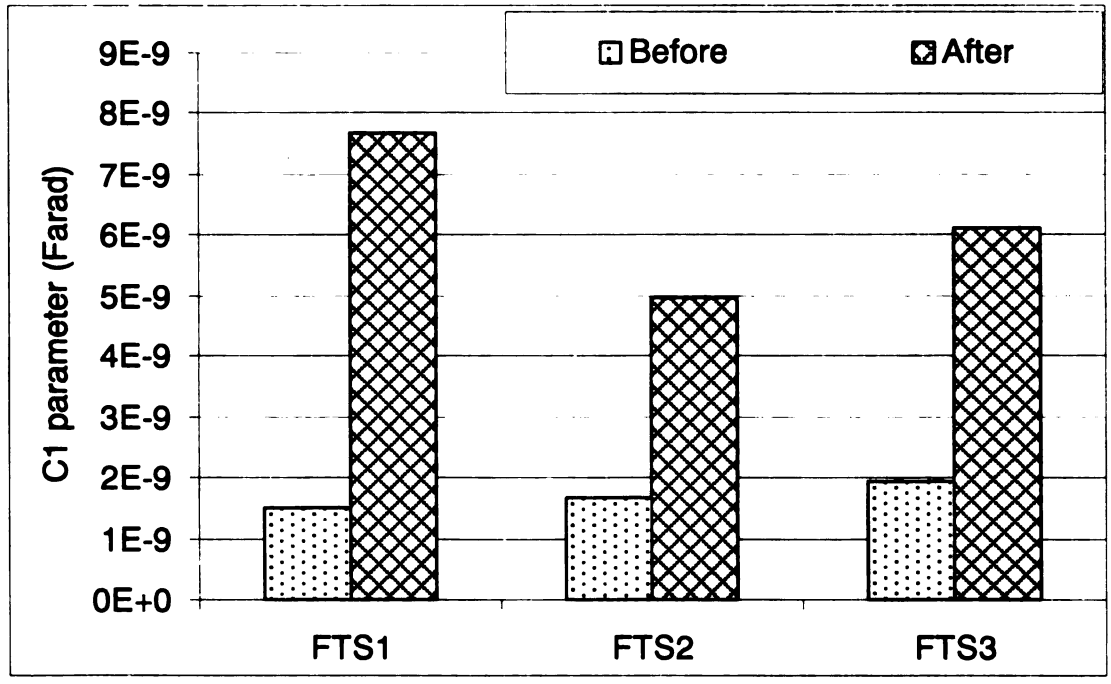

Figure 3-61 Variation of the C1 parameter before and after 300 cycles of freeze-thaw for measurements from the rebar to external sensors (legend gives the name of the specimen: FT-freeze -thaw, Sn-specimen number)

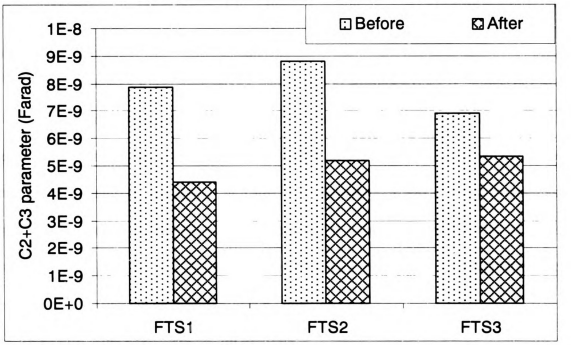

Figure 3-62 Variation of the C2+C3 parameter before and after 300 cycles of freeze-thaw for measurements from the rebar to external sensors (legend gives the name of the specimen: FT-freeze -thaw, Sn-specimen number)

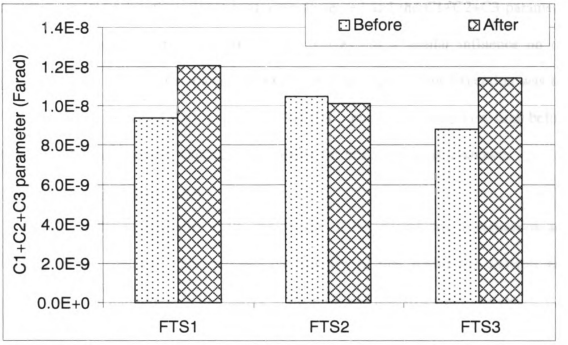

Figure 3-63 Variation of the C1+C2+C3 parameter before and after 300 cycles of freeze-thaw for measurements from the rebar to external sensors (legend gives the name of the specimen: FT-freeze -thaw, Sn-specimen number)

3.3.5 Wetting and drying

3.3.5.1 Comparison of raw impedance spectra

The magnitude of impedance before and after 300 wet-dry cycles is plotted in Figure 3-64. The concrete specimens were put in an oven to dry out the excessive water after the wet-dry experiment. The differences in the weight of the wet-dry specimens before and after wet-dry exposure are shown in Table 3-4. Exposure to 300 wet-dry cycles has a similar influence on the impedance measurements as exposure to 300 cycles of freeze-thaw. Although the decrease in impedance is observed over the entire frequency range, the decrease is largest in the low-frequency range.

3.3.5.2 Results from equivalent circuit analysis

Figures 3-65 to 3-68 show the variation of the equivalent circuit parameters for wet-dry exposure. After 300 wet-dry cycles the CPE parameter decreased significantly, the C1 parameter increased, the C2+C3 parameter decreased and the C1+C2+C3 parameter did not change significantly. The 300 wet-dry cycles has a similar influence on the equivalent circuit element parameters as 300 freeze-thaw cycles. One exception was the WDS3 specimen for which the C2+C3 and C1+C2+C3 parameters were very high before exposure and decreased after exposure. The reason for this anomaly is unknown.

3.3.5.3 Summary and Discussion

Wet-dry cycles increase the width and density of microcraks due to expansion and shrinkage of the concrete. This increases the mobility of ions within the concrete and hence reduces the magnitude of impedance in the mid- and low-frequency regions.

Table 3-4 Specimen weights before and after wet-dry testing

	Weight changes (gram)		
	Specimen 1	Specimen 2	Specimen 3
Before testing	17353	16914	16906
After testing	17336	16899	16906
Differences	-17	-15	0

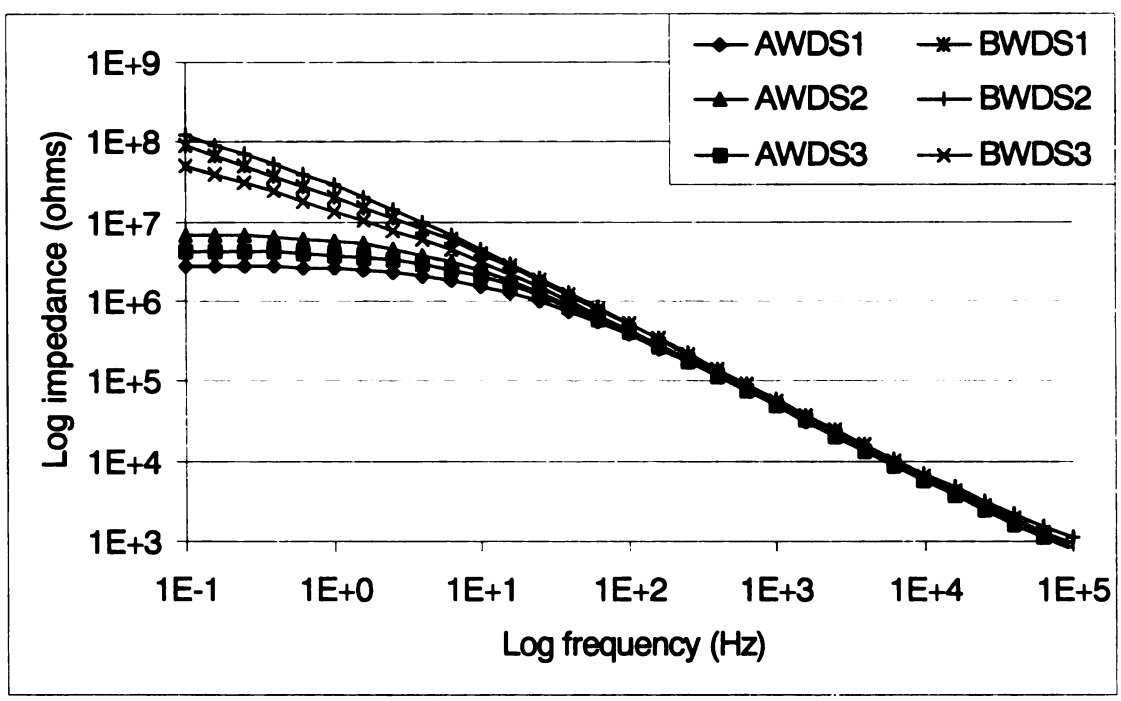

Figure 3-64 Bode magnitude plot of typical impedance spectra for specimens with chloride before and after 300 wet-dry cycles (legend gives the name of the specimen: B-before, A-after, WD-wet -dry, Sn-specimen number)

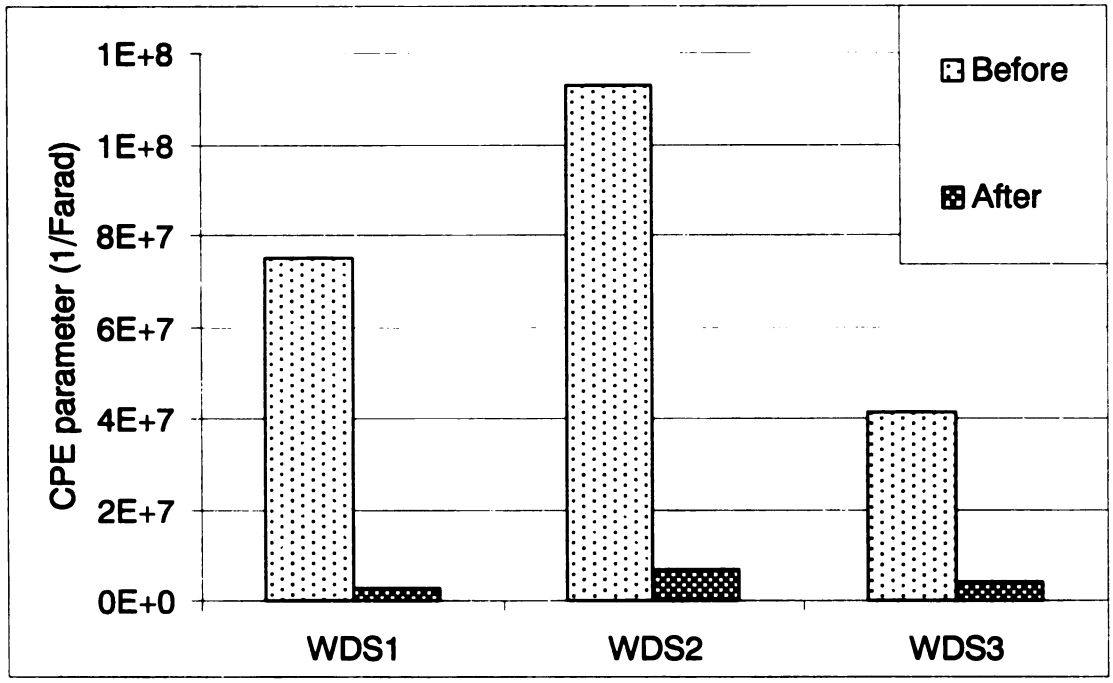

Figure 3-65 Variation of the CPE parameter from before and after 300 cycles of wet-dry for measurements from the rebar to external sensors (legend gives the name of the specimen: WD-wet -dry, Sn-specimen number)

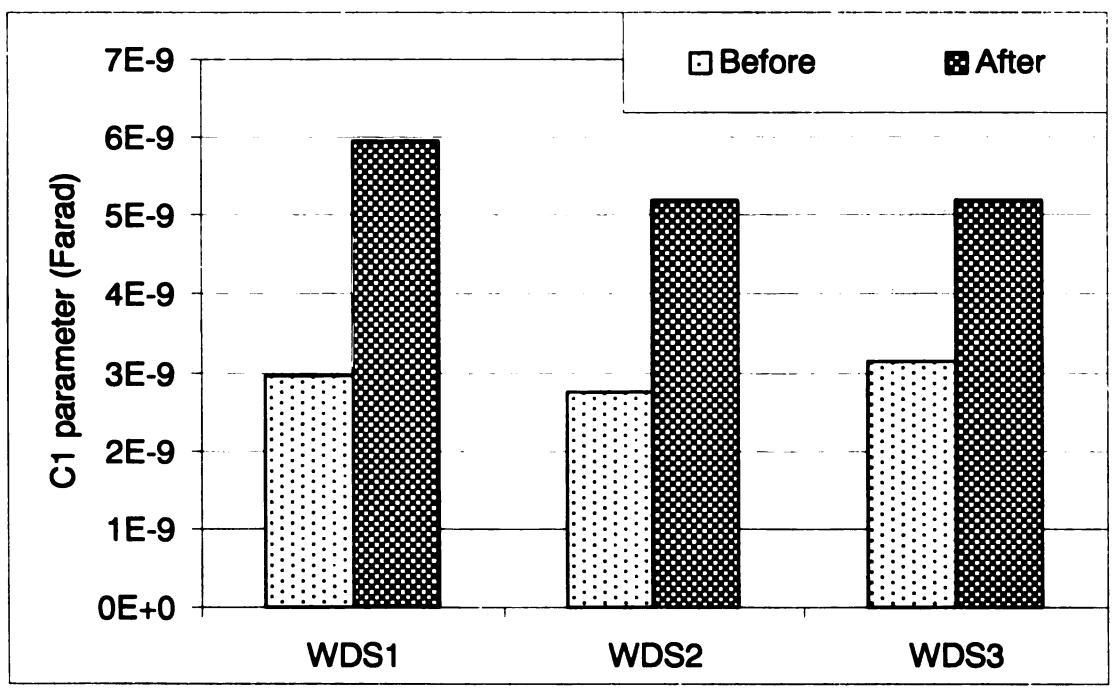

Figure 3-66 Variation of the C1 parameter before and after 300 cycles of wet-dry for measurements from the rebar to external sensors (legend gives the name of the specimen: WD-wet -dry, Sn-specimen number)

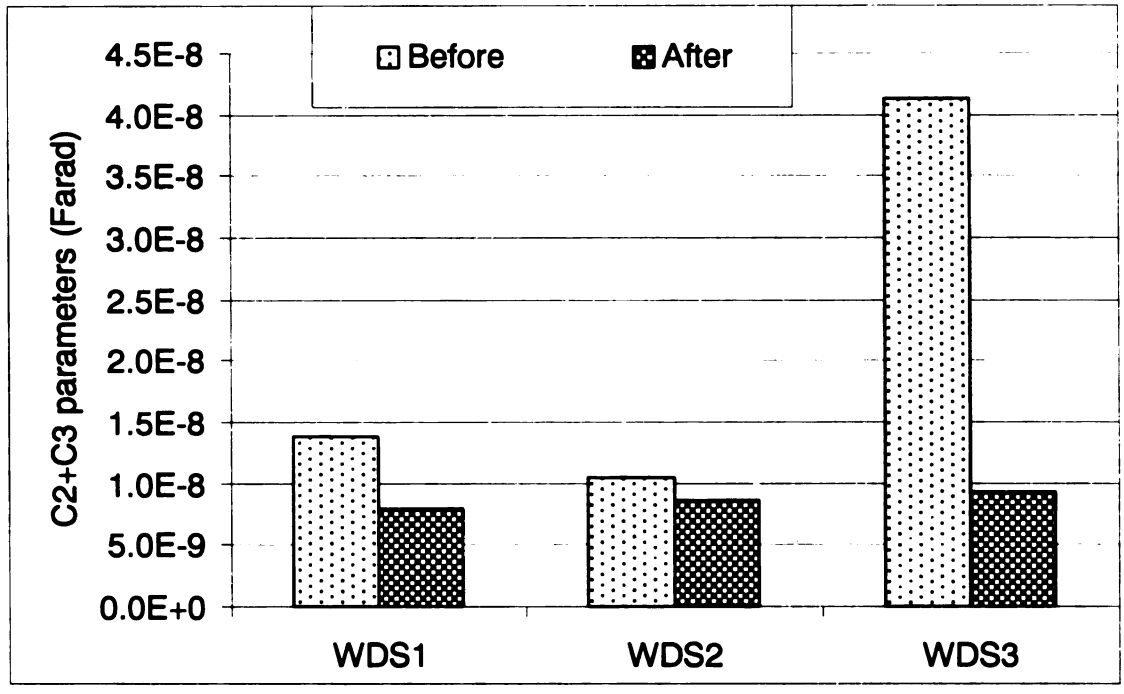

Figure 3-67 Variation of the C2+C3 parameter before and after 300 cycles of wet-dry for measurements from the rebar to external sensors (legend gives the name of the specimen: WD-wet -dry, Sn-specimen number)

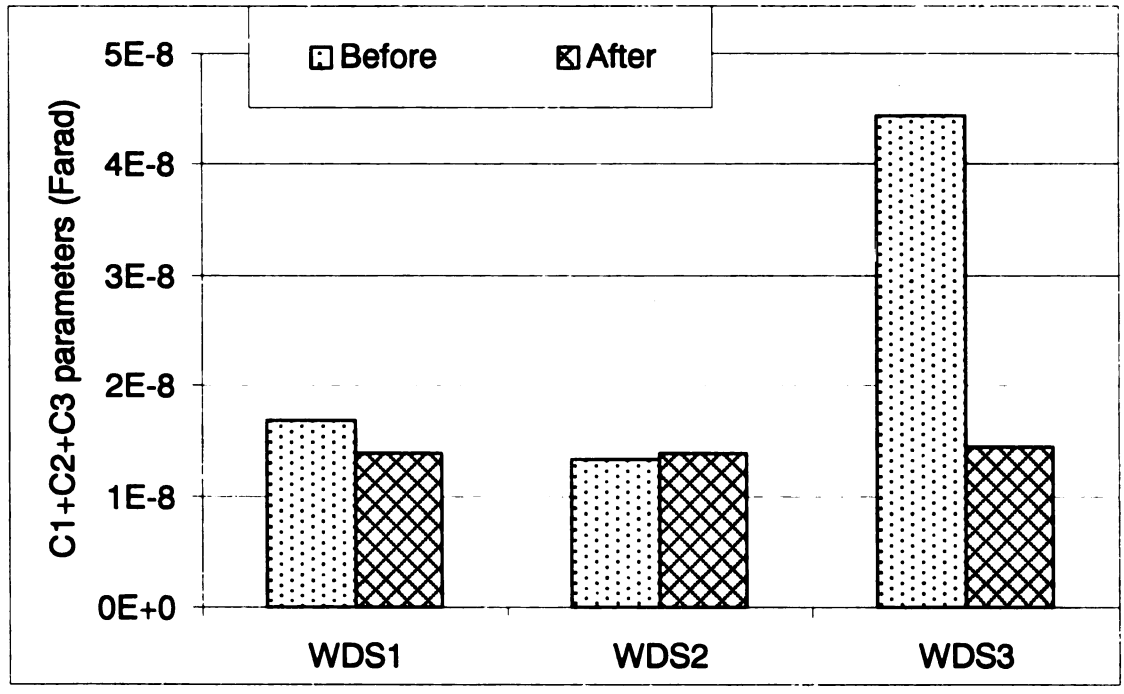

Figure 3-68 Variation of the C1+C2+C3 parameter before and after 300 cycles of wet-dry for measurements from the rebar to external sensors (legend gives the name of the specimen: WD-wet -dry, Sn-specimen number)

3.3.6 Corrosion of reinforcing bar

A constant voltage of 12 V was supplied across the two reinforcing bars to accelerate the corrosion process using an external power source. The applied current was monitored during 21 days of the accelerated corrosion test, since this has a direct correlation with the total corrosion in the reinforcing bar. Steel loss was calculated using the recorded current using (Philips 1992, Pantazopoulou 2001).

$$\Delta W(g) = \frac{I * t * Am}{z * F} \tag{3-1}$$

where ΔW is the steel loss in grams
I is the total recorded current
t is the duration of the test in seconds
Am is the atomic mass of the metal
z is valency (assuming that the rust product is mainly Fe(OH)2, 2 is used for the z value)
F is Faraday's constant

The total steel loss was about 13g for each specimen. This represents an average corrosion depth of about 0.45mm (3.6% loss) over the bar

3.3.6.1 Comparison of raw impedance spectra

Exposure to accelerated corrosion of the reinforcing bar has a similar influence on the impedance measurements as exposure to freeze-thaw and wet-dry cycles. The magnitude of measured impedances before and after accelerated corrosion are plotted in Figures 3-69. The impedance in the low- and mid-frequency range decreased. The differences in the weight of the specimens before and after the corrosion test are shown in Table 3-5. Some of the mass loss is probably due to the diffusion of corrosion products into the water used to periodically wet the specimens. The concrete specimens were put in an oven to dry out the excessive water from the corrosion experiment.

3.3.6.2 Results from equivalent circuit analysis

Figures 3-70 to 3-73 show the changes in the equivalent circuit parameters after the accelerated corrosion test. The CPE parameter decreased significantly after accelerated corrosion for 21 days. The capacitance parameters do not change significantly due to corrosion of the reinforcing bar in the concrete specimens. The C1 parameter increased slightly, and the C2+C3 and C1+C2+C3 quantities did not change significantly.

3.3.6.3 Summary and Discussion

The electrical properties of the reinforcing bar and surrounding concrete may change due to corrosion of the reinforcing bar and the presence of corrosion products in the concrete. The corrosion test was setup to study the effect of corrosion of the reinforcing bar on the impedance measurements. It is found that the corrosion of the reinforcing bar significantly lowers the impedance in the low-frequency range, but has a much smaller influence on the measured impedance in the mid- and high-frequency ranges. As a consequences, corrosion of the reinforcing bar has a significant influence on the CPE parameter from the equivalent circuit analysis, and has a much smaller influence on the capacitance parameters.

Table 3-5 Specimen weights before and after corrosion testing

	Weight changes (gram)		
	Sample 1	Sample 2	Sample 3
Before testing	17734	17755	17600
After testing	17723	17681	17564
Differences	-11	-74	-36

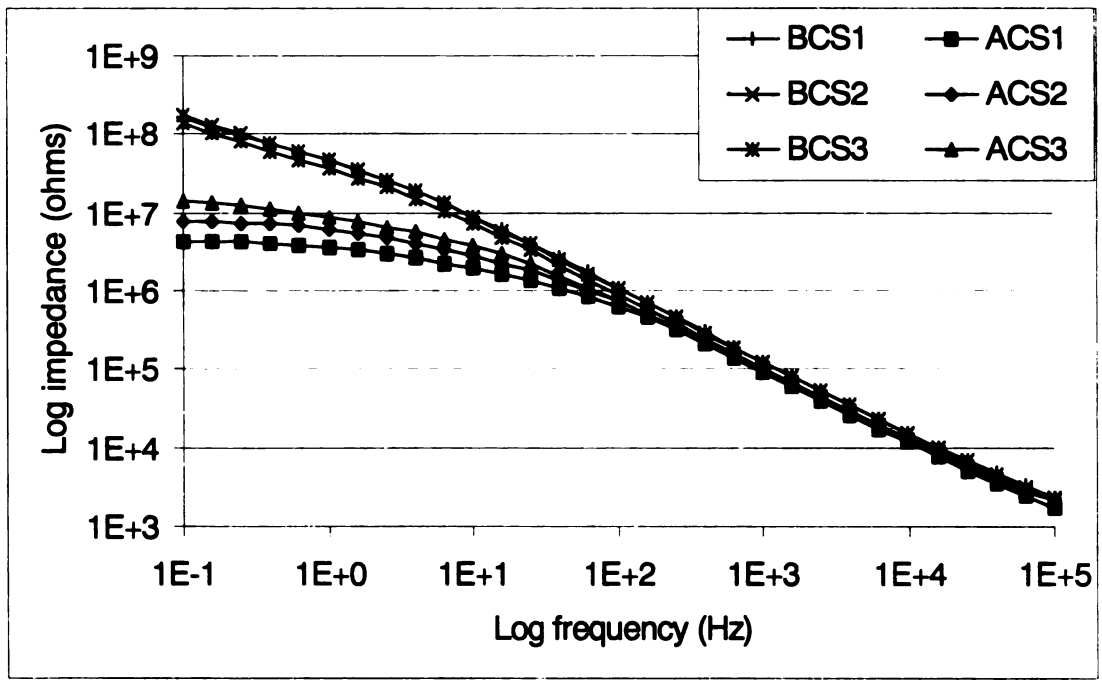

Figure 3-69 Bode magnitude plot of typical impedance spectra from the specimens with chloride for 21 days of corrosion on the rebar (legend gives the name of the specimen: B-before, A-after, C-corrosion, Sn-specimen number)

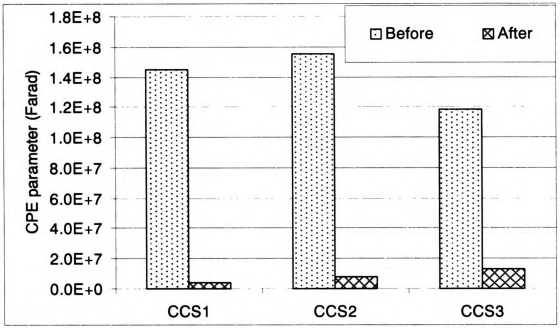

Figure 3-70 Variation of the CPE parameter from equivalent circuit analysis for specimens with chloride before and after 21 days of rebar corrosion for measurements from the rebar to external sensors (legend gives the name of the specimen: C-chloride, C-corrosion, Sn-specimen number)

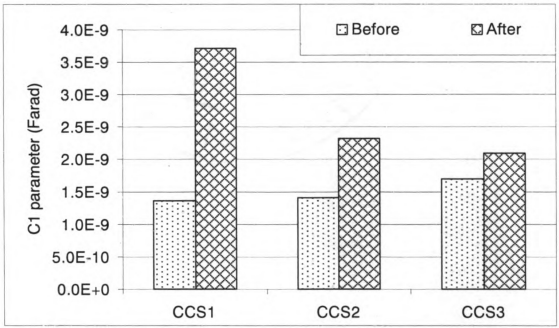

Figure 3-71 Variation of the C1 parameter from equivalent circuit analysis for specimens with chloride before and after 21 days of rebar corrosion for measurements from the rebar to external sensors (legend gives the name of the specimen: C-chloride, C-corrosion, Sn–specimen number)

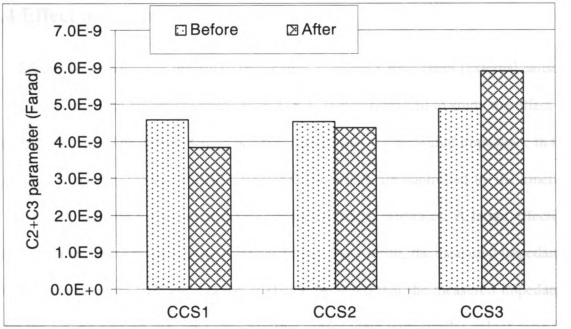

Figure 3-72 Variation of the C2+C3 parameter from equivalent circuit analysis for specimens with chloride before and after 21 days of rebar corrosion for measurements from the rebar to external sensors (legend gives the name of the specimen: C-chloride, C-corrosion, Sn-specimen number)

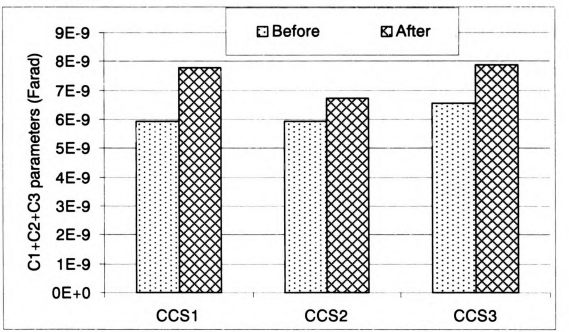

Figure 3-73 Variation of the C1+C2+C3 parameter from equivalent circuit analysis for specimens with chloride before and after 21 days of rebar corrosion for measurements from the rebar to external sensors (legend gives the name of the specimen: C-chloride, C-corrosion, Sn-specimen number)

3.4 Effect of electrode size

Figure 3-74 shows the measured impedance from the CFRP sheet (external sensor) to the different sized electrodes in the 6" x 2' x 1' slab constructed to study the effect of the electrode size. The different electrode sizes affect only the measured impedance in the very high frequency region (10,000 - 1000,000 Hz) which are controlled by the kinetics of the charge transfer processes at the electrode/electrolyte interfaces. A larger effective electrode area increases the kinetic potential energy. As a result, the measured impedance decreases in the high frequency range. It should be noted that the measured impedance from the E3, E4 and E5 sensors to the external sensor yield very similar values over the entire frequency range. This suggests that increasing the electrode size beyond a certain limit does not have a significant impact on the measured impedance. This is also reflected in the measured impedance from the stainless steel bar and the reinforcement cage to the external sensor for the eight-foot long beam (Figure 3-21). The measured impedance from the stainless steel bar and the reinforcement cage were very similar to each other even in the high frequency region.

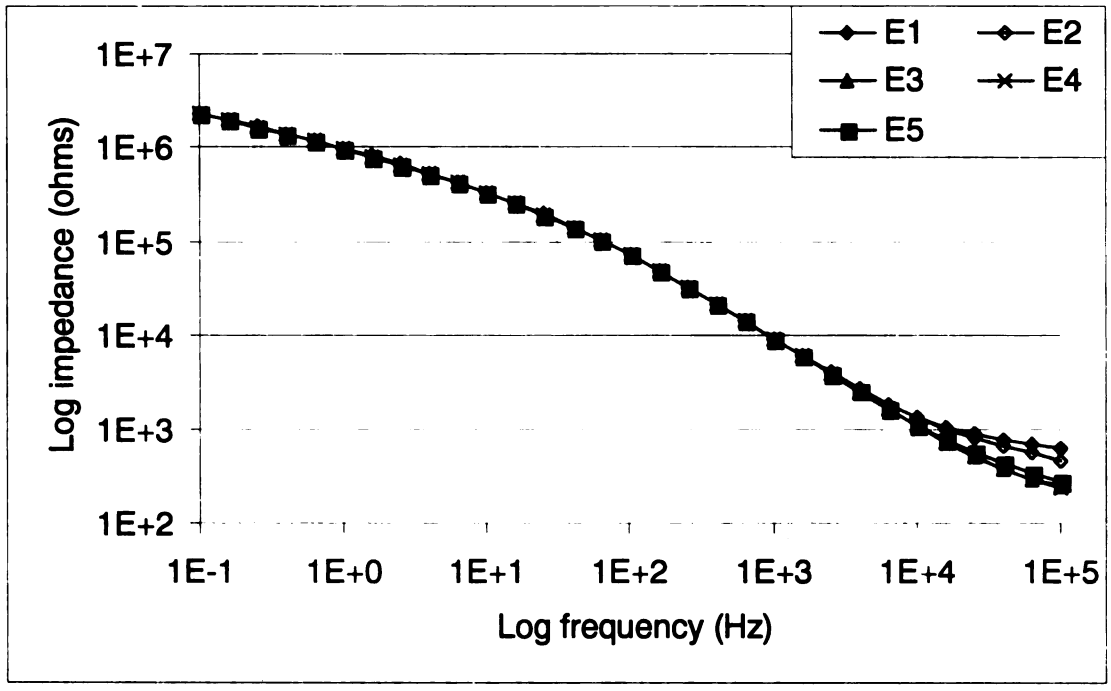

Figure 3-74 Bode magnitude plot of impedance spectra from the slab with different sized sensors (legend gives the name of the sensor: E1-0.034" dia., E2-0.25" dia., E3-0.5" dia., E4-0.59" dia., E5-0.75" dia.)

Chapter 4

Summary, Conclusions, and recommendations for Future Work

4.1 Summary

An experimental study was conducted to assess whether electrochemical impedance spectroscopy (EIS) could be used to detect the debonding of external CFRP reinforcement on concrete structures. The EIS-based sensing technology used in this study was adopted from work done by Davis et al. (1999) on composite/composite bonds.

Wedge tests were conducted with several 6" x 6" x 24" specimens and one 1.5' x 2' x 8' specimen to investigate the detection of CFRP debonding. Sensor elements (electrodes) consisted of: (a) copper tape with a conductive adhesive applied to the outside of the CFRP; (b) stainless steel wire placed in grooves on the bottom face of the concrete prior to bonding the CFRP; and (c) reinforcing bars. Experimental studies were conducted to also determine the influence of different environmental conditions on impedance measurements. The environmental conditions included: (1) variation of humidity levels; (2) variation of temperature levels; (3) chloride content in the concrete specimen; (4) 300 freeze-thaw cycles; (5) 300 wet-dry cycles; and (6) 21 days of accelerated corrosion of a reinforcing bar.

Impedance measurements were taken between pairs of sensors using a potentiostat. The measurements were analyzed by comparing the raw impedance spectra and using equivalent circuit analysis. The raw impedance measurements for different environmental conditions and different debonded lengths were compared either over the entire

frequency range or at specific frequencies. An equivalent circuit was conceived and fitted to each measured impedance spectrum and the circuit parameters were estimated. The fitted circuit parameters were compared for measurements from different environmental conditions and to different CFRP debond lengths. The raw impedance measurements and the fitted capacitance parameters (C1+C2+C3) for different debonded lengths are also fitted to the empirical formula (Equation 3-5)

4.1.1 Detection of CFRP Debonding

Variations in the measured impedance spectra and the equivalent circuit parameters due to debonding of the CFRP sheet was studied in a controlled environment (controlled temperature and humidity) and in an ambient condition (fluctuating temperature and humidity). Impedance measurements taken between the rebar and the extended copper tape sensors were most effective for assessment of the total debonded area. Impedance measurements taken between pairs of internal wire sensors were capable of revealing the location of debonded regions.

CFRP debonding increased the measured impedances over the entire frequency range when the wedge test was conducted in the controlled environment. However, when the wedge test was conducted in the ambient condition, the measured impedances from the low- and mid-frequency range were influenced by the different temperature and humidity levels. The CFRP debonding effect was most clearly observed with the impedance at high-frequencies regardless of the environmental condition. The measured impedance at a given high frequency increases exponentially as the debond length increases. It is found that different effective electrode areas (size effect) has a significant influence on the measured impedance. A larger effective electrode area decreases the magnitude of measured impedance significantly. The debonding of the CFRP was

capable of being detected without interference from environmental conditions by impedances measured in the very high-frequency range from about 10,000 to 100,000 Hz. For the large specimen, even the high frequency impedances were influenced by the environmental conditions. The increase effective electrode areas for the lorge beam reduced the impedance magnitudes, and it is postulated that this made the measurements more sensitive to environmental effects.

The CPE parameter in the equivalent circuit correlated well with debonded area in the controlled environment but was strongly influenced by variations in temperature and humidity. Capacitance parameters also correlated well with the debonded area and were not too sensitive to environmental factors. All capacitance parameters showed a linear correlation with the debonded area for the wedge test on two-foot long specimens. The sum of all capacitances (C1+C2+C3) showed the least sample-to-sample variation. For the wedge test on the large beam the sum of the capacitances (C1+C2+C3) showed an exponentially decaying variation with debonded area with high sensitivity for initial debonding up to about 10% of the total CFRP area.

The raw impedance measurements from the high frequency region and the fitted capacitance parameters (C1+C2+C3) for different debonded lengths were fitted to an empirical formula. Although the fit were always excellent, the parameters of the empirical formula vary significantly from sample to sample and therefore a formula for diagnosis cannot be readily proposed.

4.1.2 Environmental effects

The influence of short-term environmental effects including different humidity levels, different temperature levels and chloride content in the concrete on the impedance measurements were studied using small specimens. These environmental factors have a significant influence on the magnitude of impedance measured in the low- and mid-frequency range, but have a much smaller influence on the magnitude of impedance in the high-frequency range. Increased water content due to high humidity lowered the magnitude of impedance, and reduced water content due to low humidity increased the magnitude of impedance. High temperature decreased the magnitude of impedance significantly in the low- and mid-frequency range. The presence of chloride ions in concrete increased the impedance measurements in the low- and mid-frequency range.

The influence of long-term environmental conditions including freeze-thaw and wet-dry cycles and corrosion of the reinforcing bar on the measured impedance were also studied. Impedance measurements were taken before and after small concrete specimens were subjected to 300 freeze-thaw and wet-dry cycles. Impedance measurements were also taken before and after one reinforcing bar in each small specimen was subjected to accelerated corrosion to study the effect of corrosion on the measured impedance, especially when the rebar was used as a sensing element. These long-term environmental conditions had a significant influence on the measured impedance in the low-frequency range and had much less of an influence in the high-frequency range. The magnitude of impedance in the low-frequency range was reduced after the environmental exposure.

In the equivalent circuit, the R1, C1 and CPE parameters control the impedance in the low-frequency region and the C2, C3, R2 and R3 parameters control the impedance in the mid- and high-frequency regions. The different environment conditions had a

significant influence on the CPE parameter and had much less of an influence on the capacitance parameters from the equivalent circuit analysis. High temperature and high moisture content in concrete decreased the CPE parameter and increase the capacitance parameters. Low temperature and low moisture content in concrete had the opposite effects. Chloride content in concrete decreased the CPE parameter and increased the capacitance parameters. Freeze-thaw cycles, wet-dry cycles and corrosion of the rebar increased the CPE and C1 parameters and decreased the C2+C3 values. The sum of all capacitance parameters (C1+C2+C3) showed the least variation after exposure to the long-term environmental conditions.

4.2 Conclusions

Impedance measurements taken between steel reinforcement and copper tape sensors mounted on the outside of external CFRP reinforcement are effective for estimating the total debonded area of CFRP. Measurements taken in the high-frequency range (1000 – 100,000 Hz) are the most reliable since they are not strongly influenced by environmental conditions. A more reliable approach is to perform equivalent circuit analysis using the circuit used in this work, and use the sum of the capacitance parameter (C1+C2+C3) as a measure of the total debonded area of CFRP. The impedance magnitude at a given high frequency (say 100,000 Hz), and C1+C2+C3 values correlate well with the debonded area of CFRP and are not strongly affected by environmental conditions. The impedance at high frequencies is dominated by the kinetics of the charge transfer processes at the electrode/electrolyte interfaces, which appear to be influenced strongly by the debonding of the CFRP.

Impedance measurements taken between pairs of internal stainless steel wire sensors placed in grooves cut into the bottom face of concrete beams before the CFRP is bonded are effective in locating debonded regions. The magnitude of impedances at low frequencies taken between a pair of sensors in the debonded region are much higher than those taken between a pair of sensors in the bonded region. The CPE parameter from the equivalent circuit analysis is the most effective measure for detecting the location of debonded regions. The CPE parameter value corresponding to impedance measurements between sensors in the debonded area is about two orders of magnitude larger than the value corresponding to impedance measurements between sensors in the bonded area.

Short-term environmental conditions including humidity, temperature, and chloride content affect the impedance measurements at low frequencies. The short-term environmental conditions affect the rate of ions diffusion through the concrete, which is the dominant mechanism for charge transfer at low frequencies. Increased moisture content, and temperature, and the presence of chloride, increase the charge transfer rate and hence reduce the impedance at low frequencies.

Long-term environmental conditions including freeze-thaw and wet-dry cycles, and corrosion of the steel reinforcement, also affect the impedance measurements at low- and mid-frequencies. The long-term environmental conditions promote the growth of micro and macro cracks within the concrete. Repeated expansion and shrinkage due to freeze-thaw and wet-dry cycles increase micro cracking. The expansion of volume associated with corrosion of the rebar causes cracking of the concrete. The increase in voids increases the diffusion rate of ions and thereby reduces the magnitude of impedance at low frequencies.

4.3 Recommendations for Future Work

The EIS-based sensor technology shows strong promise for effective NDE of concrete structures strengthened with CFRP sheets. However, results from this purely experimental research indicate that the EIS-based impedance measurements are influenced significantly by environmental conditions and different effective electrode areas especially in the low- and mid-frequency range. It is also observed that the measured impedance can have significant sample-to-sample variation.

A significant contribution to the further enhancement of this work would be the development of a numerical approach for modeling the charge transfer process through the specimen. This can be most effectively done at the macro-scale by using a 3-D finite element model to represent the concrete structure, reinforcement and sensors and effective electrical properties to represent the current condition through the various component. The effective electrical properties of concrete would need to be characterized with respect to temperature, humidity, chloride content, and microcrack width and density. Once such a model is developed it can be used to study different structureal components reinforced with CFRP, develop optimal sensor arrangements, and develop nomographs that can be used for diagnosis of CFRP debonding.

REFERENCES

Bard, A.J., and Faulkner, L.R. (1980). *Electrochemical methods: fundamentals and application*. Interscience Publication, New York.

Buyukozturk, O., and Hearing, B. (1998). "Failure behavior of precracked concrete beams retrofitting with FRP." *Journal of composites for construction*: 138-144.

Dai, S.T., and Labuz, J.F. (1998). "Damage and failure analysis of brittle materials by acoustic emission" *Journal of Materials in Civil Engineering*, Vol. 9 (4).

Davis, G.D., Dacres, C.M. and Krebs, L.A. (1999). "In-Situ sensor to detect moisture intrusion and degradation of coatings, composites, and adhesive bonds." *Proc. Tri-Services conference on corrosion,* Myrtle Beach, South Carolina.

Davis, G.D., Krebs, L.A., Drzal, L.T., Rich, M.J., and Askeland, P. (2000). "Electro-chemical sensors for nondestructive evaluation of adhesive bonds." *J. Adhes.* 72:335-358.

Gamry Instruments, (1999). *Gamry framework system User's manual* revision 3.1.

Gamry Instruments, (April 2003) "Application notes: Equivalent circuit modeling using the Gamry EIS300 electrochemical impedance spectroscopy software." Gamry Instruments, July 2003. <http://www.gamry.com/G2/Appnotes/Reference/EISModeling/EISModeling.htm>

Karbhari, V.M., and Zhao, L. (2000). "Use of composites for 21st century civil infrastructure." *Computer Method in Applied Mechanics and Engineering* 185: 433-454.

Macdonald, J.R. (1987). *Impedance spectroscopy: emphasizing solid materials and systems* : Wiley-Interscience Publication, New York.

Mirmiran, A., Shahawy, M., and Echary, J. (1999). "Acoustic emission monitoring of hybrid FRP-concrete columns." *Journal of Engineering Mechanics*, Vol 125 (8).

Mirmiran, A., and Yunmei, W. (2001) "Damage assessment of FRP-encased concrete using ultrasonic pulse velocity." *Journal of Engineering Mechanics*, Vol 127 (2): 126-135.

Nguyen, D.M., Chan, T.K., and Cheong, H.K. (2001). "Brittle failure and bond development length of CFRP-concrete beams." *Journal of Composites for Construction.* February: 12-17.

Olajide, D., Laurence, J., and Rami M. (2000). "Ultrasonic monitoring of material degradation in FRP composites." *Journal of Engineering Mechanics* Vol. 126 (7): 704-710.

Pantazopoulou, S., Bonacci, J, Sheikh, S., Hearn, N., and Thomas, M. (2001). "Repair of corrosion-damaged columns with FRP wraps." *Journal of composites for construction.* Vol. 5 (1): 3-11.

Philips, J. (1992). "The effect of corrosion on the structural performance of new and repaired one-way slabs." PhD thesis, Dept. of Civ. Engineering, University of Toronto.

Rahimi, H., and Hutchinson, A. (2001). "Concrete beams strengthened with externally bonded FRP plates." *Journal of Composites for Construction.* February : 44-56.

Scully, J., and Kendig, M. (1989). "Basic aspects of the application of electrochemical impedance for the life prediction of organic coatings on metals." *Proc. Corrosion 89* Paper 32, NACE.

Appendix—A: Data Collection and Equivalent Circuit Analysis Procedure

This section provides a step-by-step description of the procedures used to measure impedances and perform equivalent circuit analysis. Additional information is provided in the User's Manual for the Gamry Framework software.

A-1 Software Procedure for Data Collection

The procedure described below is based on the Gamry Framework software version 3.20.

1. Connect the blue, green and white cables on the potentiostat to one sensor and the red and orange cables to the second sensor.
2. Run the Gamry Framework software.
3. From the Gamry Framework menu bar, select *Experiment*, click on *A Electrochemical Impedance*, and click on *Potentiostatic EIS* to launch the Potentiostatic EIS window.
4. Necessary information can be filled out on the Potentiostatic EIS window or retrieved from a saved template setup file.
5. To use a the saved template setup file, click on the *Restore* button located at the top of the Potentiostatic EIS window, to display the Restore Setup window.
6. From the Restore Setup window, select a proper template setup file and select a stored setup (each template setup file can contain several different setting), and then click on the Restore button (this brings back to the Potentiostatic window).
7. Specify the output file name and click the *OK* button.

A-2 Equivalent circuit analysis procedure

The procedure described below is based on The Gamry Echem Analyst application version 1.02.

1. Run the Gamry Echem Analyst application
2. Open the measured EIS data file by clicking *File* on the menu bar, clicking *Open File*, then selecting the EIS file.
3. Click *Impedance* on the menu bar and then click *Fit A Model.* This brings up the *Select Model File* window. Since the parameters of an electrical circuit which has an theoretical impedance similar to that of the measured impedance are estimated, selecting a proper equivalent circuit is very important.
4. Once the proper equivalent circuit model is selected, the *Impedance Fitting* window is displayed. The nonlinear least squares fitting procedure requires initial values to be specified. The initial values for each equivalent circuit are stored with the circuit. To check whether the initial values are reasonable for the measured data, click *Preview* in the *Impedance Fitting* window.
   4.1. If the impedance generated by the equivalent circuit does not match the measured impedance, then the initial value should be changed to obtaina better match. The initial values for the equivalent circuit element parameters used in this research are listed in Table A-1. Figure A-1 shows the fitted impedance using poor initial values.
   4.2. The C1, R1 and CPE parameters controls the fitted impedance in the low-frequency range and the C2, R2, C3 and R3 parameters controls the fitted impedance in the mid- and high-frequency ranges. Use the *Preview* function and

adjust the initial value of the parameters. If the initial values are within a factor of 100 and the shapes of the impedance spectra generated by the initial values are similar to the measured spectra then the equivalent circuit model will usually yield a good fit.

4.3. Once reasonable initial values are obtained, the fitting program will converge on parameters that yield a theoretical impedance close to the measured impedance. Figure A-2 shows the fitted impedance with the initial values of the parameters and the fitted impedance from the final converged values of the parameters. The fitting program uses a Levenberg-Marquardt non-linear least square fitting algorithm.

5. To finalize the fitting process, click the *Calculate* button in the *Impedance Fitting* window.

Table A- 1. Initial values of equivalent circuit element parameters

Parameter	Rebar to External		Internal to Internal		Internal to External	
	Low	High	Low	High	Low	High
R1	1.0E+03	1.0E+07	1.0E+08	1.0E+08	1.0E+05	1.0E+08
C1	1.0E-07	1.0E-08	1.0E-08	1.0E-10	1.0E-08	1.0E-10
R2	1.0E+01	1.0E+03	1.0E+04	1.0E+04	1.0E+04	1.0E+04
R3	1.0E+01	1.0E+04	1.0E+06	1.0E+06	1.0E+06	1.0E+06
C3	1.0E-07	1.0E-08	1.0E-08	1.0E-10	1.0E-08	1.0E-10
CPE1	1.0E+06	1.0E+07	1.0E+08	1.0E+08	1.0E+05	1.0E+08
Alpha	0.6	0.6	0.6	0.1	0.1	0.1
C2	1.0E-07	1.0E-08	1.0E-08	1.0E-10	1.0E-08	1.0E-10

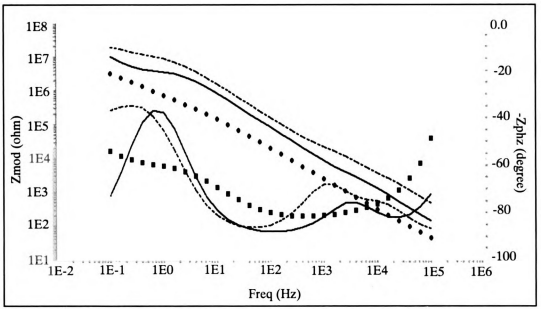

Figure A- 1 Measured impedance from rebar to external sensors and impedance of the equivalent circuit using poor initial values for parameters: Dots are the measured values, dotted line is the fitted impedance using initial values, and solid line is the fitted impedance with the final values

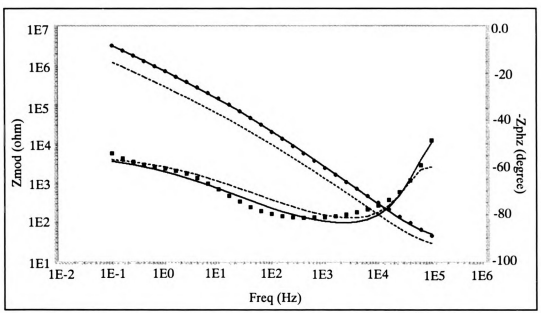

Figure A- 2 Measured impedance from rebar to external sensors and impedance of the equivalent circuit using good initial values for parameters: Dots are the measured values, dotted line is the fitted impedance using initial values, and solid line is the fitted impedance with the final value